

# Kinetic properties of heteromeric kinesin-2 from *Caenorhabditis elegans*

Dissertation zur Erlangung  
des akademischen Grades  
„Doktor der Naturwissenschaften“ (Dr. rer. nat.)

an der Fakultät für Biologie  
der Ludwig-Maximilians-Universität München

Angefertigt am Institut für Zellbiologie  
der Ludwig-Maximilians-Universität München  
unter der Betreuung von Hr. Prof. Dr. Manfred Schliwa

vorgelegt von  
Süleyman Kösem

München, 2014

1. Gutachter: Hr. Prof. Dr. Manfred Schliwa
2. Gutachter: Fr. Prof. Dr. Angelika Böttger

Dissertation eingereicht am: 12. Mai 2014

Tag der mündlichen Prüfung: 13. Oktober 2014

# **Ehrenwörtliche Versicherung**

Ich versichere hiermit an Eides Statt, dass die vorgelegte Dissertation von mir selbständig und ohne unerlaubte Hilfe angefertigt wurde. Ich habe weder anderweitig versucht eine Dissertation einzureichen oder eine Doktorprüfung abzulegen, noch habe ich diese Dissertation oder Teile derselben einer anderen Prüfungskommission vorgelegt.

München, den

Süleyman Kösem



# Publications

## Articles

Kösem S., Okten Z, Ho TH, Trommler G, Koonce MP, Samereier M, Müller-Taubenberger A., A non-mitotic CENP-E homolog in *Dictyostelium discoideum* with slow motor activity. Biochem Biophys Res Commun. 2013 Feb 15; 431(3):490-5. doi: 10.1016/j.bbrc.2013.01.030. Epub 2013 Jan 16.

Brunnbauer M, Mueller-Planitz F, Kösem S., Ho TH, Dombi R, Gebhardt JC, Rief M, Okten Z., Regulation of a heterodimeric kinesin-2 through an unprocessive motor domain that is turned processive by its partner. Proc Natl Acad Sci U S A. 2010 Jun 8; 107(23):10460-5.

## Poster Presentations

Kösem S., Oekten Z., What makes the Kinesin like Protein (KLP) 11/11 chimeric construct unprocessive?, ASCB 51th int. meeting, 2012, San Francisco, USA.

Kösem S., Oekten Z., What makes the Kinesin like Protein (KLP) 11/11 chimeric construct unprocessive? DGZ/FEBS Workshop "The spider's web: how microtubules organize cellular space" 2011, Dresden, Germany.

Kösem S., Oekten Z., What makes the Kinesin like Protein (KLP) 11/11 chimeric construct unprocessive?, EMBO annual meeting 2010, Barcelona, Spain.

Kösem S., Vukajlovic M., Schliwa M., Oekten Z., Autoregulation of heteromeric kinesin-2 from *C. elegans*, DGZ annual meeting, 2010, Regensburg, Germany.

# Table of contents

|  |    |
|--|----|
| Summary .....  | 1  |
| Zusammenfassung .....  | 3  |
| Introduction .....   | 5  |
| 1. The cytoskeleton and cellular motility.....                         | 5  |
| 1.1. The cytoskeleton .....  | 5  |
| 1.2. Cellular motility driven by motor proteins.....                   | 6  |
| 2. Kinesin superfamily .....   | 8  |
| 2.1. Functional anatomy of kinesins .....                              | 9  |
| 2.1.1. Structural elements involved in force generation.....           | 9  |
| 2.1.2. Structural elements involved in autoregulation .....            | 10 |
| 2.2. Model of Processive movement by kinesins .....                    | 10 |
| 2.3. Regulation of kinesin motors .....                                | 13 |
| 3. Kinesin-2 subfamily .....   | 14 |
| 3.1. Kinesin-2 involved in IFT in <i>C.elegans</i> sensory cilia ..... | 16 |
| 4. Aims of this thesis .....   | 18 |
| 4.1. Mechanism of autoinhibition .....                                 | 18 |
| 4.2. Mechanism of processivity .....                                   | 19 |
| Materials and methods .....  | 21 |
| 1. Materials .....   | 21 |
| 1.1. Reagents and other Materials.....                                 | 21 |
| 1.2. Plasmids and Vectors .....  | 21 |
| 1.3. Oligonucleotides (Primers).....                                   | 22 |
| 1.4. Bacterial Strains .....   | 25 |
| 1.5. Media and Cultivation of <i>E.coli</i> .....                      | 25 |
| 1.6. Antibodies and peptides .....                                     | 25 |
| 2. Methods .....   | 26 |
| 2.1. Molecular biology methods .....                                   | 26 |
| 2.1.1. Agarose gel electrophoresis .....                               | 26 |
| 2.1.2. DNA isolation from agarose gels .....                           | 26 |
| 2.1.3. Determination of DNA concentration .....                        | 26 |

## Table of contents

---

|   |           |
|---|-----------|
| 2.1.4. Purification of plasmid DNA .....  | 27        |
| 2.1.5. DNA cleavage with restriction enzymes .....  | 27        |
| 2.1.6. Dephosphorylation of 5' –ends of DNA.....  | 27        |
| 2.1.7. Ligation of DNA fragments .....  | 27        |
| 2.1.8. Transformation of chemically competent <i>E.coli</i> cells .....                               | 28        |
| 2.1.9. Identification of transformed <i>E.coli</i> .....  | 28        |
| 2.1.10. Polymerase chain reaction (PCR).....  | 28        |
| 2.1.11. Generation of constructs .....  | 29        |
| 2.1.12. Baculovirus expression system .....   | 32        |
| <b>2.2. Biochemical methods .....</b>   | <b>36</b> |
| 2.2.1. SDS-polyacryl amide gel electrophoresis (SDS-Page).....  | 36        |
| 2.2.2. Determination of protein concentration .....   | 37        |
| 2.2.3. Determination of tubulin concentration .....   | 38        |
| 2.2.4. Purification of porcine brain tubulin .....  | 38        |
| 2.2.5. Tubulin polymerization .....   | 39        |
| 2.2.6. Microtubule stimulated ATPase assay .....  | 40        |
| 2.2.7. Multiple motor gliding filament assay .....  | 42        |
| 2.2.8. Single molecule motility assay .....   | 44        |
| 2.2.9. Analysis of single molecule experiment .....   | 45        |
| 2.2.10. Protein purification.....   | 45        |
| 2.2.11. Gel filtration chromatography .....   | 48        |
| 2.2.12. Microscopy.....   | 48        |
| 2.2.13. Mass spectrometry (MS) .....  | 50        |
| <b>Results.....</b>   | <b>51</b> |
| 1. Experimental Concept .....   | 51        |
| 2. Kinesin-2 (KLP11/20) subunits from <i>C.elegans</i> exhibit low sequence homology .....            | 53        |
| 3. KLP11/20 exhibits a helix breaker position within its stalk region .....                           | 54        |
| 4. Expression, purification, and quality control of the constructs .....                              | 55        |
| 4.1. Size-exclusion chromatography of the full-length constructs .....                                | 57        |
| 4.2. Size exclusion chromatography of the truncated constructs .....                                  | 59        |
| 5. Kinetic properties of the wild type KLP11/20 and its chimeric KLP20/11 .....                       | 61        |
| 6. The kinetic contributions of the KLP11 and KLP20 subunits to the heterodimeric KLP11/20 motor..... | 63        |
| 7. Relieving auto-regulation in KLP11/20 by tail mutations .....                                      | 64        |

## Table of contents

---

|  |                                    |
|--|------------------------------------|
| 7.1. Removing the kink in the tail domain eliminates the auto-regulation in KLP11/20 .....             | 65                                 |
| 7.2. Removing the kink in the homodimeric KLP11/11 does not affect the motor's activity.....           | 67                                 |
| 7.3 Monomeric KLP11 and KLP20 constructs are kinetically equivalent .....                              | 69                                 |
| 8. Dimerization brings about the observed kinetic distinctions in KLP11/11 and KLP20/20 chimeras ..... | 71                                 |
| 9. The suppression of the KLP11/11 activity is relieved by flexible residues .....                     | 73                                 |
| 10. Homodimeric KLP20/20 is processive, KLP11/11 is not.....   | 74                                 |
| 11. KLP11/11 GCN4 motors with flexible extensions between the head domains are processive .....        | 75                                 |
| 12. Summary of results.....  | 78                                 |
| Discussion.....  | 80                                 |
| 1. Kinesin-2 (KLP11/20) from <i>C.elegans</i> is auto-regulated.....                                   | 80                                 |
| 2. Monomeric head domains are almost equivalent .....  | 82                                 |
| 3. Homodimeric KLP11/11 combinations are suppressed due to steric hindrance .....                      | 82                                 |
| 4. Neck linker region and kinetic activity.....  | 85                                 |
| 5. Neck linker region and processivity .....   | 86                                 |
| Summary and Outlook.....   | 88                                 |
| Literature .....   | 90                                 |
| Curriculum Vitae .....   | Fehler! Textmarke nicht definiert. |



# Summary

The cytoskeleton of eukaryotic cells is an essential and highly dynamic structural network of fibers protecting the cell from deformation, providing cellular scaffold and enabling cellular motility for spatial organization. Motor proteins are responsible for intracellular trafficking as well as morphological activities in eukaryotic cells, using actin filaments and microtubules as tracks. Cytoskeletal motor proteins (Myosins, dyneins and kinesins) can be described as ATP-driven “nano-machines” that are responsible for directed intracellular movements. The kinesin superfamily contains several hundred members divided into at least 14 family designations. Vast majority of kinesins are homodimeric, some are homotetrameric, or monomeric. The heterodimeric kinesin-2 from *C. elegans* consists of three subunits: two different kinesin-like motor subunits encoded by kinesin like proteins (KLP) 11 and 20 and one non-motor subunit termed KAP (Kinesin associated protein).

However, why kinesin-2 combines two different subunits and which advantages this provides for the whole motor remains elusive. Are the subunits kinetically not equivalent as they also differ in size? Does KLP11/20 regulate its catalytic activity by a tail mediated mechanism similar to kinesin-1 and kinesin-3? Testing kinesin-2's catalytic activity and its regulation as well as of its subunits by molecular engineering has enabled the dissection of the kinetic properties of the subunits KLP11 and KLP20 constituting the heterodimeric KLP11/20 motor from *C. elegans*.

Four main conclusions were drawn from these analyses. First, wild type KLP11/20 is auto-regulated and this inhibition can be relieved either by swapping the relative head positions (KLP20/11) or by replacing the flexible kink position by stiff residues (KLP11EE/20EE) or by removing the KLP11 subunit (KLP20/20). Second, the dimerization of two KLP11 vs. two KLP20 head domains either by the wild type tail or by the unrelated molecular zipper GCN4 results in motors with distinct kinetic properties. Third, the GCN4-mediated dimerization of the KLP11 subunit results in an unprocessive motor whereas the corresponding dimerization of the KLP20 subunit results in a processive motor. Fourth, introducing flexible residues between the

## Summary

---

KLP11 head domains is sufficient to impart processivity onto the homodimeric KLP11/11 GCN4 motor.

## Zusammenfassung

Das Zytoskelett von eukaryontischen Zellen ist ein essentielles und sehr dynamisches strukturelles Netzwerk von Fasern, das die Zelle vor Verformung schützt, zelluläre Stabilität bietet und Mobilität für die räumliche Organisation ermöglicht. Indem sie die Aktinfilamente und die Mikrotubuli als Schienen benutzen, sind Motorproteine sowohl für den intrazellulären Transport als auch für die morphologischen Aktivitäten in eukaryotischen Zellen verantwortlich. Zytoskelett Motorproteine (Myosine, Dyneine und Kinesine) können als ATP betriebene "Nanomaschinen" bezeichnet werden, die für gerichtete intrazelluläre Bewegungen verantwortlich sind. Die Kinesin -Superfamilie umfasst mehrere hundert Mitglieder, die in mindestens 14 Familienstämme unterteilt werden können. Die überwiegende Mehrheit der Kinesine bilden Homodimere, während einige Homotetramere oder Monomere sind. Das heterodimere Kinesin-2 aus *C. elegans* besteht aus drei Untereinheiten: zwei unterschiedlichen Kinesin ähnlichen Motoreinheiten, welche durch die Kinesin Like Proteins (KLP) 11 und 20 kodiert werden, sowie einer nicht-Motoruntereinheit die als KAP (Kinesin associated protein) bezeichnet wird.

Doch warum Kinesin-2 zwei unterschiedliche Untereinheiten kombiniert und welche Vorteile dies für den ganzen Motor bietet bleibt ungeklärt. Sind die Untereinheiten etwa kinetisch nicht gleichwertig, da sie sich auch in der Größe unterscheiden? Reguliert KLP11/20 seine katalytische Aktivität durch einen Schwanz vermittelten Mechanismus ähnlich wie bei Kinesin-1 und Kinesin-3? Die Untersuchung der katalytischen Aktivität und dessen Regulierung sowohl von Kinesin-2 als auch von seinen Untereinheiten mit Hilfe der Molekulartechnik hat zur Aufklärung der kinetischen Eigenschaften der Untereinheiten KLP11 und KLP20, die den heteromeren KLP11/20 Motor aufbauen, beigetragen.

Aus diesen Analysen wurden vier haupt Schlussfolgerungen gezogen: (1) Wildtyp KLP11/20 ist auto-reguliert und diese Hemmung kann entweder durch Vertauschen der relativen Kopfpositionen (KLP20/11) oder durch den Austausch der flexiblen Knick-Position durch steife Elemente (KLP11EE/20EE) oder durch Entfernen der KLP11 Untereinheit aufgehoben werden (KLP20/20). (2) Die Dimerisierung von zwei

KLP11 und zwei KLP20 Kopf Domänen zu einem Motor entweder durch den Wildtyp-Schwanz oder durch den molekularen ‚Zipper‘ GCN4 führt zu zwei unterschiedlichen Motoren mit verschiedenen kinetischen Eigenschaften. (3) Die GCN4-vermittelte Dimerisierung von zwei KLP11 Untereinheiten führt zu einem unprozessiven Motor während die Dimerisierung von zwei korrespondierenden KLP20 Untereinheiten einen prozessiven Motor liefert. (4) Die Einführung flexibler Reste zwischen den Kopfdomänen bei KLP11 ist ausreichend, um dem Homodimeren KLP11/11 GCN4 Motor Prozessivität zu verleihen.

# Introduction

## 1. The cytoskeleton and cellular motility

The cytoskeleton of eukaryotic cells is an essential and highly dynamic structural network of fibers protecting the cell from deformation, providing a cellular scaffold and enabling cellular motility for spatial organization. Technical and experimental improvements in the last decades have made possible to provide unequivocal evidence that motor proteins are responsible for intracellular trafficking as well as morphological activities in eukaryotic cells, using actin filaments and microtubules as tracks. Motor proteins are capable of converting chemical energy from adenosine triphosphate (ATP) hydrolysis into mechanical work in order to transport vesicles and organelles along filaments [1, 2]. The segregation of chromosomes in mitosis and meiosis [3, 4], asymmetric localization of morphogens in early embryos or the transport of secretory vesicles in vertebrates or mRNA in yeast [5] are well known processes that require molecular motors.

### 1.1. The cytoskeleton

Filamentous actin (F-actin), microtubules and intermediate filaments constitute the eukaryotic cytoskeleton [6] accompanied by a large number of accessory proteins, responsible for proper function and maintenance of these three filament types [7].

Intermediate filaments, have a diameter of about 10nm, protect cells against mechanical stress and provide cell integrity. The intermediate filament monomers are elongated fibrous proteins and have no enzymatic activity. So far, no evidence is available that they serve as tracks for molecular motors.

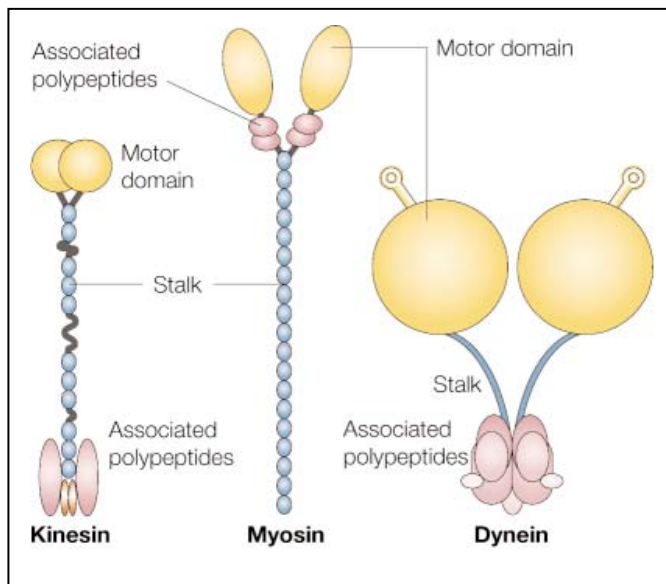
F-actin and microtubules are polar structures containing a fast growing plus (+) and a slow growing minus (-) end. In contrast to intermediate filaments, both types serve as tracks for molecular motors. The F-actin is a flexible two stranded helical polymer with a diameter of 6 to 8 nm, composed of actin subunits (also called microfilaments). They are built from so-called globular actin monomers (G-Actin) containing ATP in their ATP-binding clefts [8, 9] that polymerize in an oriented way to F-Actin [10].

Numerous accessory proteins (actin binding proteins, ABPs) form actin bundles, regulate the length of the filament, its orientation and structure or cross-link the filaments to each other or even to microtubules, ending in an actin network, concentrated at the cell cortex that serves as tracks for myosin motors.

Microtubules (MTs) are cylindrical polymers with a diameter of 24 nm composed of guanosine triphosphate (GTP) binding  $\alpha$ - and  $\beta$ -tubulin heterodimers. In contrast to G-actin which uses ATP for polymerization, the tubulin heterodimer uses GTP to polymerize into microtubules. The head-to-tail arrangement of the subunits generates a linear structure termed protofilament, which gives polarity to the filaments. It is known, that *in vivo* often 13 laterally arranged protofilaments form the microtubule [11]. MTs are highly dynamic structures, characterized by spontaneous elongation and shrinking phases [12]. This process, named dynamic instability is coupled to GTP hydrolysis and is controlled by numerous proteins [13]. *In vivo*, the minus end of MTs is anchored at the microtubule-organizing centre (MTOC) by the gamma ( $\gamma$ )-tubulin complex [14], in close proximity of the nucleus, whereas the plus end grows out towards the cell periphery. Typically, MTs radiate from the cell centre to the cell cortex, allowing long range transports. Similar to actin filaments, a number of proteins termed MT-Associated Proteins (MAPs) are responsible for the dynamics and maintenance of the MTs [15]. MT stabilization in *in vitro* assays is accomplished with the anticancer drug taxol, which effectively promotes the assembly of tubulin monomers to MTs [16] and prevents the MTs from shrinking. So far, two classes of motor proteins, kinesins and dyneins are capable of using MTs for long distance transport of cell organelles.

### **1.2. Cellular motility driven by motor proteins**

Cytoskeletal motor proteins can be described as ATP-driven “nano-machines” that are responsible for directed intracellular movements. Three different groups of motor proteins evolved to power such transport: Myosins, which are responsible for actin based motility, and two types of MT based motors, kinesins and dyneins (Figure 1).



**Figure 1. The three motor protein ‘prototypes’.** The catalytic domains of the motors are depicted in yellow, followed by the stalk, shown in blue. Associated polypeptides are shown in purple. (From Woehlke *et al.* 2000 [17])

The actin-based myosin and the microtubule-based kinesin motors were initially considered unrelated [17]. Mechanistically, a fundamental difference is the nucleotide-dependent interaction of the motors with their filaments. That means in detail, that myosin hydrolyses ATP while detached from actin, whereas kinesin hydrolyses ATP while attached to the microtubule [18]. So the structural similarity of the core of their catalytic domains came as a surprise [19] (see Figure 1). Furthermore there were also striking similarities of the kinesin core to structural elements of G-Proteins [20]. The similarity is particularly apparent in the nucleotide active site, which consists of three loops called the P-loop, Switch I, and Switch II [21]. The vast majority of the members in the myosin super family are involved in plus-end directed transport on F-actin. Myosin VI is so far the only motor that drives minus-end directed transport. Kinesin super family also comprises members that are mostly involved in plus-end directed transport on the microtubule, whereas some members are minus-end directed and bi-directional kinesins, respectively [22-25].

Dyneins are so far the only family of motor proteins that are exclusively involved in minus-end directed transport. Dyneins can be divided into two groups: cytoplasmic dyneins and axonemal dyneins, which are also named ciliary or flagellar dyneins.

It has to be mentioned that beside motor protein driven motility, there is a polymerization driven motility, which is accomplished by rearrangements of the cytoskeleton. This type of motility is controlled by assembly and disassembly

processes of microfilaments and/or microtubules including a vast number of regulatory proteins. Polymerization driven motility is, for example, responsible for migration of fibroblasts or macrophages by building up a leading edge containing assembled actin filaments.

## 2. Kinesin superfamily

The first kinesin was discovered more than two decades ago as a novel ATPase involved in neuronal microtubule based motility. The name kinesin comes from the greek word “kinein” for “to move” [26, 27]. The kinesin superfamily already contains several hundred members, which are identified based on the sequence homology of the kinesin motor domains and is divided into at least 14 family designations [28].

In contrast to dyneins, the members of the kinesin superfamily show large morphological diversity. Their roles in cells vary from transport of vesicles and organelles to mediation of proper cell division, as well as the movement of chromosomes [4, 29, 30]. The best studied motor proteins within the kinesin family are the founding members, also known as conventional kinesins or kinesin-1 [31].

Kinesin subfamilies can be classified on the basis of their directionality (plus-end or minus-end directed movement on microtubules), or the localization of the catalytic domain (N-terminal, internal, or C-terminal, i.e. N, I, or C-type) or by their variable polypeptide chain composition (monomers, homodimers, heterodimers, etc.) [32]. It is reported, that the direction of kinesin movement is correlated with the location of the head domains, i. e. kinesins with their motor domain located at the N-terminus move towards the plus-end of MTs, whereas kinesins with their motor domains located at the C-terminus move to the minus-end of the MTs [22-25]. Interestingly there is also a group of kinesins having their motor domains located in the middle of the protein, as in case of the kinesin-13 family. The members of this group are capable of moving in both directions by lattice diffusion on the MT filament and accumulate at the ends of MTs where they are associated with microtubule depolymerization [33, 34]. Vast majority of kinesins described above are homodimeric, some are homotetrameric, or monomeric.

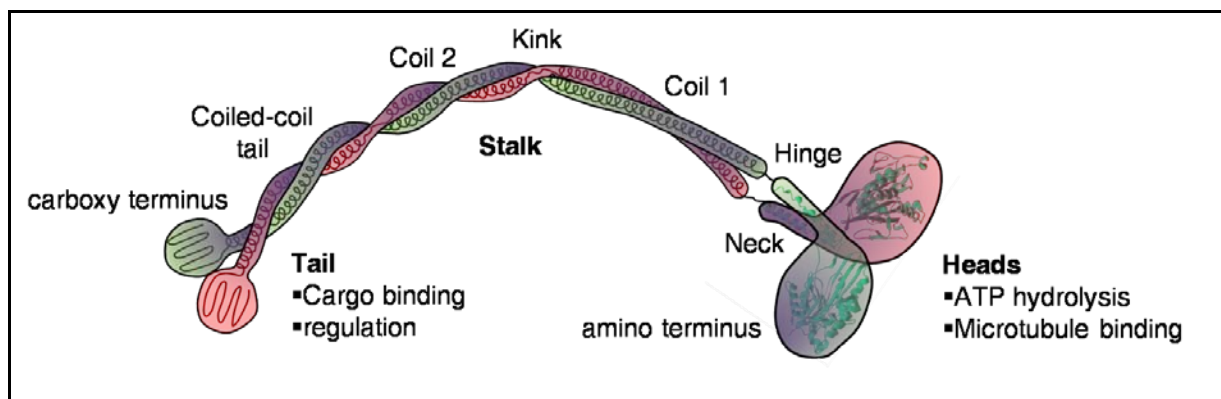
One noteworthy exception is the Kinesin-2 subgroup, also known as heteromeric kinesin [35], Kif3 [36] or simply heterokinesin [37]. Here, two distinct polypeptides



heterodimerize into one double-headed motor which in turn C-terminally associates with a non-motor subunit [38-40], termed Kinesin Associated Protein or KAP, to form a heterotrimeric complex in vivo and in vitro [41]. So far, all kinesin-2 motors were shown to move towards the plus-end of the microtubule [35].

## 2.1. Functional anatomy of kinesins

Typically kinesins are composed of three main domains (Figure 2): a globular head domain containing the neck linker region, responsible for catalytic activity, a  $\alpha$ -helical stalk region, necessary for dimerization of two kinesin chains and a tail domain [38-40] responsible for cargo binding and regulation [17, 42].



**Figure 2. Domain organization of the conventional kinesin heavy-chain dimer.** The conventional kinesin is a homodimer containing two heavy chains, with a head, stalk and tail domain. The catalytic head domains (~350 amino acids) are responsible for force production via ATP hydrolysis, converting chemical energy into mechanical work, as well as for binding to the microtubule track. The stalk region (~50 nm) contains several coiled-coil segments, mediating the homodimerization of the subunits to a double headed motor protein. The small globular tail domains (~20 nm) at the distal C-terminal end are implicated in cargo binding and regulation. The overall size of the molecule is about 80 nm [43]. (Adapted from Woehlke and Schliwa, 2000 [17])

### 2.1.1. Structural elements involved in force generation

Molecular motors power intracellular transport of different cargoes along cytoskeletal tracks by converting free energy from ATP hydrolysis into mechanical work. The chemical cycle of ATP hydrolysis needs to be coupled to a mechanical cycle of motor interaction with its filament [44, 45], resulting in a displacement of the motor along the cytoskeletal track.

The catalytic elements of the kinesin motors are the motor domains, also named head domains, which are followed by a neck region connecting the motor head to the stalk. These two elements of the kinesins are the most highly conserved regions

(about 30 to 40% sequence identity [33, 36, 37]). The motor domain and the neck linker are necessary and sufficient to couple the ATP hydrolysis to mechanical work.

Depending on the nucleotide state of the molecule, the neck-linker is found in different positions relative to the head domains [46] (Figure 3). Being also responsible for MT binding through a microtubule interaction site, the globular head is playing a crucial role in the 'mechanochemical' cycle of kinesin motor proteins [17].

### **2.1.2. Structural elements involved in autoregulation**

Figure 4 illustrates the flexible kink region found in the middle of the coiled-coil stalk which mediates the auto-regulatory folding of kinesin [47]. The resulting interaction of the globular tail domain located at the distal C-terminus with the head domains has been demonstrated to suppress the motor's ATPase [48-56]. Specifically, this interaction significantly slows down the ADP release from the catalytic head domains, leading to a reduced motor activity, while the motors affinity to microtubules is not affected [49, 51, 57-59]. In the folded state, the globular tail domains are in close proximity to the head domains, allowing a basic level of regulation [17].

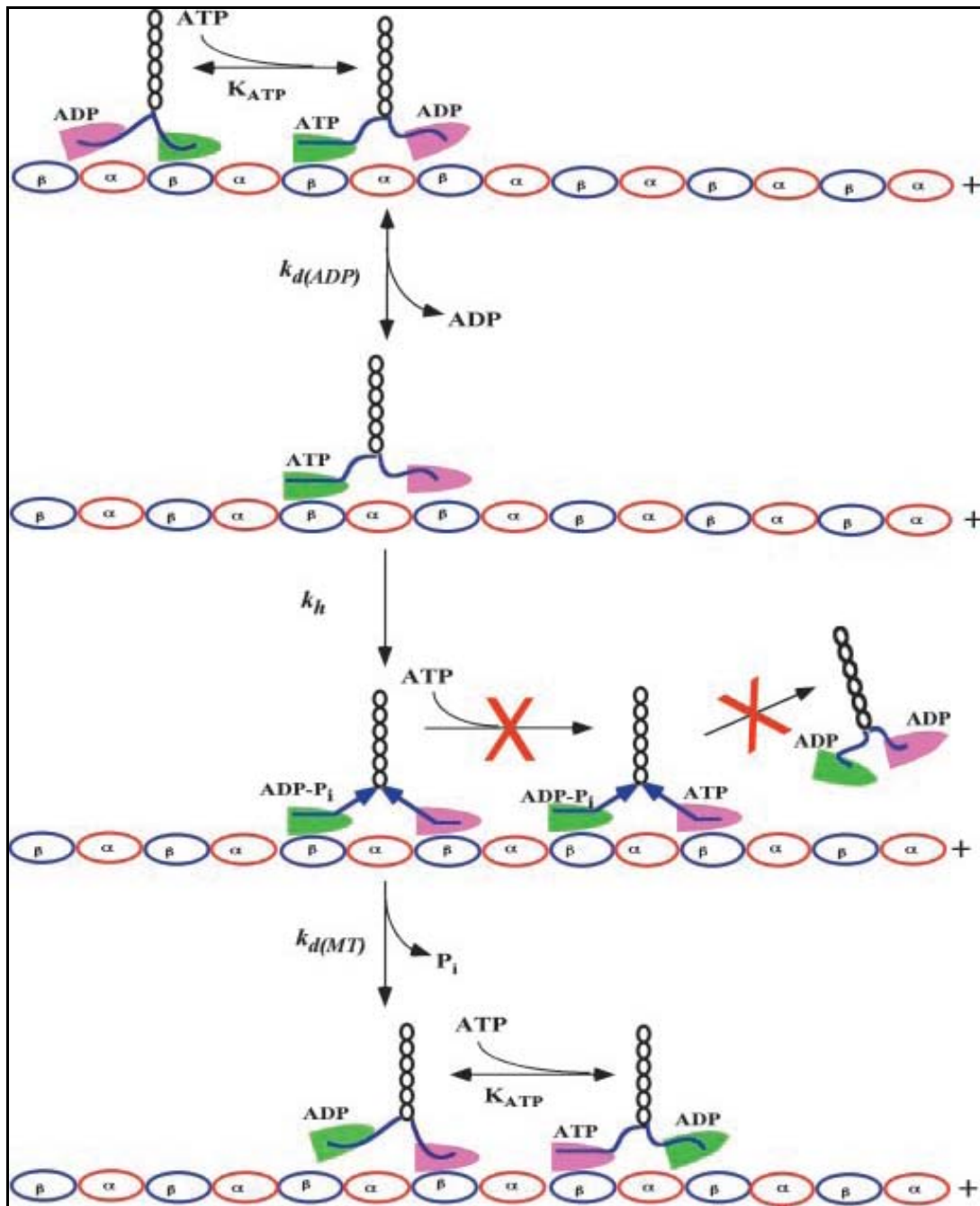
### **2.2. Model of Processive movement by kinesins**

Depending on specific physiological functions, some motors move processively, whereas others move in a non-processive manner. Processive movement is achieved by taking consecutive steps on the cytoskeletal track without falling off. Conventional kinesin is a processive molecular motor [60, 61] moving in 8 nm steps on its microtubule track, representing the distance between  $\beta$ -tubulin subunits of a microtubule [62]. Having directly coupled the stepping to the ATP hydrolysis, in each step one ATP molecule is consumed [63, 64].

Processivity in conventional kinesin is brought about by dimerization of two heavy chains via the stalk domain to a homodimer. The various models of processivity have common, that the two motor domains of the molecule have to remain enzymatically "out of phase", which means that at least one head is strongly bound to microtubules at any given time [65, 66]. This implies that there must be some form of communication between the two motor head domains for a possible processive movement, to prevent the motor from dissociating from its track. The alternated ATPase cycles between the two heads, where one head is kept bound to the

microtubule, while the other head detaches and moves forward [67], ensures consecutive stepping. Conventional kinesin regulates the behavior of its heads by using a nucleotide dependent change in its affinity to microtubules [68-70]. This means in detail, that in solution both motor heads tightly bind ADP until the first head attaches to the filament. Upon binding of the first head (Figure 3, green motor head) to microtubules, ADP is released and the motor locks onto the filament. The mechanochemical cycle is initiated by binding of ATP to the attached (green) leading motor head. Binding of ATP leads to rapid docking of the leading head's neck linker, which throws the tethered rear head (magenta) forward. The new rear head can be released again only if it binds and hydrolyses a new ATP molecule. During this hydrolysis process, the new leading head is allowed to find its next proper microtubule binding site, where it releases its ADP and locks onto the filament [71]. In this intermediate state, both heads are tightly bound to the filament and the neck-linkers are strained (Figure 3, blue arrows). With a mechanism preventing ATP from binding to the new leading head while it is experiencing rearward strain, ATP hydrolysis is followed by the dissociation of the rear head, while the leading head holds on [65]. At this point, both heads have exchanged their roles and the motor walks hand-over-hand, which represents the widely accepted model for processive stepping [72-76].

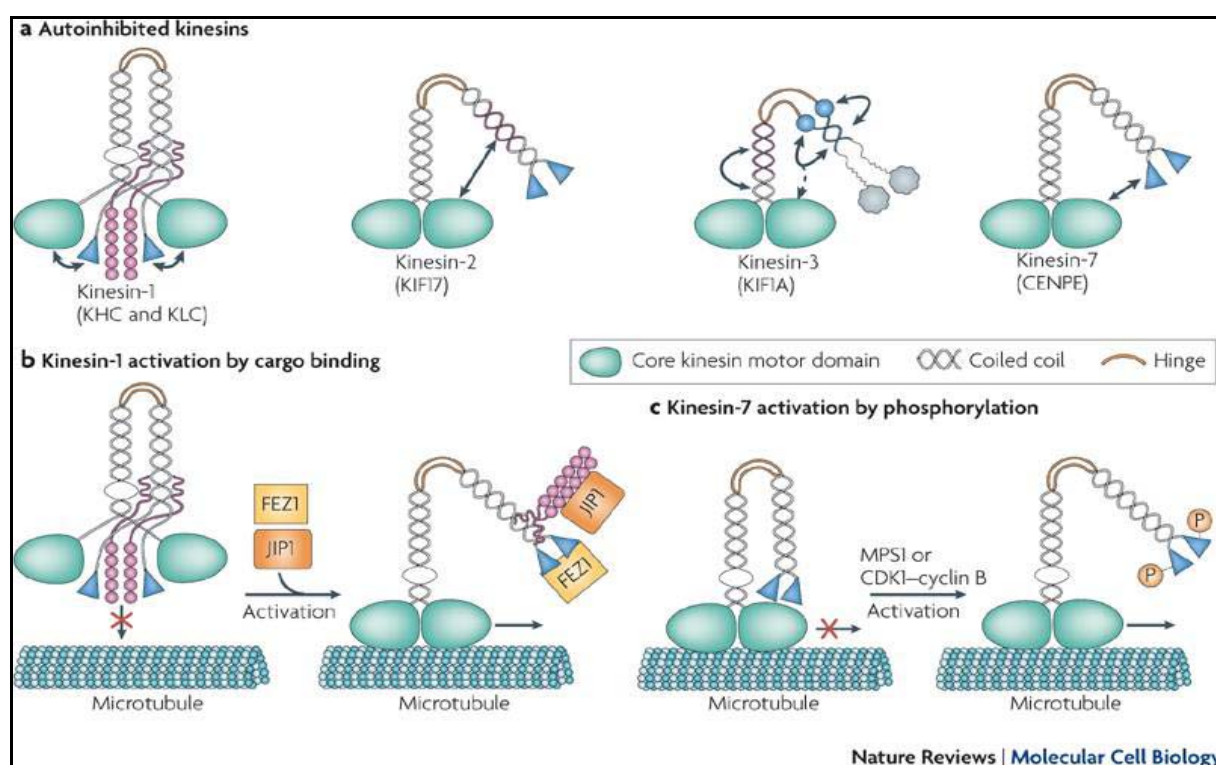
Based on a hand-over-hand model, it was believed that processive motility requires two heads acting precisely coordinated to stay out of phase while walking to the plus-end of the microtubule. So the discovery of a minus-end-directed [77], dimeric and non-processive motor like Ncd (Non-claret-disjunctional) [78], as well as the observation that a monomeric single-headed motor, mouse Kif1A, moving processively came as a surprise [79]. Kif1A has evolved a unique mechanism where it can maintain contact to the negatively charged carboxyl terminus of microtubule dimers via a positively charged surface loop [79]. In contrast to a directed movement of conventional kinesin, Kif1A shows back-and-forth movement with a net directional bias [17, 80] during its movement. So, processivity in the field of kinesins is still controversial and requires further investigations to be fully understood.



**Figure 3. First two steps of kinesin on microtubules.** The heads are distinguished by magenta and green shading connected by neck linkers colored in blue to the black coiled coil region. The mechanochemical cycle is initiated by the binding of ATP to the attached, green motor domain, and is characterized by the equilibrium constant  $K_{ATP}$ . This leads to the rapid docking of this motor domain's neck linker, which throws the tethered rear (magenta) motor forward in the direction of the next tubulin binding site. The release of ADP from the new leading head (magenta) is followed by ATP hydrolysis that leads to the binding of both heads at the same time to the filament. This places the two neck linkers under mechanical strain, depicted as blue arrows. In the absence of any mechanism to prevent it, ATP could then bind to the empty, leading head domain and then become rapidly hydrolyzed. This would lead to the dissociation of the motor from the track after only two turnovers. The red X indicates that this does not happen. It must exist a mechanism to prevent ATP from binding to the leading head while it is experiencing rearward strain. Instead, the ATP hydrolysis is followed by the dissociation of the rear head, characterized by rate constant  $k_d(MT)$ , which occurs concomitantly with phosphate release (from Rosenfeld *et al.*, 2003 [65]).

### **2.3. Regulation of kinesin motors**

Because kinesins use a considerable amount of ATP to function as motors, it is essential to have mechanisms preventing the cell from unnecessarily wasting energy. It is believed that kinesins are regulated at several levels [81] to avoid futile ATP consumption, including associated light chains, phosphorylation, binding to its cargo or intramolecular folding [17] (Figure 4). Electron microscopy and FRET experiments provided evidence that without cargo bound, kinesin is in a folded and inactive conformation [56, 82]. This inhibitory folding is enabled by a flexible kink in the middle of the stalk [49, 50, 52]. Folding of the protein brings the carboxyl terminus of the tail and the N-terminal head domains in close proximity to inhibit the catalytic activity of the motor [48-56]. Competitive cargo binding to the C-terminal end of the tail disengages the catalytic heads and activates the motor. This is also true for an artificial cargo such as a silica bead [83]. A recent crystal structure of kinesin-1 in complex with its tail domain provided the structural evidence that the head-tail interaction creates a “lock down” preventing the movement of the motor domains that is needed to undock the neck linker and release ADP [84].



**Figure 4. Autoinhibitory mechanisms used by kinesin motors.** **a)** Inactive kinesin-1, Kif17, Kif1A and CENPE (Centromere associated protein E) assume a folded conformation that enables an inhibitory and direct motor-to-tail interaction. Double arrows indicate regions that interact in the folded, inactive conformation and dotted arrows indicate plausible interactions. **b)** Upon interaction of two binding partners (FEZ1, fasciculation and elongation protein-1 and JIP1, Jun N-terminal kinase-interacting protein1) with kinesin-1, its autoinhibition is relieved. **c)** Upon phosphorylation of CENPE by kinases MPS (Monopolar spindle protein 1) and CDK1 (Cyclin-dependent kinase 1); its activation is initiated (from Verhey and Hammond, 2009 [85]).

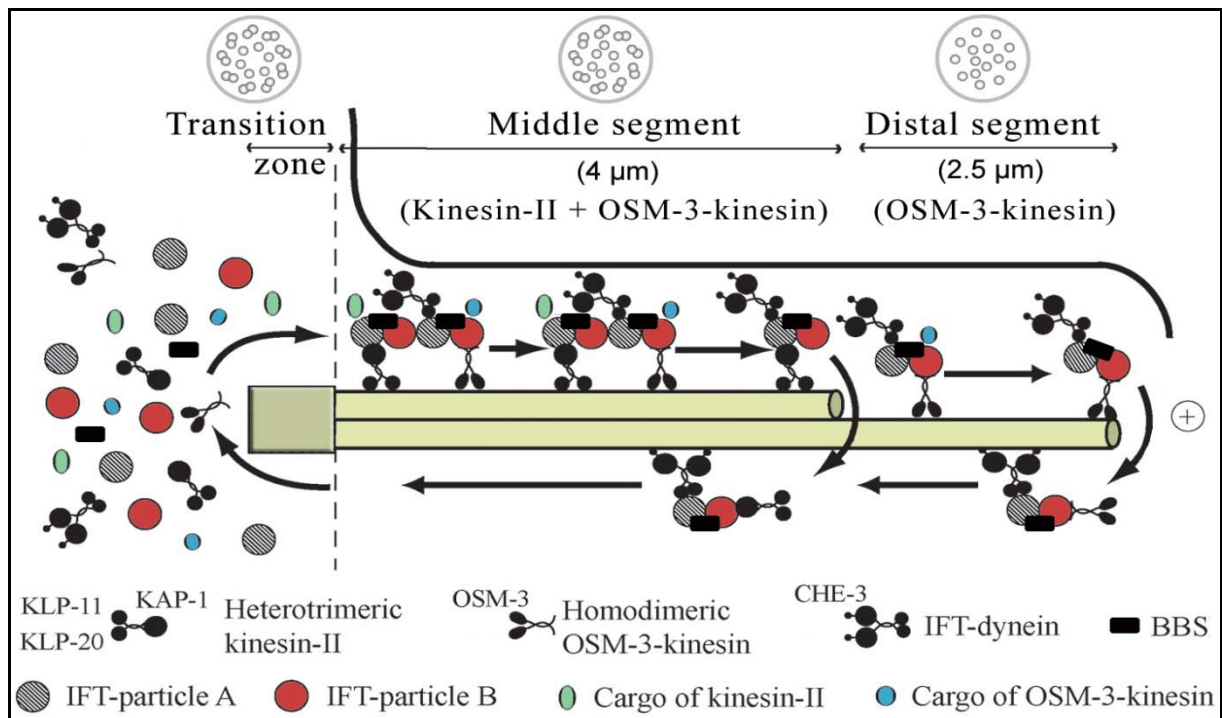
### 3. Kinesin-2 subfamily

Kinesin-2 family members are a class of diverse plus-end directed motor proteins [35, 86]. Having homodimeric as well as heterotrimeric members with different functions, kinesin-2 members are found in many organisms. In mammals, kinesin-2 is highly enriched in the testes and, to a lesser extent, in many other tissues, suggesting non-neuronal functions. In the frog, it is found in melanophores and unfertilized eggs [87]. In echinoderms, kinesin-2 is found in both embryos and sperm, where it localized to the mitotic spindle and midpiece and flagellum, respectively [40]. This diversity of distribution suggests that these kinesins perform different tasks in different cell types, a hypothesis supported by an expanding wealth of evidence. Being essential for assembly and maintenance of cilia and flagella [41, 88-90] as well as for proper function of these structures [41, 90-96], a co-evolution of both can be assumed.

Kinesin-2 and homologues have been identified in almost every species examined and studying these homologues has aided in the identification of many different potential functions for the kinesin-2 motor complex in numerous contexts. The best established function of kinesin-2 is its role in ciliary transport. Intraflagellar transport or IFT was detected using a differential interference microscopy (DIC) in *Chlamydomonas*, where bidirectional movement of granule-like molecules beneath the flagellar membrane could be observed [97, 98]. Experiments with mutant *Chlamydomonas* cells containing temperature sensitive homologues of kinesin-2 could provide evidence, that kinesin-2 is responsible for transport of the raft complex and transport of the components used for cilia construction and maintenance to the tip of the flagella [41, 95, 97] in numerous cell types and organisms. In addition, kinesin-2 guarantees proper IFT in other essential processes like vision [99] or chemosensory behavior in metazoans which rely on specialized cilia [100, 101].

Besides IFT transport, many other functions of kinesin-2 family members have been discovered. Chromosome segregation [102] and cytokinesis [103], mitotic spindle assembly [104], organelle sorting and anterograde transport in axons [39, 105, 106], endoplasmic reticulum (ER) and Golgi membrane transport [107], dispersion of melanosomes [108], signal transduction [109-111] as well as localization of RNA [112] are just some of the well known processes where kinesin-2 plays an important role.





**Figure 5. Intraflagellar transport (IFT) in *C. elegans*.** Components of the IFT machinery and ciliary cargo assemble at or near the transition zone (basal body). Heterotrimeric kinesin-2 and homodimeric OSM-3 kinesin, separately bind IFT particles and transport these together with IFT-dynein and cargo along the middle segment in the anterograde (+) direction. In the distal segment, OSM-3 kinesin alone transports the IFT particles and dynein/cargo. BBS (Bardet-Biedl syndrome) proteins act to stabilize the association between the motors and IFT particles. Components of the IFT machinery and presumably other ciliary molecules are recycled back to the base of the cilium using the IFT dynein molecular motor. The lengths of the transition zone (1 μm), middle segment (4 μm) and distal segment (2.5 μm) regions are shown (for amphid cilia) along with transverse view schematics of the microtubule arrangements (on top). (Adapted from Inglis *et al.*, 2007 [113].)

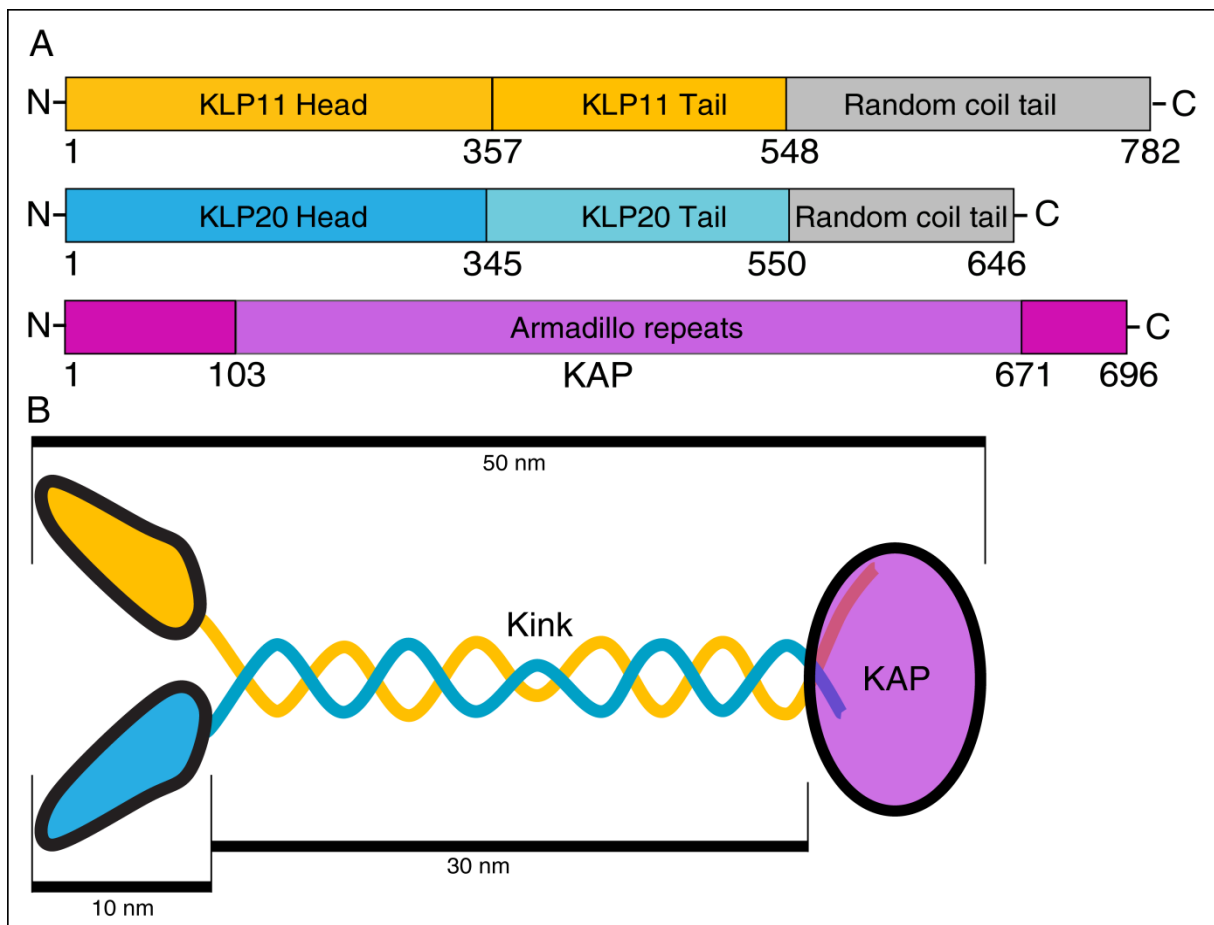
### 3.1. Kinesin-2 involved in IFT in *C. elegans* sensory cilia

The heterotrimeric kinesin-2 in *C. elegans* consists of three subunits (Figure 6): two different kinesin-like proteins (KLP) 11 and 20 that are members of the KIF3A/3B or KRP85/95 kinesin subfamilies and one non-motor subunit termed KAP (Kinesin associated Protein) [40, 114].

During IFT, heterotrimeric KLP11/20 acts in concert with the homodimeric Osm-3 kinesin-2 to assemble and maintain cilia of chemosensory neurons (Figure 5) [28, 86, 115-117]. *In vivo*, KLP11/20 alone moves with an average velocity of 0.5 μm/s and Osm-3 alone moves at 1.3 μm/sec, respectively. The observed intermediate velocity in the middle segment in mutants most likely results from the concerted action of both motors [115, 116, 118]. Furthermore, investigations on Osm-3 by Imanishi *et al.* 2006 [119] showed that Osm-3 kinesin is an auto-regulated motor *in vitro*. Additionally, ATPase activity and processivity were both dramatically stimulated by replacing the



flexible residues located in the middle of the stalk that was reminiscent of the kink position found in kinesin-1 (Figure 4). The removal of the kink in Osm-3 also changed the conformation of the motor from a compact to an extended form [119]. Taken together these results strongly argue for the existence of a flexible kink in the homodimeric kinesin-2 Osm-3 which allows the motor to adopt a folded, auto-regulated conformation as was demonstrated for the conventional kinesin-1 (Figure 4).



**Figure 6. Domain organization of the heterotrimeric kinesin-2 from *C. elegans*.** **A)** Schematic overview of the two motor subunits and Kinesin associated protein (KAP) with amino acid positions, building up the heterotrimeric motor in *C. elegans*. Interestingly both N-terminal motors differ in size of their head domains, as well as in size of their C-terminal located tail domains, whereas KLP11 (orange) contains 782 amino acids, which are 136 amino acids more than KLP20 (blue). The accessory subunit KAP contains about 10 armadillo repeats, which is conserved among kinesin-2 kinesins and is reported to interact with cargo. **B)** Model showing the structure of kinesin-2 from *C. elegans*. Head domains have a size about 10 nm and are shown in orange (KLP11) and in blue (KLP20) dimerized via their tail domains (about 30 nm). Kink region, responsible for bending is located within the tail domains. The accessory subunit KAP has a globular overall structure. The size of all subunits is about 50 nm (adapted from Cole 1999 [40])

## 4. Aims of this thesis

Structural comparison of conventional kinesin and kinesin-2 shows, that these two motors have similar overall structures: two motor heads located at the N-terminus, dimerized by a stalk and a C-terminal located tail region with the accessory subunit (KAP). Interestingly, structural similarity of both motor proteins exists although significant sequence homology is limited to the catalytic head domains [86]. Nevertheless, KLP11/20 kinesin-2 from *C. elegans* and conventional kinesin use the rod domains to ensure heterodimerization and homodimerization, respectively, to assemble a proper functioning motor protein [38, 40]. However, why kinesin-2 combines two different head domains and which advantages this provides for the whole motor needs to be determined. Testing kinesin-2's catalytic activity and its regulation as well as that of its individual subunits could illuminate the question why evolution favoured the generation of a heterotrimeric motor.

### 4.1. Mechanism of autoinhibition

Investigations of conventional kinesin and kinesin-2 motors so far have shown that autoinhibition is a possible mechanism of controlling their activity [81, 119, 120]. One main aim of this thesis is to investigate whether KLP11/20 is regulated by a similar mechanism to prevent futile energy consumption or not. The KLP11 and KLP20 subunits assembling kinesin-2 expose high sequence homology in the catalytic head domains, whereas the rod domains lack a significant sequence homology. Consequently, having two different although related motor subunits varying also in size (KLP11: 782 amino acids and KLP20: 646 amino acids) raises the question, whether both head domains are used for different purposes. Is possibly only one of the head domains autoregulated by the tail domains, while the other head performs a different task? One aspect favouring an autoregulation of the molecule is a helix breaker position probably serving as a hinge located in the wild type KLP11 tail domain. Are one of the head domains or maybe both motor heads kept in stand by modus by bending of the tail domains over the head domains at this position when they are not in use?

Assuming that KLP11/20 activity is controlled by autoinhibition, there were different possibilities to turn on the motor's activity. Eliminating the kink region responsible for

the bending of the molecule via exchange of the amino acids in the kink was one possibility. Another option was to remove the complete native tail domain to exclude any influence on the head domains and replacing it with an artificial GCN4 leucine zipper with strong propensity to form coiled-coils to ensure homodimerization. At last, by reducing the motor to its monomeric head domains including the neck regions eliminated every disturbance of motor activity caused by the tail domains. Additionally, the monomeric constructs were released of a possible mutual influence of the head domains which might occur in the case of homodimerization.

All generated constructs were assayed in ATPase assays for their ATP turnover ( $k_{\text{cat}}$ ) and the affinity for microtubules ( $K_{\text{m}}$ ) as well as for ATP. Furthermore, with the exception of monomeric constructs, all motors were tested in multiple motor gliding filament assays for their gliding velocities.

### 4.2. Mechanism of processivity

The ability of kinesin motors walking along the microtubule track without dissociating, called processivity is not totally understood. Initially, it was believed that processive movement requires two head domains acting in concert, until the discovery of a single headed processive Kif1A motor [79] disproved this theory. The cooperation partner of KLP11/20, Osm-3, was turned processive only by mutations in the hinge region of the molecule in *in vitro* assays [119]. So, probing for the processive movement properties of KLP11/20 was essential since a hinge region within the motor protein was also present. During processive movement, a crucial role is played by the neck and neck-linker regions of the molecule, which is believed to be responsible for generating an intramolecular strain. It is widely accepted that this intramolecular strain [65, 75, 121-123] is responsible for 'gating', a mechanism that allows the two head domains to communicate their enzymatic state to each other to stay out of phase during stepping.

This work is focused on the processivity of KLP11/20 from *C. elegans*. What does it take to be a processive motor? This was the leading question accompanying the investigations regarding processive movement of kinesin-2. Additionally, it was intended to illuminate the question what the minimum requirement for a motor protein is to display processive movement. By investigating single molecule behavior of all

constructs including different tail variations it was intended to answer whether both subunits as homodimeric motor combinations were processive or not. Furthermore, by introducing flexible residues (glycine and serine repeats) in the neck region of KLP11 it was intended to investigate the influence of intramolecular strain on the processive behavior of kinesin-2. For this purpose, single molecule assays with homodimeric KLP11 and KLP11 GS constructs zipped together with GCN4 were performed. These assays provided insight into the individual behavior of a single molecule, which otherwise is inaccessible in bulk measurements. With single molecule assay, one is able to determine the processivity index and velocity of a motor protein under zero load conditions. With four SfGFP (Superfolder Green Fluorescent Protein) dyes tagged to homodimeric GCN4 constructs of KLP11, KLP11 GS repeats, and KLP20 were investigated in single molecule assays via TIRF (Total internal reflection fluorescence) microscopy. Their individual processivity behavior has been elucidated to better understand the overall structure and kinetic properties of this special heterotrimeric protein within the kinesin family members.

# Materials and methods

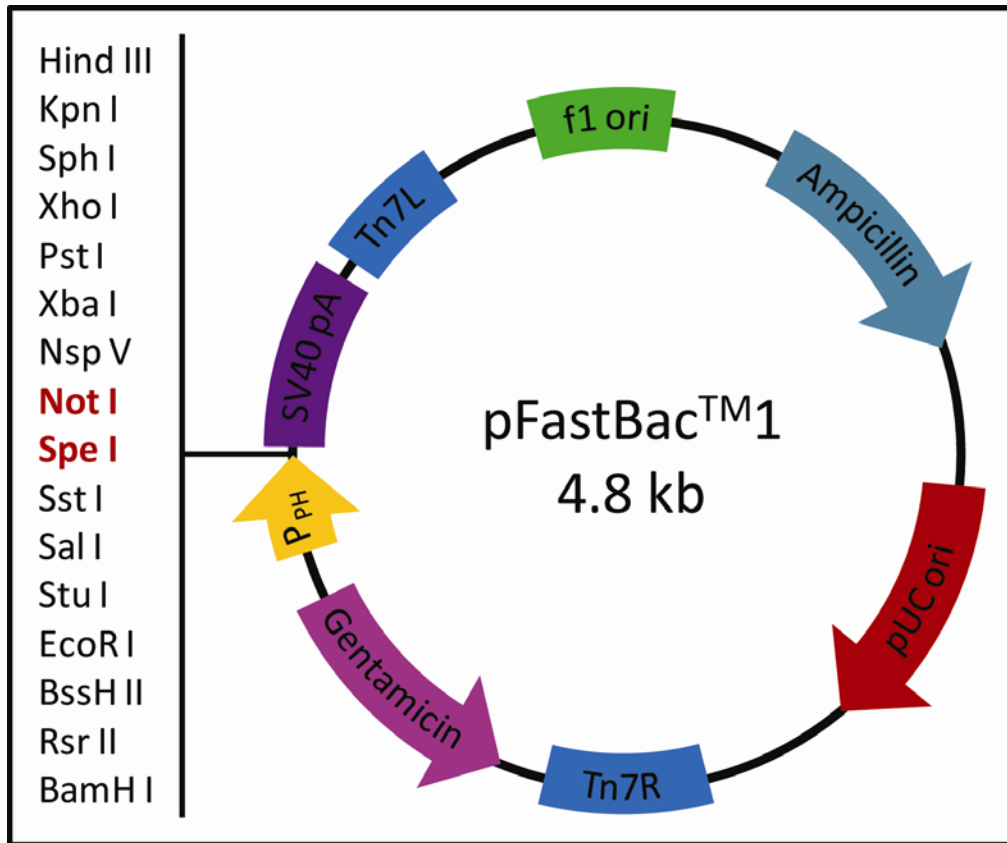
## 1. Materials

### 1.1. Reagents and other Materials

Unless stated otherwise chemicals were purchased from BioMol (Hamburg), Biorad (Munich), Braun (Melsungen), Fluka (Buchs, Swiss), Invitrogen (Karlsruhe), Merck (Darmstadt), Millipore (Munich), PeqLab (Erlangen), Roche (Mannheim), Roth (Karlsruhe), Serva (Heidelberg) or Sigma-Aldrich (St. Louis, U.S.A.) and were of "p.a." quality. Other materials were mainly purchased at Greiner (Munich), Nunc (Wiesbaden), Qiagen (Hilden), Peske (Karlsruhe) and Sarstedt (Nümbrecht).

### 1.2. Plasmids and Vectors

The full-length DNA sequences of KLP11 and KLP20 cloned into the pDest8 vector (Invitrogen) by Prof. Jonathan Scholey (University of California, Davis). All further *C. elegans* kinesin constructs used in this work were derived from these sequences with the help of either primers or by synthesis. Full-length and Flag-tagged KLP11-EE and KLP20-EE constructs were synthesized by Sloning (Puchheim, Germany). All constructs were cloned into pFastBac1<sup>TM</sup> (Invitrogen) plasmid (Figure 7).



**Figure 7. Map of pFastBac1™ vector.** All constructs were cloned into the multiple cloning site (MCS) via NotI and SpeI restriction sites (red). This allowed to integrate genes of interest under the control of the strong polyhedrin promoter (orange), ensuring overexpression of the target protein. Other characteristics of this plasmid were gentamicin and ampicillin resistance for selection, the translocation sites Tn7L and Tn7R to translocate the target gene into the bacmid and f1 and pUC origins for replication.

### 1.3. Oligonucleotides (Primers)

Oligonucleotides for PCR and sequencing were designed manually and purchased from Biomers (Ulm). The primers used in this study are shown in Table I and II.

#### 1.3.1. Cloning primers

**Table I. Cloning primers used in this study**

| Primer                                   | Primer sequence   |
|--|---|
| KLP11_FL_pFastBac1_SpeI/NotI_C-Term Flag |   |
| 3_FL_KLP11_Fw (#26)                      | 5'-aggactagtagtggtggaataatga aaaaatcttcaaa<br>acaggagactgt caaagtaattgtgagatgtcg-3' |
| 2_FL_KLP11Rev                            | 5'-tatgcggccgctcacttgcgtcat cgtcctttagtcg<br>ccgccattctg gcttcttctcatgaaccg-3'      |

# Materials and methods

| KLP20_FL_pFastBac1_SpeI/NotI_2_C-Term Flag      |   |
|---|---|
| 4_FL_KLP20_Fw                                   | 5'-aggactagtagtggaaggtgctgaaa<br>aagtgaagtagtggtacgatgtcg tcc-3'                    |
| 4_FL_KLP20_Rev2                                 | 5'-tatgcggccgctcacttgcgtcat cgtcctttagtcgccgc<br>ctgtgag caattgtttagtcg-3'          |
| KLP-20 head+KLP-11 tail_C-Term Flag (Chimera 1) |   |
| 4_FL_KLP20_Fw                                   | 5'-gaattccaagaagaaattgaaatgc tccg-3'  |
| 2_FL_KLP11Rev                                   | 5'-cggagcatttcaatttcttcttga attc<br>cctgagctgagcatcc-3'                             |
| KLP-11 head+KLP-20 tail_C-Term Flag (Chimera 2) |   |
| 2_FL_KLP11_Fw                                   | 5'-aggactagtagtgaataatcttcaa aacagg<br>agactgtcaaagtaattgt gagatgtcg -3'            |
| 4_FL_KLP20Rev2                                  | 5'-tatgcggccgctcacttgcgtcat cgtcctttag<br>tcgccgcctgtgag caattgtttagtcg -3'         |
| KLP11_Mono_pFastBac1_SpeI/NotI_Flag             |   |
| 3_FL_KLP11_Fw (#26)                             | 5'-aggactagtagtggtgaaataatgaaaaatcttcaaa<br>acaggagactgt caaagtaattgtgagatgtcg-3'   |
| 2_KLP11_Mono_Rev                                | 5'-gcgcggccgctcacttgcgtcatc gtccttgt<br>agtcgccccaatttct tcttgaattctcgc-3'          |
| KLP20_Mono_pFastBac1_SpeI/NotI_Flag             |   |
| 4_FL_KLP20_Fw                                   | 5'-aggactagtagtggaaggtgctgaaa<br>aagtgaagtagtggtacgatgtcg tcc-3'                    |
| 4_Mono_KLP-20_Rev                               | 5'-gcgcggccgctcacttgcgtcatcgtcctttagtcg<br>ccgccaatttcc agctgaaacttctgagc-3'        |
| KLP11_GCIN4_2xGS_2xSfGFP_Flag                   |   |
| 3_FL_KLP11_Fw (#26)                             | 5'-aggactagtagtggtgaaataatga aaaaatcttcaaaa<br>caggagactgt caaagtaattgtgagatgtcg-3' |
| Apal_KLP11_GCIN4_2xGS_Rev                       | 5'-tatgggcccagagccagagccaatttc<br>ttcttgaattctcgc-3'                                |
| KLP11_GCIN4_8xGS_2xSfGFP_Flag                   |   |

|                     |  |
|---------------------|--|
| 3_FL_KLP11_Fw (#26) | 5'-aggactagtatggtggaaataatgaaaaatcttcaa<br>aacaggagactgt caaagtaattgtgagatgtcg-3'          |
| KLP11_8X GS_Apa_Rev | 5'-tatgggcccagagccagagccagagccagagccagagc<br>cagagccagagc cagagccaatttcttcttgaattctcgag-3' |

### 1.3.2. Sequencing primers

**Table II. Sequencing primers used in this study**

| Primer              | Primer sequence                      |
|---------------------|--------------------------------------|
| KLP11 full-length   |                                      |
| KLP-11 #1           | 5'-gagctagctatttgaaatttatca gg-3'    |
| KLP-11 #2           | 5'-ggatgcgaaatctgccatattcct tatcg-3' |
| KLP-11 #3           | 5'-cgtaggatctgaagaagatggaagg-3'      |
| KLP-11 #4           | 5'-cgggtgtctttacacgatcatctggt gcc-3' |
| KLP20 full-length   |                                      |
| KLP-20 #1           | 5'-ggaatctggagattaaggaaagacc gg-3'   |
| KLP-20 #2           | 5'-ccacgctgagatacgcaaactgtgc g-3'    |
| KLP-20 #3           | 5'-gcaatgagctgaaggatgctcgagc gg-3'   |
| pFastBac1           |                                      |
| Polyhedrin Promoter | 5'-cctataaatattccggattattcat accg-3' |
| P10 Promoter        | 5'-cggacctttaattcaaccc-3'            |
| M13Fw               | 5'-gttttcccagtcacgac-3'              |
| M13Rev              | 5'-caggaaacagctatgac-3'              |



## 1.4. Bacterial Strains

*Escherichia coli* (*E. coli*) strain XL1-blue (Stratagene, Amsterdam) was used for plasmid amplification. MAX Efficiency<sup>®</sup> DH10Bac<sup>™</sup> competent *E. coli* cells (Invitrogen, Karlsruhe) were used for bacmid generation.

## 1.5. Media and Cultivation of *E. coli*

*E. coli* cells were grown according to standard methods (Sambrook *et al.* 1989 [124]) on agar plates or shaking at 240 rpm at 37°C.

|                            |  |
|----------------------------|--|
| S.O.C medium:              | 2% Tryptone, 0.5% yeast extract, 10 mM NaCl, 2.5 mM KCl, 10 mM MgCl <sub>2</sub> , 2% 1 M Glucose  |
| LB-ampicillin medium/agar: | 1% Tryptone, 0.5% yeast extract, 0.5% NaCl, 100 µg/ml Ampicillin, (1.5 % agar)   |
| Bluo-Gal LB:               | 1% Tryptone, 0.5% yeast extract, 1% NaCl, 50 µl/ml kanamycin, 7 µg/ml gentamycin, 10 µg/ml tetracycline, 100 µg/ml Bluo-Gal, 40 µg/ml IPTG |
| DH10 selection medium:     | LB, 50 µl/ml kanamycin, 7 µg/ml gentamycin, 10 µg/ml tetracycline  |

## 1.6. Antibodies and peptides

Antibodies were mainly used for purification of specific tagged proteins. Others were used for testing the labeling quality of microtubules with fluorophores or for single molecule assays. FLAG peptides were used for purification of Flag tagged proteins. The antibodies and peptides used in this study are shown in Table III.

**Table III. Antibodies used in this study**

| Antibody  | Company                           |
|---|-----------------------------------|
| Anti-FLAG <sup>®</sup> M2 affinity gel                  | Sigma-Aldrich, St. Louis (U.S.A.) |
| Anti-FLAG <sup>®</sup> Biotinylated M5, monoclonal      | Sigma-Aldrich, St. Louis (U.S.A.) |
| Anti-FLAG <sup>®</sup> M2-Cy3 <sup>™</sup> , monoclonal | Sigma-Aldrich, St. Louis (U.S.A.) |
| Anti-β Tubulin-Cy3 <sup>™</sup> , monoclonal            | Sigma-Aldrich, St. Louis (U.S.A.) |
| Biotinylated anti GFP                                   | Vector, CA (U.S.A.)               |
| FLAG <sup>®</sup> peptides                              | Sigma-Aldrich, St. Louis (U.S.A.) |

## 2. Methods

### 2.1. Molecular biology methods

#### 2.1.1. Agarose gel electrophoresis

DNA fragment separation according to their size was performed by electrophoresis in 1% agarose gels in TAE buffer. To avoid contamination with substances inhibiting a ligation, high purity agarose was used for preparative gels. To visualize the acquired DNA fragments on the gel, 1% ethidium bromide (10mg/ml) was added to the liquid agarose. The DNA samples were mixed with 1/5 volume of 6 x DNA loading dye before loading. Electrophoresis was done at 90 mV for 20 to 60 minutes. DNA bands were detected by UV illumination and documented using the Eagle Eye II CCD camera system (Stratagene, Heidelberg). A standard 1 kb DNA ladder was always loaded on the gel, to determine correct DNA bands.

|                      |   |
|----------------------|---|
| 50 x TAE:            | 2 M Tris, 0.57% acetic acid, 50 mM EDTA, pH 8.0             |
| 6 x DNA loading dye: | 30% glycerol, 0.25% bromphenol blue, 0.25% xylene<br>cyanol |

#### 2.1.2. DNA isolation from agarose gels

DNA bands of interest were cut of the stained high purity agarose gel with a scalpel and transferred to a sterile Eppendorf vial. After weighing the extraction of DNA fragments was performed with the Qiaquick<sup>®</sup> Gel Extraction kit (Qiagen) according to the manufacturer's protocol. Elution of DNA was done in 30 to 50 µl Qiagen elution buffer, depending on the intensity of observed DNA bands on the agarose gels.

#### 2.1.3. Determination of DNA concentration

DNA concentration was determined spectrophotometrically by measuring the extinction at a wavelength ( $\lambda$ ) 260nm ( $E_{260}$ ) of the 1:100 diluted sample (in (DEPC)-water) after calibration of the photometer with a buffer control. The concentration of the initial sample was calculated by simply multiplying the determined extinction by five. An  $E_{260}$  of 1.0 was corresponding to 50 µg/µl DNA as referred by Sambrook *et al.* 1989 [124].

### **2.1.4. Purification of plasmid DNA**

Plasmid DNA was prepared using the Qiagen-Plasmid-Kit from overnight shaking cultures inoculated with single colonies selected from the transformation reaction. For small scale preparations (3 ml), the cells were pelleted at 2,500 x g for 7 minutes at 4°C (Rotanta 460R swinging bucket centrifuge, Hettich) followed by plasmid DNA isolation using the QIAprep<sup>®</sup> Miniprep kit (Qiagen) according to the manufacturer's protocol. DNA was eluted in 50 µl Qiagen Elution Buffer and stored at -20°C.

### **2.1.5. DNA cleavage with restriction enzymes**

Plasmid DNA or PCR products destined for analytical restriction were incubated with max. 1 µl of enzyme in a 10 µl reaction mix according to the manufacturer's manual (New England Biolabs, NEB). A typical digestion included 2 to 5 µl of mini-prep DNA (0.1 to 0.5 µg/µl) and was performed at the temperature optimum of the respective restriction enzyme. This guaranteed about 1 to 5 U Enzyme per 1 µg DNA.

For plasmid DNA or PCR products destined for preparative restriction, about 5 to 10 µg of DNA were incubated with about 5 U/µg DNA of each enzyme for 1 h at the temperature optimum of respective enzymes. Heat inactivation of restriction enzymes was carried out by incubation at either 65°C or 85°C for 20 min depending on the used enzymes. All digested samples were analysed on agarose gels.

### **2.1.6. Dephosphorylation of 5' –ends of DNA**

To circumvent the probability of religation of linearized vector DNA, the restricted DNA is dephosphorylated at 5' –ends by incubation with Antarctic Phosphatase (AP, NEB). For this purpose, about 1 µg of cut DNA was incubated with 5 U of AP in AP-Buffer (10 x) for 1 h at 37°C. The AP was subsequently heat inactivated at 65°C for 20 min.

### **2.1.7. Ligation of DNA fragments**

Restricted and purified vector and DNA fragments ligation was mediated by T4 DNA Ligase (NEB, Frankfurt) in an ATP containing ligase buffer provided by the manufacturer. Typically, the ligation reaction contained 40 U T4 DNA Ligase and was performed by mixing vector and insert in a 1:3 or 1:5 ratio, mainly depending on the concentration of isolated DNA. Vector DNA was incubated without insert as re-ligation control. The ligation was carried out overnight at 16°C.

### 2.1.8. Transformation of chemically competent *E. coli* cells

For transformation, chemically competent *E. coli* XL1-Blue cells were slowly thawed on ice. Usually, 10 µl of DNA from ligation reactions were mixed with 200 µl of XL1-Blue competent cells and incubated on ice for 20 min. Subsequently, the mixture was placed on a 42°C heat block for 1 min to perform a heat shock. Then the reaction was cooled on ice for 2 min and was supplemented with 200 µl of S.O.C medium. After incubation for 1 hour at 37°C on a shaker, the mix was plated on LB agar plates with 100 mg/ml ampicillin and was incubated overnight at 37°C.

### 2.1.9. Identification of transformed *E.coli*

After an overnight incubation of transformed *E.coli*, 2 to 8 medium-size colonies were selected to inoculate 3 to 4 ml of LB-Amp medium per colony. Incubation was performed overnight in a shaker device at 220 rpm and 37°C. Mini-plasmid preparation was carried out after pelleting the cells at 2,500 x g for 10 min at 4°C by using the QIAprep® Miniprep kit (Qiagen) according to the manufacturer's protocol. The DNA was checked with appropriate restriction endonucleases and analyzed on agarose gels. All plasmids with the expected restriction fragments were sequenced at the Sequencing Service of the LMU (Ludwig-Maximilians-University, Munich, Germany). For this, 150 to 300 ng of purified DNA was mixed with 3.3 pmol sequencing primer in 1 x DNA elution buffer (DNA-EB). Sequencing was then carried out with the "Cycle, Clean & Run" program using BigDye v3.1.

### 2.1.10. Polymerase chain reaction (PCR)

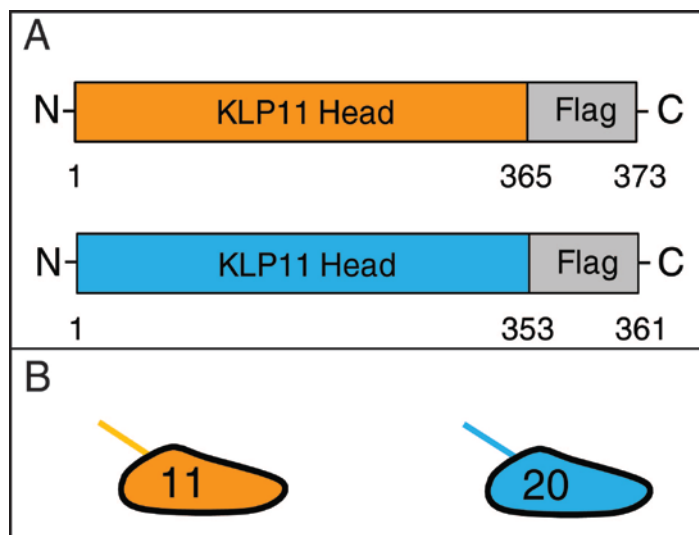
PCR reactions use thermostable DNA polymerases and an excess of specifically designed oligonucleotides to amplify parts of a known sequence from a DNA template [125]. Repeated denaturing, annealing and elongation cycles (typically 30 to 50 cycles) lead to an exponential amplification of the specific DNA fragments. The reaction mixture contained the standard reaction buffer (1 x *Pfx50*<sup>TM</sup> PCR mix) with 400 µM of each dNTP, 0.5 µM 5'-and 3'-primer, approximately 20 ng template DNA and 2.5 U high fidelity *Pfx50*<sup>TM</sup> DNA polymerase (Invitrogen) in a volume of 50 µl and was performed in a thermo block (MWG Biotech, Primus 96<sup>plus</sup>).

### 2.1.11. Generation of constructs

All constructs have been cloned by PCR on the original full-length cDNA in linearized pDest8 vector into pFastBac1™ (Invitrogen) plasmid or have been synthesized from known sequences containing full-length kinesin-2 constructs.

#### 2.1.11.1. Monomeric KLP11 and KLP 20 constructs

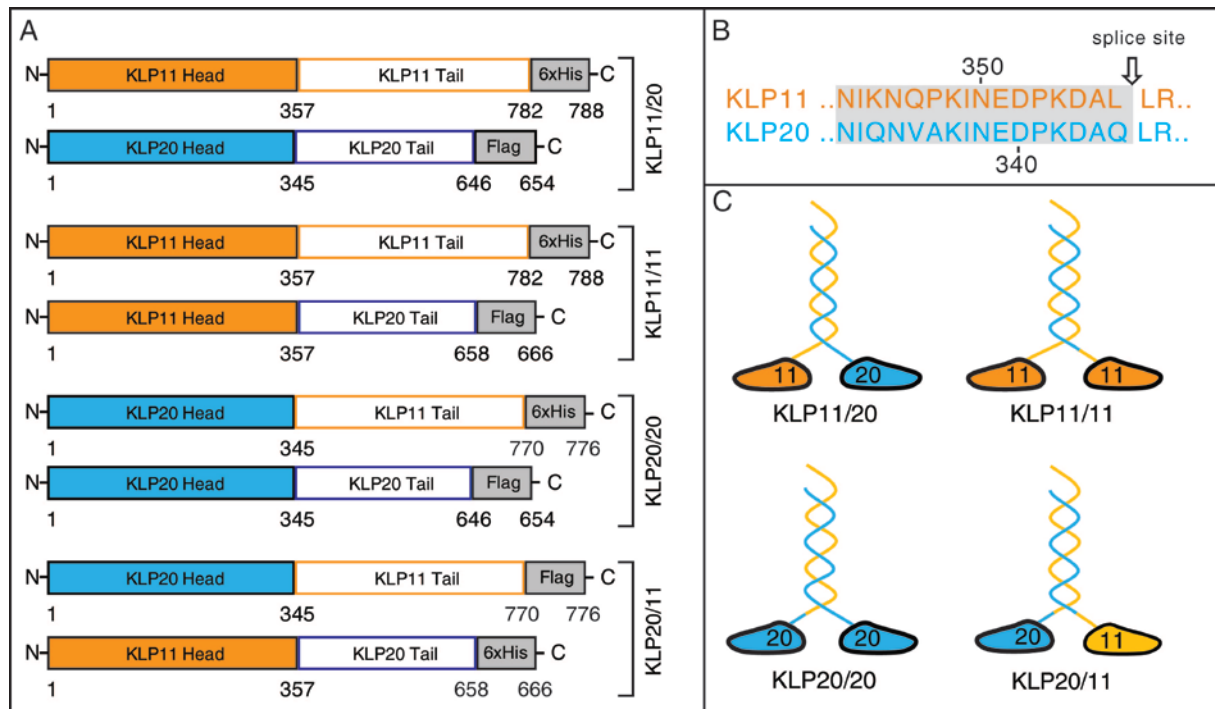
Monomeric KLP11 and KLP20 constructs consisting of just the head domains and the neck, conjugated to Flag tag (Figure 8) have been generated by PCR on the pDest™8 vector.



**Figure 8. Monomeric head domain architecture of kinesin-2.** **A)** Schematic overview of the generated KLP11 and KLP20 monomeric constructs with amino acid positions. **B)** Models, depicting the structure of monomeric motors.

#### 2.1.11.2. Full-length, wild type KLP11 and KLP20 constructs

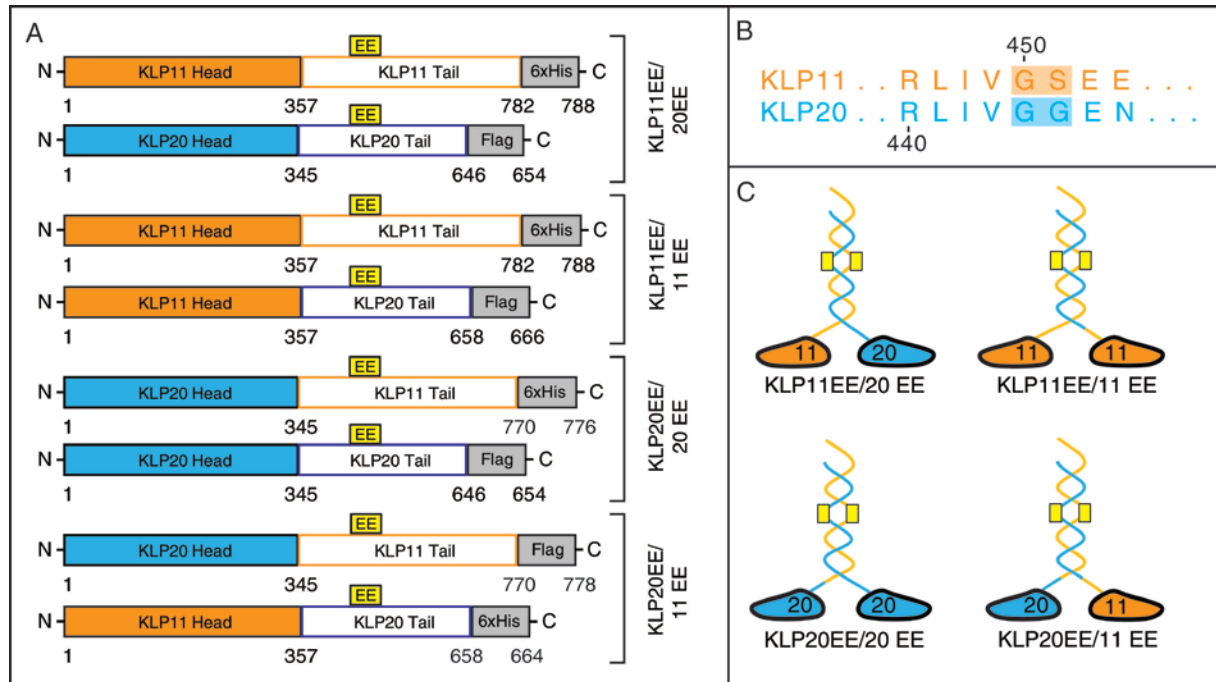
The C-terminally Flag or 6xHis tagged full-length constructs were cloned into the pFastBac1 vector (Figure 7) using specific primers (section 1.2.3). Figure 9 depicts an overview of all full-length, wild type tail constructs used in this work.



**Figure 9. Full-length, wild type tail constructs.** **A)** Overview of the generated constructs with amino acid positions and the corresponding purification tags. **B)** Chimeric constructs were generated using the splice site following the neck linker (highlighted in gray) by exchanging the tail domains. **C)** Schematics of the target kinesin-2 dimers. (Adapted from Brunnbauer *et al.*, 2010 [126])

### 2.1.11.3. Full-length ‘EE tail’ constructs

Constructs containing the G451/S452 (Glycine/Serine) mutation into the E451/E452 (Glutamic acid/Glutamic acid) for KLP11 and G444/G445 (Glycine/Glycine) mutation into E444/E445 (Glutamic acid/Glutamic acid) for KLP20 were generated by partial gene synthesis using unique restriction sites in the respective constructs. The C-terminally Flag or 6xHis tagged full-length ‘EE tail’ constructs were cloned into the pFastBac1 vector. Figure 10 depicts an overview of all full-length, ‘EE tail’ constructs used in this work.

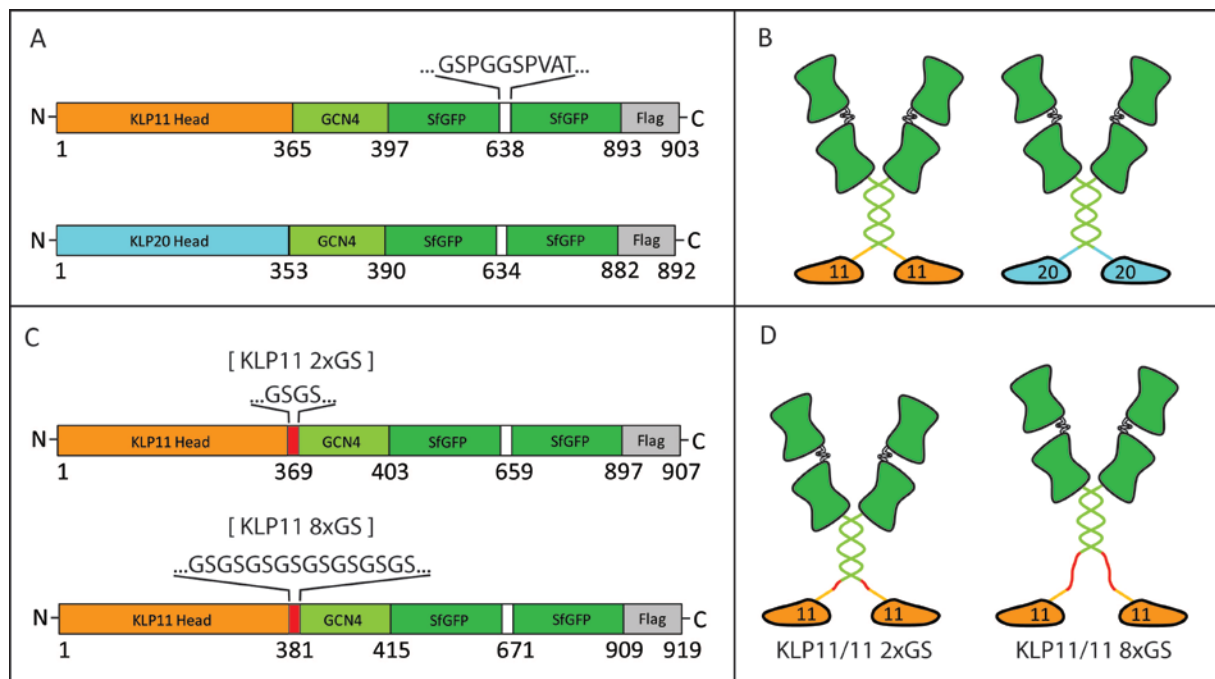


**Figure 10. Full-length, 'EE tail' constructs.** **A)** Overview of the generated constructs with amino acid positions and the corresponding purification tags. Box with EE marks introduced point mutation position of the EE amino acids (yellow). **B)** The KLP11 EE mutant was generated by point mutation at the positions 450 and 451 (light orange box, GS exchange) and the KLP20 EE mutant by point mutation at the positions 444 and 445 (light blue box, GG exchange). **C)** Schematics of the target 'EE tail' kinesin-2 dimers. (Adapted from Brunnbauer *et al.*, 2010[126])

#### 2.1.11.4. GCN4 tandem Superfolder GFP (SfGFP) constructs

To enhance the fluorescent signal in single molecule assays, we generated homodimeric constructs conjugated to four Superfolder GFP molecules. The fluorophore SfGFP was synthesized by GenScript (NJ, USA) and cloned into pFastBac1 vector containing only the head domains of desired constructs. Tandem SfGFP constructs were generated by initially cloning a SfGFP molecule with 10 amino acids in front as a gap, conjugated to an existing KLP11 GCN4 SfGFP (Ascl/NotI restriction site) or a KLP20 GCN4 SfGFP (ApaI/NotI restriction site) construct via restriction enzymes.

KLP11 constructs with elongated neck regions (GS repeats) were generated with specific primers (see section 1.2.3.1) and ligated into plasmids containing only GCN4 2xSfGFP with individual tag (ApaI/SpeI restriction site, Figure 11).



**Figure 11. Domain architecture of homodimeric GCN4 motor constructs fused to tandem SfGFP.** **A)** Overview of generated KLP11/11 and KLP20/20 constructs with amino acid positions. To guarantee correct folding of the second SfGFP protein, a flexible region of 10 amino acids were introduced, adapted from Cai *et al.*, 2007 [127] (white box). **B)** Schematics of homodimeric motors, zipped together via GCN4 (light green), conjugated to tandem Superfolder GFP (green, barrel shape). **C)** Overview of generated KLP11/11 GS (red box) constructs with amino acid positions. **D)** Schematics of homodimeric KLP11/11 GS constructs with elongated neck regions.

## 2.1.12. Baculovirus expression system

Protein overexpression was carried out using the eukaryotic Bac-to-Bac baculovirus expression system (Invitrogen). This eukaryotic expression system has the advantage, that all the protein expression and processing machinery which is necessary for a correct biological function of the protein of interest is present like in higher eukaryotes. [128]. Proteins of interest isolated from this system are close to their native forms and show correct biological function [129].

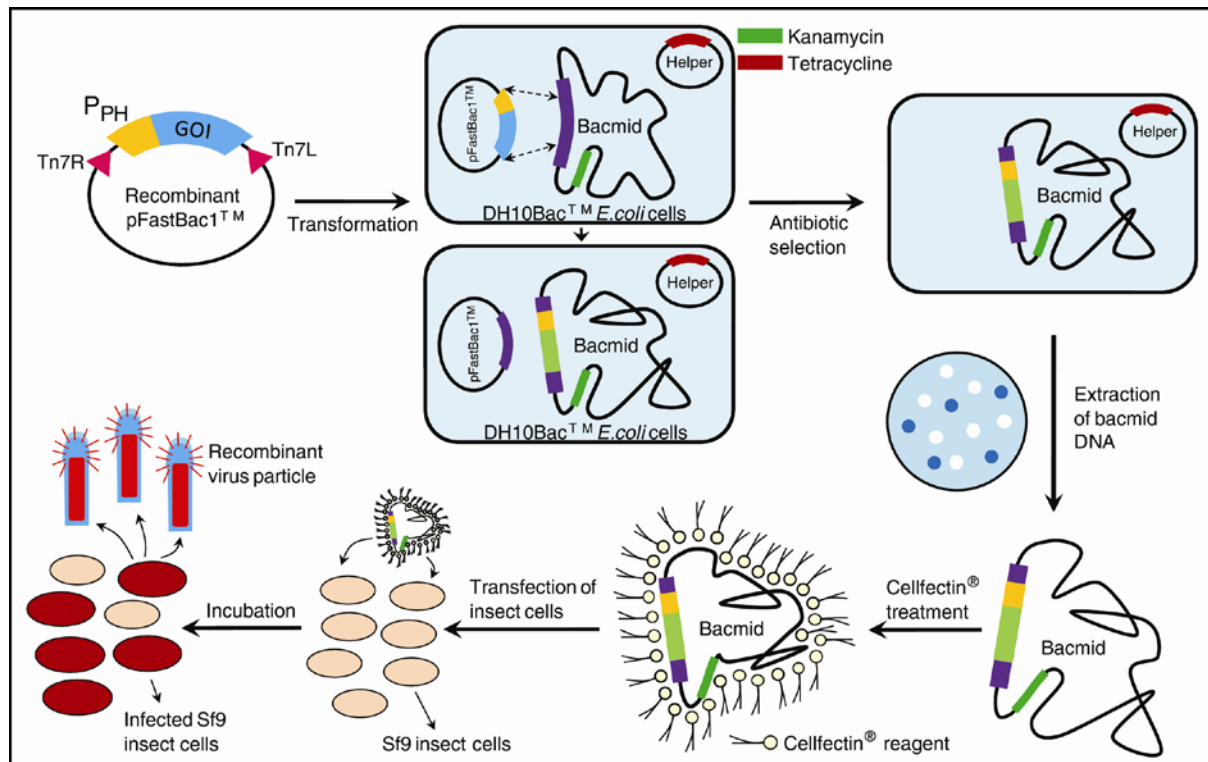
### 2.1.12.1. Generation of Baculovirus shuttle vectors (bacmids)

In order to transpose the amplified recombinant pFastBac1™ vector containing the desired construct into the baculovirus shuttle vector (bacmid), transformation into either chemically competent MAX Efficiency® DH10Bac™ *E. coli* cells by heat shock was performed. This strain contains beside a helper plasmid coding for a transposase and tetracycline resistance, the *Autographa californica nuclear polyhedrosis virus* (AcNPV) bacmid. This bacmid has a kanamycin resistance marker and a mini-attTn7 cassette, which is embedded in the *LacZα* peptide. Recombinant



bacmid generation is achieved by site-specific transposition between the mini-Tn7 element of the pFastBac1<sup>TM</sup> donor vector and the mini-attTn7 attachment site on the bacmid [130]. With successful transposition, the *LacZ $\alpha$*  gene on the bacmid is disrupted, and therefore the complementation process and functional  $\beta$ -galactosidase formation, which in turn enables for blue-white screening for successful insertion of the gene of interest (Figure 12).

For transformation, MAX Efficiency<sup>®</sup> DH10Bac<sup>TM</sup> *E. coli* cells (50  $\mu$ l) were thawed on ice and incubated with approximately 10 ng DNA for 30 min on ice. After heat shock transformation for 1 min at 42°C, the cells were cooled for 2 min on ice and supplemented with 900  $\mu$ l of S.O.C medium. The transformed cells were incubated in a shaker device at 220 rpm for 4 hours at 37°C. After incubation, 100  $\mu$ l of dilutions 1:10, 1:100, 1:1000 in S.O.C. medium were plated on Bluo-Gal LB (section 1.4) plates for blue-white selection and were incubated for 48 hours at 37°C. To exclude false positive results, white colonies were again plated on Bluo-Gal LB agar plates and incubated for another 48 hours at 37°C to regrow white colonies.



**Figure 12. Bacmid generation in DH10Bac<sup>TM</sup> *E. coli* cells and virus amplification in Sf9 cells.** Recombinant pFastBac1 plasmid containing the gene of interest (GOI) is transformed into competent DH10 MAX Efficiency<sup>®</sup> DH10Bac<sup>TM</sup> *E. coli* cells. Via site specific transposition, the gene of interest is transposed into the *lacZα* gene of the bacmid. Because the *lacZα* gene is now disrupted, blue/white selection of colonies containing the recombinant bacmid is possible. By using ampicillin, gentamycin and kanamycin as selection markers, the bacmid is amplified and extracted. After Cellfectin<sup>®</sup> treatment, Sf9 insect cells are transfected with bacmid containing the GOI. First recombinant virus generation (P0) is harvested after an incubation time of 4 to 7 days. (Adapted from BacuVance<sup>TM</sup> Baculovirus Expression System (GenScript) and Zimmermann D., Involvement of Myosin V in organelle transport and its unconventional interaction with microtubules, 2012)

#### 2.1.12.2. Isolation of bacmid DNA

Single white growing colonies were picked and inoculated in 6 ml DH10 selection medium supplemented with gentamicin, kanamycin and tetracycline and incubated overnight in a shaker device at 220 rpm and 37°C. After pelleting the cells in a Rotanta 460R swinging bucket centrifuge (Hettich) at 2,500 x g for 15 minutes at 4°C, plasmid isolation and purification was performed. According to the Qiagen<sup>®</sup> Miniprep kit, solutions P1, P2 and P3 were used, while all centrifugation steps were performed at 16,000 x g at room temperature in a table centrifuge. After resuspending in 200 µl of P1 buffer, cells were lysed in 200 µl of P2 lysis buffer and incubated for 5 min at room temperature. This was followed by 200 µl of P3 buffer and incubation for 10 min on ice and a centrifugation step of 1 min. The supernatant containing the plasmid DNA was transferred into a clean tube and mixed with 500 µl isopropanol and

incubated for 30 min on ice. The isopropanol precipitated DNA was pelleted by centrifugation for 30 min. After removing the supernatant, the pellet was washed in 350  $\mu$ l ethanol (70%) and centrifuged again for 1 min. The supernatant was discarded and the pellet was completely air-dried and kept for 10 min at 37°C for a better dissolving. The pellet was subsequently dissolved in 40 to 50  $\mu$ l of double-distilled water and stored at -20°C.

### **2.1.12.3. Transfection of Sf9 insect cells with recombinant bacmid**

For every construct to be transfected in Sf9 cells, 2 ml of freshly diluted Sf9 cells at a density of  $0.5 \times 10^6$  cells/ml were pipetted into one well of a 6-well tissue culture plate and incubated light protected for 20 to 30 min at 28°C. Here the cells had the opportunity to become adherent to the surface of the culture plate. Meanwhile, 5 to 15  $\mu$ l bacmid DNA was covered with 5  $\mu$ l of the cationic lipid Cellfectin® transfection reagent (Invitrogen) (Figure12) into 200  $\mu$ l Sf-900 II serum free medium (SFM). Cellfectin® is a 1:1.5 (m/m) liposome formulation of the cationic lipid N, N<sup>I</sup>, N<sup>II</sup>, N<sup>III</sup>-tetramethyl-N, N<sup>I</sup>, N<sup>II</sup>, N<sup>III</sup>-tetrapalmitylspermine (TM-TPS) and dioleoyl phosphatidylethanolamine (DOPE) in membrane-filtered water, which is able of coating the DNA and enabling transfection. The mixture was incubated for 20 to 30 minutes at 28°C, and 800  $\mu$ l of SFM was added. After removing the medium from the Sf9 cells, a double washing step with each 2 ml of SFM was performed. As next, the mixture of DNA and Cellfectin® was given to adherent Sf9 cells and the tissue culture plate was sealed and incubated for 5 hours at 28°C. After that, the mixture was removed and cells were covered with 3 ml of supplemented fresh Sf-900 II SFM medium (10% serum and 1% gentamicin, 10mg/ml). Depending on the infection degree of the baculoviruses, the cells were incubated 3 to 4 days at 28°C. A clear indication for infection were cells with increased cell size or detached cells, which were formerly adherent leading to holes in the cell lawn.

The initial virus generation (P0) was harvested by taking up the supernatant with a syringe and pressing it through a micro filter with 0.22  $\mu$ m pore size.

### **2.1.12.4. Amplification of baculoviruses**

The low titer P0 generation of viruses was used as stock for amplification of larger volumes of uninfected cells to get viruses with high titers. Typically, 20 to 30 ml of  $1 \times 10^6$  cells/ml were inoculated with 5% vol. of P0 virus and incubated, depending on infection degree light protected on cell plates for 4 to 7 days at 28°C. The second virus generation, P1 was used as stock for both, cell plate and shaking culture (V generation of viruses) amplification of viruses. Here, usually 60 to 100 ml of  $1 \times 10^6$  cells/ml were inoculated with 10% vol. of P1 virus and treated like P1 virus amplification for the case of plate amplification, whereas the shaking culture was kept in a shaking device for 4 to 6 days at 110 rpm and 28°C. The density of the shaking culture during infection was kept at  $1 \times 10^6$  cells/ml while the volume was kept constant (If needed, Sf9 cells were inoculated with additional virus). The so generated P2 and V1 virus generations were stored light protected at 4°C.

### **2.1.12.5. Protein expression in Sf9 cells**

For protein expression, all proteins were over-expressed in Sf9 insect cells either from plates or suspension culture. 50 to 1000 ml freshly diluted Sf9 cells to a density of  $2 \times 10^6$  cells/ml were infected with usually 10 to 20% vol. of recombinant virus encoding for the gene(s) of interest. The infected cells were kept for 48 to 72 hours in a shaker device at 110 rpm and 28°C or in an incubator at 28°C. Harvesting was achieved at 2,500 x g for 15 minutes at 4°C (Rotanta 460R swinging bucket centrifuge, Hettich).

## **2.2. Biochemical methods**

### **2.2.1. SDS-polyacryl amide gel electrophoresis (SDS-Page)**

SDS-Page is a method for separation of protein bands according to their size, under denaturing conditions [131]. Depending on amount and expected size of proteins, typically 8 to 12% polyacryl amide gels were used. Usually, probes were mixed with 1/5 volume of SDS 6 x sample buffer and boiled at 95°C for 2 min before loaded onto the gel. A protein standard (unstained High Molecular Weight ladder) was always loaded on the gel. The gels were run for 40 to 60 minutes in 1 x TAE buffer at 20 to 60 mA with 240 V limit. Gels were stained for 30 to 60 min in Coomassie Blue

solution, rinsed with ddH<sub>2</sub>O and destained with 10% acetic acid. Gels were photographed with a CCD camera (Eagle Eye System, Stratagene) or scanned (Epson 1200 Photo) for documentation.

|                                 |  |
|---------------------------------|--|
| PAA solution:                   | 30% acrylamide, 0.8% bisacrylamide (Biorad)  |
| Running buffer:                 | 25 mM Tris-HCl, 0.1% SDS, 192 mM glycine   |
| 10 x buffer for stacking gel:   | 500 mM Tris-HCl, pH 6.8, 0.4% SDS  |
| 10 x buffer for separating gel: | 1.5 M Tris-HCl, pH 8.8, 0.4% SDS   |
| 6 x Laemmli sample buffer:      | 300 mM Tris-HCl, pH 6.8, 15 mM EDTA, 12% SDS,<br>30% glycerol, 15% β-mercaptoethanol, 0.06%<br>bromphenol blue |
| Coomassie staining solution:    | 10% acetic acid, 50% methanol, 0.25 % Coomassie<br>Brilliant Blue R250 (Sigma)                                 |

### 2.2.2. Determination of protein concentration

The protein concentration was determined either with Bradford reagent [132] or using Bovine Serum Albumin (BSA)-standard loaded on SDS-PAGE gels.

With Bradford, for each measurement, a standard curve was measured in parallel using BSA as reference. The absorbion at E<sub>630</sub> was measured with a microplate reader (Dynatech MR 5000) and the protein concentration was determined using BSA standard as reference.

With SDS-PAGE gels, usually 2 to 5 different known BSA concentrations were loaded next to the proteins of interest and the gel was prepared for imaging (section 2.2.1). The image of the gel was corrected as desired and the intensity of the BSA protein bands was analyzed with ImageQuant imaging software. After determining the intensities of the protein bands of interest and relating them to the values obtained from the BSA standards, the absolute concentration was transferred into the molar concentration of the protein using following equation:

$$c_{\text{molar}} (\text{Mol}) = c_{\text{absolute}} (\text{mg/ml}) / \text{MW (kDa)}$$

#### Equation 1

### 2.2.3. Determination of tubulin concentration

The concentration of microtubule suspensions was calculated after denaturation in guanidium-HCl by measuring the  $E_{280}$  in the photometer. 10  $\mu$ l of a 1/10 and a 1/5 dilution of microtubules in the used buffer system was mixed with 90  $\mu$ l of 6,6 M guanidium-HCl. After mixing, the absorbtion at  $E_{280}$  was measured against a blank containing 10  $\mu$ l buffer and 90  $\mu$ l guanidium-HCl. Assuming a molecular weight of 100000 g/mol for a tubulin dimer, the microtubule concentration was determined with the following formula [133]:

$$(E_{280} / 1.03) * \text{final dilution of MT (100 or 50)} = x \mu\text{M MT}$$

### Equation 2

### 2.2.4. Purification of porcine brain tubulin

For tubulin purification, about 700 g pig brain halves were obtained from the local slaughterhouse and put on ice immediately. After removing blood vessels and connective tissue, about 350 g of brain tissue were mixed with Buffer A and homogenized in a pre-cooled warring blender (Braun, Germany) and centrifuged at 26,000 x g for 70 min at 4°C (J2-21M/E centrifuge and JA-14 Rotor, Beckman-Coulter). The supernatant was gently mixed with pre-warmed 25% glycerol (final concentration v/v, Roth) and 2 mM  $\text{Na}_2\text{ATP}$ . To polymerize the tubulin, this mixture was incubated in a constant shaking water bath for 30 min at 35°C. The microtubules were sedimented by centrifugation at 200,000 x g for 45 min at 32°C (pre-warmed L8-70M Ultracentrifuge and 45Ti Rotor, Beckman-Coulter). The pellets were resuspended in 5 ml Buffer C and homogenized on ice in dounce homogenizers (Wheaton) for 25 min. depolymerization of microtubules was accelerated by frequent homogenization in-between. The homogenate was centrifuged at 150,000 x g for 30 min at 4°C (pre-cooled L8-70M Ultra-centrifuge and 42Ti Rotor, Beckman-Coulter). The supernatant was allowed again to polymerize by adding 2 mM  $\text{Na}_2\text{ATP}$  and incubation at 35°C for 30 min. This was followed again by a sedimentation step at 125,000 x g for 30 min at 35°C (pre-warmed L8-70M Ultracentrifuge and 42.1Ti Rotor, Beckman-Coulter). The tubulin pellets were dissolved and homogenized on ice for 25 min in Buffer B (high ionic strength) to a final volume of 50 ml. This step was helpful to remove traces of microtubule-associated proteins (MAPs). The

homogenate was then centrifuged again at 150,000 x g for 30 min at 4°C (pre-cooled L8-70M Ultracentrifuge and 42.1Ti Rotor, Beckman-Coulter). The supernatant was inoculated with 10% DMSO and 2 mM Na<sub>2</sub>ATP and polymerized at 35°C for 30 min. The microtubules were pelleted once more at 125,000 x g for 60 min at 35°C (pre-warmed L8-70M Ultracentrifuge and 42.1Ti Rotor, Beckman-Coulter) and resuspended in 5 ml Buffer D. Homogenization was again performed on ice for 30 min, followed by a centrifugation at 135,000 x g for 30 min at 4°C (pre-cooled L8-70M Ultracentrifuge and 42.1Ti Rotor, Beckman-Coulter), in order to remove precipitates. To remove last traces of remaining MAPs, the supernatant was loaded on a gravity-flow phosphocellulose P11 material filled column, pre-equilibrated with 100 ml Buffer D. Tubulin was collected dropwise in Buffer D, while protein level was checked in parallel with Bradford reagent. The eluted tubulin was supplemented with 0.1 mM GTP and was shock-frozen in aliquots in liquid nitrogen. Tubulin was stored at -70°C.

Buffer A: 0.1 M PIPES-NaOH, 2 mM EGTA, 1 mM MgSO<sub>4</sub>, 1 mM DTT, 100 µM ATP

Buffer B: 0.5 M PIPES-NaOH, 1 mM EGTA, 1 mM MgSO<sub>4</sub>, 1 mM DTT, 1 mM ATP

Buffer C: 0.1 M PIPES-NaOH, 1 mM EGTA, 1 mM MgSO<sub>4</sub>, 1 mM DTT, 1 mM ATP

Buffer D: 0.1 M PIPES-NaOH, 1 mM EGTA, 1 mM MgSO<sub>4</sub>, 1 mM DTT, 50 µM ATP

All buffers were adjusted to pH 6.9 at 4°C.

### **2.2.5. Tubulin polymerization**

Tubulin polymerization to microtubules occur above a critical concentration and a critical temperature under GTP consumption [134]. Microtubules were polymerized in varying amounts with the help of taxol (4 mM), a microtubule stabilizing agent. Taxol binds to the β-subunit of tubulin heterodimers and prevents them from dissociating (Xiao et al 2006, PNAS). Because aggregated tubulin disturbs polymerisation of tubulin monomers to microtubules and disables the accurate determination of microtubule concentration as needed for ATPase measurement, it had to be removed. This was achieved via a clear spin before further steps were performed at 200,000 x g for 5 min at 4°C (Optima-TL ultra-centrifuge and TLA120 Rotor, Beckman-Coulter).

#### **2.2.5.1. Polymerization of tubulin for motility assays**

To obtain fluorescently labeled microtubules for microscopic assays, fluorescent Atto488 (Atto-Tec, Siegen, Germany)-labeled or Cy3 (Sigma)-labeled tubulin was mixed in a ratio of 1:15 with unlabeled tubulin prior to clear spin.

Tubulin destined for single molecule assays, where microtubules function as cytoskeletal tracks, were additionally to the fluorescent tubulin, supplemented with biotinylated tubulin in a molar ratio of 1:15.

Polymerization was induced by the addition of 1 mM GTP to the mixture and incubation for at least 30 min at 37°C. The polymerized microtubule filaments were stabilized by adding 20 µM Taxol to the reaction and incubating over night at 37°C.

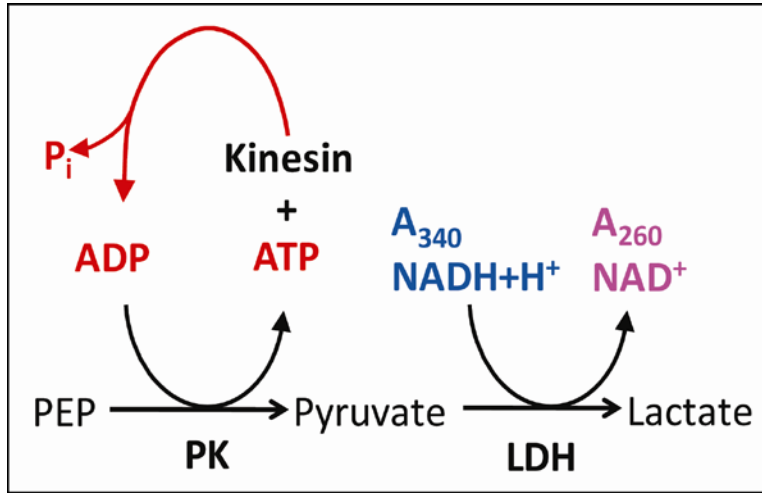
#### **2.2.5.2. Polymerization of tubulin for ATPase activity assays**

For ATPase assays, after clear spin and initial polymerization of tubulin to microtubules (same conditions as in section 2.2.5.1), one additional centrifugation step at 200,000 x g for 15 min at 30°C (Optima-TL ultra-centrifuge and TLA120 Rotor, Beckman-Coulter) was performed through a sucrose cushion (40% sucrose in 1x12A25 Buffer and 20 µM taxol). With this step unpolymerized tubulin was removed from polymerized microtubules. The pelleted microtubules were washed twice with 12A25 Buffer containing 20 µM taxol and then resuspended in this buffer.

#### **2.2.6. Microtubule stimulated ATPase assay**

The microtubule-stimulated steady state ATP turnover was measured in a coupled enzymatic assay. In this assay, ATP hydrolysis is linked to the oxidation of NADH to NAD<sup>+</sup> by the enzymes lactate dehydrogenase (LDH) and pyruvate kinase (PK) [133] (Figure 13). PK requires phosphoenolpyruvate (PEP) as co-substrate and converts ADP to ATP, thus guaranteeing a constant ATP concentration during the reaction.





**Figure 13. Coupled enzymatic steady-state ATPase assay.** The motor hydrolyzes ATP to ADP and inorganic phosphate. The regenerating system (PK) recycles the consumed ADP back into ATP, keeping up a constant ATP level in the system. For each ATP molecule regenerated, one NADH molecule is oxidized by lactate-dehydrogenase (LDH) to NAD<sup>+</sup>. By measuring the absorbance decrease at 340 nm, the ATP consumption can be calculated.

The NADH oxidation can be observed in the photometer by its decrease in extinction at 340 nm. Consequently, the oxidation of one NADH molecule is coupled to hydrolysis of one ATP molecule by a motor protein. ATPase activities of motor proteins were analyzed at different microtubule or ATP concentrations. The decrease of NADH concentration over time was followed photometrically and determined applying the law of Lambert-Beer:

$$\Delta E/t = (\epsilon \cdot \Delta c(\text{NADH}) \cdot d) / t$$

**Equation 3** (Haid *et al.* 1975 [135])

with  $\Delta E/t$  being the output value of extinction over time,  $\epsilon$  being the extinction coefficient of NADH at 340 nm ( $\epsilon_{\text{NADH at 340 nm}} = 6.22 \text{ Mol}^{-1} \cdot \text{cm}^{-1}$ ) and  $d$  being the diameter of the well.  $K_M$  and  $k_{\text{cat}}$  were determined by change of absorbance-decay over 30 min and plotted against microtubule concentration ( $K_M$  for MT) or ATP concentration ( $K_M$  for ATP) and the values were fitted to a hyperbolic function, describing Michaelis-Menten kinetics.  $K_M$  represents the half maximal activation constant, whereas the catalytic constant  $k_{\text{cat}}$  expresses the maximal number of ATP that is hydrolyzed per kinesin head per time. It was calculated as follows:

$$k_{\text{cat}} = (\Delta c(\text{ATP}) / \Delta t) / c(\text{kinesin})$$

**Equation 4**

The assay was performed in 12A25 buffer at 27°C over 30 min with a spectrophotometer (Bio Tek, Bad Friedrichshall, Germany). The reaction volume was

50  $\mu$ l and consisting of 37  $\mu$ l microtubule dilution in 12A25 buffer with 20  $\mu$ M Taxol as described above, 10  $\mu$ l protein dilution with desired protein concentration (7.7  $\mu$ l) and regeneration system (2.3  $\mu$ l), and also 3  $\mu$ l of 15 mM Mg-ATP mixed in this order. Because the reaction starts with ATP, it was crucial to add it just before the assay was started. The measurement was performed in 96-well plates (Greiner) with an area size  $A = 0.15 \text{ cm}^2/\text{well}$ .

|                          |   |
|--------------------------|---|
| 12A25 buffer:            | 12 mM Aces-KOH, 25 mM KAc, 2 mM MgAc, 0.5 mM EGTA, pH 6.8                 |
| ATP regeneration system: | 1.5 mM NADH in 100 mM HEPES, 3 mM PEP in 12A25, 1.6 U/ml PK, 2.2 U/ml LDH |
| Taxol:                   | 4 mM in DMSO  |
| Mg-ATP:                  | 100 mM ATP in H <sub>2</sub> O, 100 mM MgCl <sub>2</sub>                  |

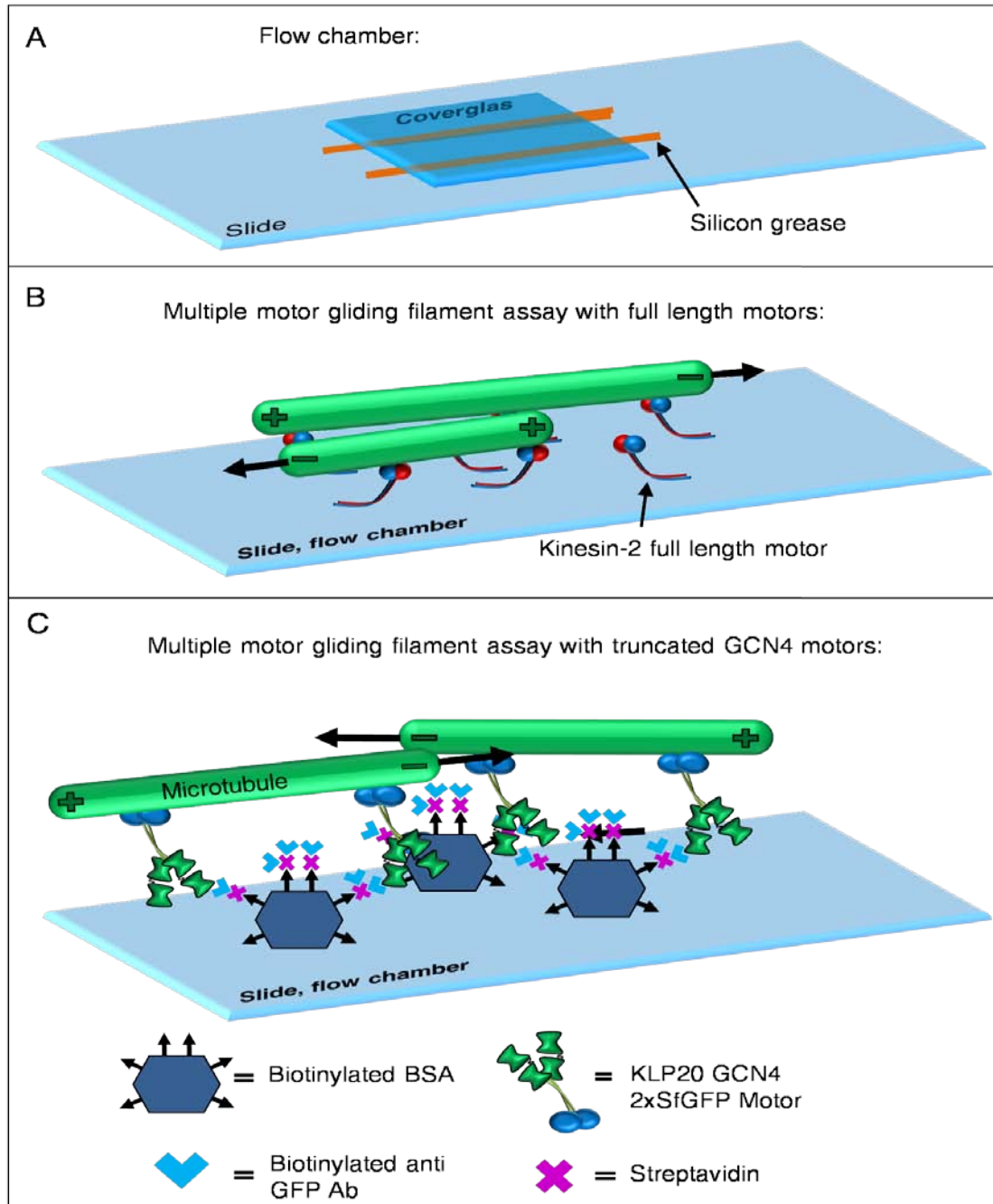
### 2.2.7. Multiple motor gliding filament assay

Kinesin motors bind non-specifically via their tail domains on microscope coverslips while the motor domains stay flexible (Figure 14). Gliding assays were performed following standard methods [60] in BRB80 buffer. Here, the protein's maximum velocity is determined indirectly via the speed of single fluorescently labeled microtubules.

For full-length kinesin motors, a flow chamber (volume 10  $\mu$ l) was generated using silicone grease (GE Bayer, Germany) and a glass slide covered by a coverslip (Figure 14). Flow chambers were incubated with 10  $\mu$ l of protein for 4 minutes. Unbound motors were washed with 34,5  $\mu$ l of motility buffer containing Cy3-labeled microtubules [136], a oxygen scavenger system, glucose and casein. ATP was given to motility buffer prior to use. Fluorescently labeled microtubules were either followed over time by a Axiovert 200 microscope (Zeiss, Germany) and the velocity was measured using the manufacturer's software (Zeiss, Germany) or with the below described TIRF microscope.

For kinesin motors where the tail domains were removed (Figure 11), a binding to the microscope coverslips was no longer possible. In this case, the flow chamber was coated with 1 mg/ml BBSA (Sigma), 1 mg/ml streptavidin (Sigma) and biotinylated anti-GFP antibodies (Vector, CA/USA; Biozol Diagnostika Vertrieb GmbH, Eching),

with washing steps with 1 mg/ml BSA and BRB buffer in between. After this special treatment of the chamber, motor proteins bound to the antibody coated surface (Figure 14) via their SfGFP.



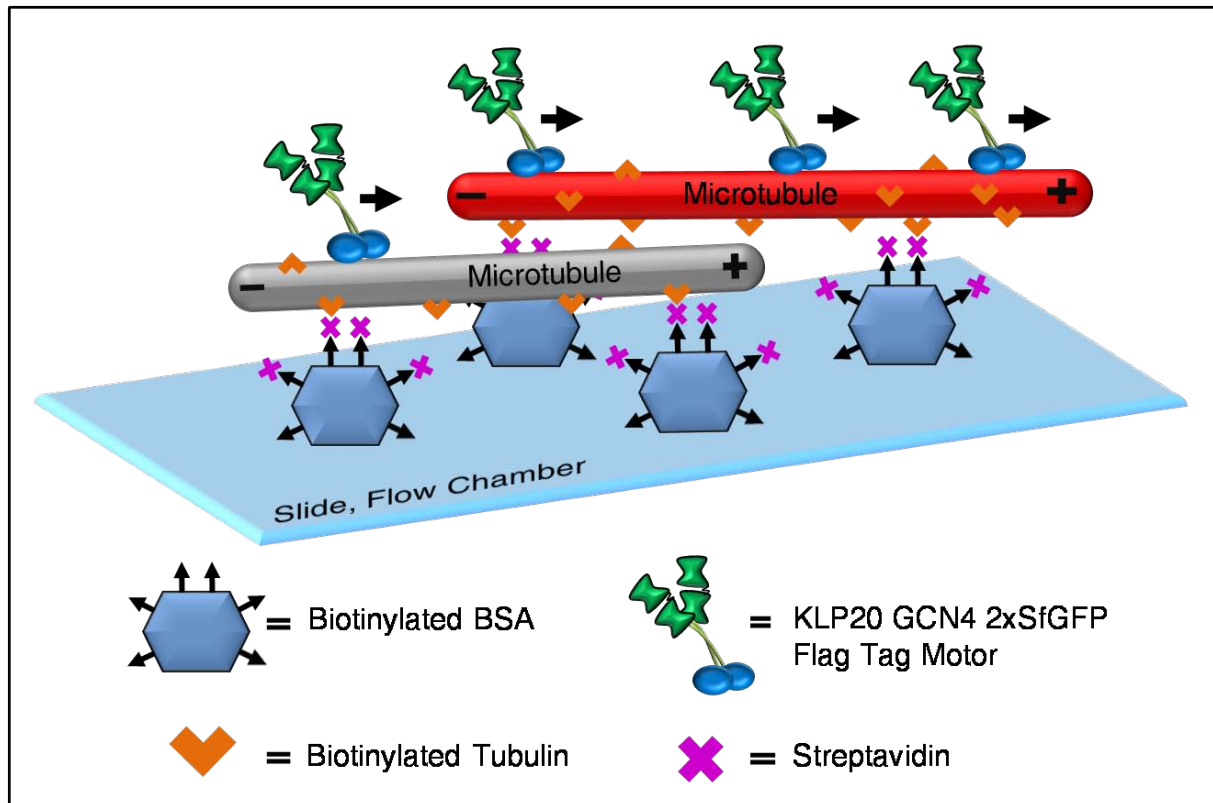
**Figure 14. Multiple motor gliding filament assay.** **A)** Flow chamber preparation with an object slide, a cover slip and silicon grease, generating a chamber with a volume of about 10  $\mu$ l. **B)** Inside a flow chamber, full-length kinesin motors stick to glass surface via their tail domains, while the head domains protrude into the matrix containing motility mixture with fluorescently labeled microtubules. By doing their step cycle, the motors push the filaments forward, indicated by black arrows. Minus end of the filaments is leading, because the motors are plus end directed [86]. **C)** A combination of sticky biotinylated BSA, streptavidin and a biotinylated anti GFP antibody was necessary to attach the GCN4 motors to the surface via their Superfolder GFP inside a flow chamber.

BRB80 buffer: 80 mM PIPES, pH 6.9, 100 mM KAc, 2 mM MgCl<sub>2</sub>, 1 mM EGTA, 1 mM DTT

Motility buffer: 0.145 mg/ml glucoseoxidase (Sigma, G2133), 0.0485 mg/ml catalase (Sigma, C3155), 0.2 mg/ml casein, 0.4% glucose, 200 mM KAc, 1 mM DTT, in BRB80

### **2.2.8. Single molecule motility assay**

Single molecule motility assays (Figure 15) were carried out following the procedure given in Vale et al. (1996) [20]. The flow chamber was coated similar to the multiple motor gliding assay until the streptavidin step. 10 to 20  $\mu$ l of biotinylated, fluorescently labeled (Cy3) and not labeled microtubule dilution mixture was flushed into the chamber and incubated for 5 min before removing unbound filaments with washing buffer containing 1 mg/ml BSA in BRB80 buffer. Motor proteins were attached to microtubule tracks by supplementing the motility buffer with 1mM non-hydrolyzable ATP analogue AMP-PNP and incubating for 4 min. After checking the immobilized Superfolder GFP labeled motors with a TIRF microscope, motility buffer containing 2 mM ATP was washed into the chamber and the movements of the motor proteins were recorded with a CCD camera.



**Figure 15. Single molecule assay with GCN4 motors.** A mixture of biotinylated, fluorescently labeled and not labeled microtubules (Cy3 (red), not labeled (gray)) were immobilized on the surface by a combination of biotinylated BSA and streptavidin. The run of a homodimeric motor conjugated to four Superfolder GFP molecules on their microtubule track was obtained and recorded with a TIRF microscope. Arrows indicate the plus end directed run of a motor protein.

### 2.2.9. Analysis of single molecule experiment

Superfolder GFP tagged protein movements on immobilized microtubules were determined from frame by frame analysis with the help of Cell<sup>^</sup>R software (Olympus Biosystems, Germany). The velocity of motor proteins translocating along their cytoskeletal track microtubules was determined manually and calculated simply by dividing the traveled distance by the elapsed time. All further data and statistical analysis was carried out using IgorPro software (WaveMetrics, Inc., Portland, U.S.A.).

### 2.2.10. Protein purification

Sf9 insect cells were infected with baculoviruses coding for genes of interest and cells were harvested as described by centrifugation. From this point on, all steps were performed either on ice or 4°C.

### 2.2.10.1. Protein purification via 6xHis tag with Ni-NTA agarose beads

Harvested cells were lysed in 10% vol. (of the initial cell suspension volume) of ice-cold His tag lysis buffer with the help of a pipetboy (Integra Biosciences, Germany) for 2 to 4 min. After centrifugation at 65,000 x g for 10 min and 4°C (Beckmann L8-M, rotors 70.1 Ti, 50.2 Ti, or Beckmann Optima TL, rotor TLA 100.3), the pellet was discarded. The supernatant, containing the protein of interest was incubated rotating with pre-washed Ni-NTA coated sepharose beads (Ni-NTA agarose, Qiagen) for 1 hour (250 µl Ni-NTA material for 5 ml cell lysate) at 4°C. After incubation, beads were 3 to 4 times washed with 1 ml of ice-cold His washing buffer in an Eppendorf reaction tube to eliminate unbound protein. Elution of 6xHis tagged proteins was performed by incubating with 0.5 to 1% vol. (of lysis suspension volume) of His elution buffer containing 500 mM imidazole for 45 min at 4°C. Eluted proteins were shock-frozen in liquid nitrogen and stored at -70°C.

|                     |   |
|---------------------|---|
| PIPES basic buffer: | 80 mM PIPES, 300 mM KAc, 1 mM MgCl <sub>2</sub> , 1 mM DTT and 100 µM ATP                           |
| Lysis buffer:       | basic buffer, 1% Triton-X 100, protease inhibitor cocktail (cOmplete, Roche), 20 mM imidazole, pH 8 |
| Washing buffer:     | basic buffer, 40 mM imidazole, protease inhibitor cocktail (cOmplete, Roche), pH 8                  |
| Elution buffer:     | basic buffer, 500 mM imidazole, protease inhibitor cocktail (cOmplete, Roche), pH 7.5               |

### 2.2.10.2. Protein purification via 6xHis tag with Dynabeads®

Protein purification with Dynabeads® His tag isolation and pulldown (Life Technologies, Darmstadt, Germany) was performed analogous to the His tag purification with Ni-NTA agarose beads according to the manufacturer's protocol. The advantage of this method was a lower background and a faster purification due to shorter incubation times. Harvested Sf9 cells were lysed and cleared as described. Meanwhile, four times with 500 µl in washing buffer washed beads were cleared in a DynaMag™ (Life Technologies, Darmstadt, Germany) magnet in between. 50 µl (2 mg) beads were mixed and incubated rotating with 700 µl supernatant, containing protein of interest up to 30 min at 4°C. After incubation, beads were washed again

with 500 µl His washing buffer and cleared with the magnet in between. Elution was performed rotating up to 10 min at 4°C. The mixture was applied to the magnet and the supernatant containing the protein of interest was transferred to a clean tube. Eluted proteins were shock-frozen in liquid nitrogen and stored at -70°C.

### **2.2.10.3. Protein purification via Flag tag**

Harvested cells were lysed in 10% vol. (of the initial cell suspension volume) of ice-cold Flag tag lysis buffer with the help of a pipetboy (Integra Biosciences, Germany) for 2 to 4 min. The homogenate was cleared by centrifugation at 65,000 x g for 10 min and 4°C (Beckmann L8-M, rotors 70.1 Ti, 50.2 Ti, or Beckmann Optima TL, rotor TLA 100.3). The supernatant, containing the protein of interest was incubated rotating with 2 to 3% vol. (of lysis solution volume) of anti-FLAG antibody agarose resin (Anti-FLAG M2<sup>®</sup> Affinity Gel, Sigma) for 1.5 hours at 4°C. After incubation, beads were 3 to 4 times washed with 1 ml of ice-cold Flag washing buffer 1, followed by 3 to 4 times washing with Flag washing buffer 2 in an Eppendorf reaction tube with centrifugation steps in-between, to eliminate unbound protein. Elution of Flag tagged proteins was performed by incubating with 2 to 5% vol. (of lysis suspension volume) of Flag elution buffer containing an excess of FLAG-peptides (Sigma) for 45 min at 4°C. If desired, another elution step with 1 to 2.5% vol. (of lysis suspension volume) of elution buffer was performed for 45 min at 4°C. Eluted proteins were shock-frozen in liquid nitrogen and stored at -70°C.

|                     |  |
|---------------------|--|
| PIPES basic buffer: | 80 mM PIPES, 300 mM KAc, 1 mM MgCl <sub>2</sub> , 1 mM DTT, and 100 µM ATP                               |
| Lysis buffer:       | basic buffer, 1% Triton-X 100 and protease inhibitor cocktail (cOmplete, Roche)                          |
| Washing buffer 1:   | basic buffer with 500 mM KAc, 5 µM ATP, 0.1% Tween 20, and protease inhibitor cocktail (cOmplete, Roche) |
| Washing buffer 2:   | basic buffer with 200 mM KAc, 1 mM EGTA, 5 µM ATP, and protease inhibitor cocktail (cOmplete, Roche)     |
| Elution buffer:     | basic buffer with 100 µg/ml FLAG-peptide and protease inhibitor cocktail (cOmplete, Roche)               |

### 2.2.10.4. Co-immunoprecipitation assays

Constructs consisting of a combination of Flag tagged and His tagged subunits required a tandem purification of proteins. Harvesting was performed as described (section 2.1.10.5) and Flag tag purification was carried out (section 2.2.10.3). After checking eluted protein amounts via SDS-PAGE, usually 500 µl elution was incubated with 150 µl Ni-NTA material for the case of Ni-NTA agarose purification, or with 50 µl magnetic beads for the case of Dynabeads<sup>®</sup> His tag isolation. Elution was carried out as described above.

### 2.2.11. Gel filtration chromatography

Gel filtration chromatography or size exclusion chromatography is a method based on the ability of gel filtration media like Superose to separate complex protein mixtures, primarily according to their molecular size.

To check whether the motor proteins were in a dimeric or aggregated state, gel filtration was carried out with a Superdex 200 10/300 GL gel filtration column (GE Healthcare) at a Äkta purifier 100 (GE Healthcare) according to manufacturer's manual. Standard protein purification as described above was performed until to the elution step. After washing proteins, an extra 3 to 4 times washing step with 1 ml of ATP free gel filtrations buffer was performed, to eliminate a possible ATP disturbance of the system. The proteins were eluted in gel filtration buffer. If needed, an additional concentration step by dialysis into gel filtration buffer or by centrifugation in an Amicon<sup>®</sup> Ultra centrifugal filter unit (10 kDa exclusion size, Millipore) was performed. The volume loaded on the column was about 150 µl.

Gel filtration buffer: 80 mM PIPES, 200 mM KAc, 1 mM MgCl<sub>2</sub>, 1 mM DTT, and 1 mM EGTA

### 2.2.12. Microscopy

The *in vitro* motility properties of motors investigated in this study were performed via fluorescence-microscopy techniques. Epifluorescence microscopy was used for studying primarily multiple motor filament gliding assays, whereas total internal reflection fluorescence (TIRF) microscope was used for studying single molecule motility assays.

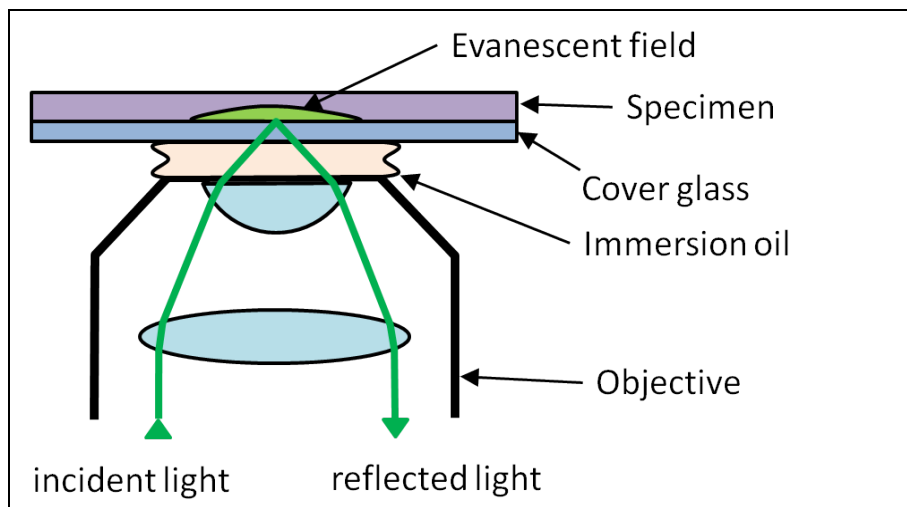


### **2.2.12.1. Epifluorescence microscopy**

With this type of microscope, it is possible to illuminate subjects of interest conjugated to a fluorophore and detect them via a coupled camera device. The illumination is not only restricted to the focus plane, but also to the whole sample, leading sometimes to high background signalling. The background is reduced only by using an emission filter. Axiovert 200 M epifluorescence microscope (Zeiss, Germany) with a 100 x, N.A. 1.4 Oil objective lens and an AxioCaM MRm CCD camera was used to study proteins of interest. Illumination was carried out via a mercury lamp (FluoArc 01.26D, Jena GmbH, Germany), while band-pass filters facilitated excitation of fluorophores at 488 and 532 nm. Depending on each experiment and illumination time, sequences of 30 to 300 frames were recorded and analysed by AxioVision software (Zeiss, Germany).

### **2.2.12.2. TIRF microscopy**

With TIRF microscopy, it is possible to selectively illuminate objects conjugated to fluorophores that are really close to the surface and avoid excitation of fluorophores in the bulk [137]. This is achieved by the use of an emerging evanescent wave caused by the reflection of a laser beam at the glass-water interface. It is necessary, that the immersion oil has a similar refractive index as the cover slip and that the medium has a lower refractive index than the cover slip (Figure 16). Depending on the angle, the wavelength of the laser beam and the refractive indices, the evanescent wave penetrates the sample only to a depth of about 150 to 200 nm [138], because the intensity decays exponentially with the distance to the glass-water interface.



**Figure 16. Objective-type TIRF microscope.** The incident light is guided through the objective, refracted by the high numerical aperture lens and brought to a critical angle to the glass-water interface. The reflected light goes back through the objective to the dichroic mirror. The evanescent field is generated from the total internal reflection of the laser beam at the glass-water boundary, where only a thin layer of the specimen is excited (adapted from Sako and Uyemura, 2002 [139]).

Single SfGFP fused motor proteins were investigated using an objective-type TIRF microscope (IX71, Olympus), equipped with a plan objective lens (100 x, N.A. 1.65 Oil) and a front-illuminated CCD camera (C-9100, Olympus). Excitation of fluorophores was achieved with the help of a solid-state laser at 488 or 532 nm wavelength. Depending on each experiment and illumination time, sequences of 200 to 600 frames were recorded and analysed with Cell<sup>^</sup>R software (Olympus Biosystems, Germany).

### 2.2.13. Mass spectrometry (MS)

Mass spectrometry is an analytical method where charged particles are analysed according to their mass-to-charge ratio. This is achieved mainly by a couple of typical MS procedures: First, the particle is ionized by an ion source and charged particles (ions) are generated; second, the separation of the ions is carried out by a mass analyser, according to their mass-to-charge ratio by an electric or magnetic field; and third, a mass spectrum is generated with the help of a detector system according to the collected mass data [140]. Additionally to sequencing, proteins of interest were analyzed and confirmed by mass spectrometry by the Zentrallabor für Proteinanalytik (ZfP) of the LMU.

# Results

## 1. Experimental Concept

To dissect the kinetic properties of kinesin-2 from *C. elegans*, different motor constructs have been designed and generated (Figure 17). 'Wild-type tail' constructs were generated to answer the question whether this heterodimeric construct is autoinhibited via a bending of the tail domains, as observed already with conventional kinesin [47-56]. Homodimeric 'wild-type tail' constructs addressed the question whether the subunits differ in their kinetic behavior. These motor combinations were additionally expected to illuminate the question if in case the motor was autoinhibited, which subunit was regulated by autoinhibition. 'EE tail' combinations, eliminating a regulatory effect by the tail domains, were generated to investigate the motors under constitutively activated conditions. 'GCN4 tail' constructs were designed to eliminate any influence of the tail domains, be it intra- or intermolecular. The motor combinations so generated should be fully active. To study the single molecule behavior of the 'GCN4-tail' motor combinations with the help of four Superfolder GFP (SfGFP) molecules per motor under zero load conditions with TIRF microscopy was essential. The observations should illuminate the question regarding the processive behavior of each subunit as a homodimeric motor. Monomeric head domains including the neck regions were generated to investigate whether both catalytic subunits lacking a tail region were kinetically equivalent. 'GCN4 tail' KLP11 constructs containing variable GS repeats in their neck regions were designed to understand KLP11 subunits suppression in different assays. Additionally, these constructs were examined to understand the role of the neck linker length and its influence on the catalytic activity of the motor as well.

## Results





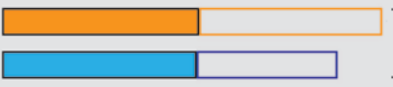

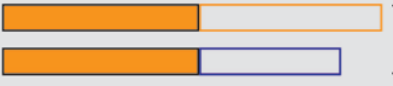


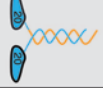



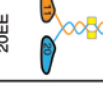
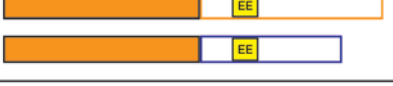
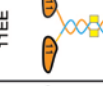

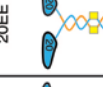

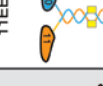
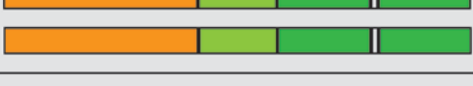

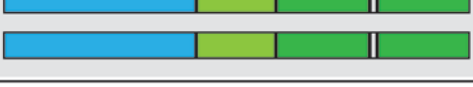




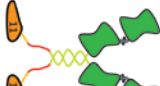
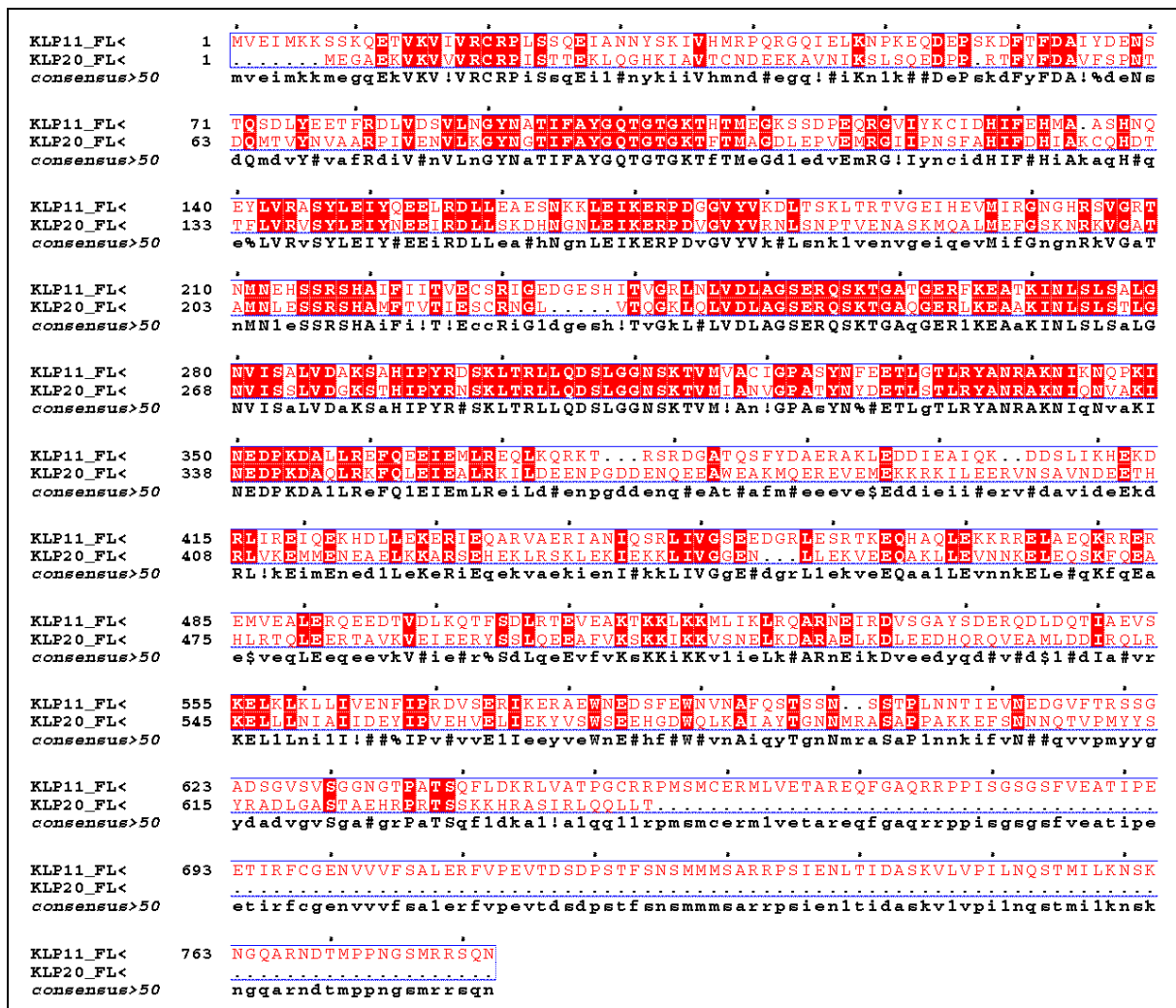
| Generated constructs                            |   | Planned experiments  | ATPase | Filament gliding | Single molecule |
|---|---|--|--------|------------------|-----------------|
| Monomeric constructs                            |  11 Monomer      |     | Y      | N                | N               |
|   |  20 Monomer      |     | Y      | N                | N               |
| Kinesin-2 constructs containing wild-type tails |  KLP11/20        |     | Y      | Y                | N               |
|   |  KLP11/11        |     | Y      | Y                | N               |
|   |  KLP20/20        |     | Y      | Y                | N               |
|   |  KLP20/11        |     | Y      | Y                | N               |
|   |  KLP11EE/20EE    |     | Y      | Y                | N               |
|   |  KLP11EE/11EE  |   | Y      | Y                | N               |
| Kinesin-2 constructs containing EE mutations    |  KLP20EE/20EE  |   | Y      | Y                | N               |
|   |  KLP20EE/11EE  |   | Y      | Y                | N               |
|   |  KLP11/11      |   | Y      | Y                | Y               |
|   |  KLP20/20      |   | Y      | Y                | Y               |
| Kinesin-2 constructs with flexible extensions   |  KLP11/11 2xGS |  | Y      | Y                | Y               |
|   |  KLP11/11 8xGS |  | Y      | Y                | Y               |

Figure 17. Generated constructs and designated experiments.

## 2. Kinesin-2 (KLP11/20) subunits from *C. elegans* exhibit low sequence homology

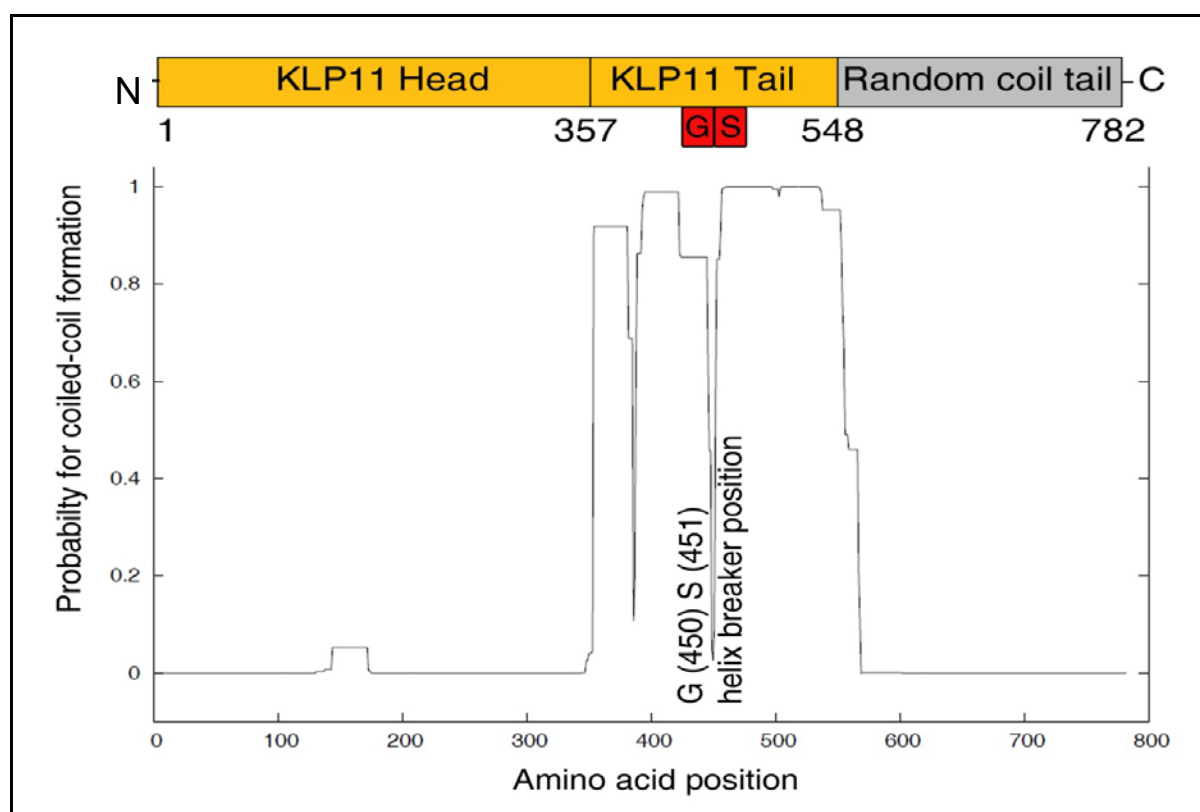
Although related, sequence alignments performed with BLASTP 2.2.27 and MultAlin [141-143] showed that the full-length KLP11 (782 amino acids (aa), 88.7 kDa) and KLP20 (646 amino acids, 73.5 kDa) subunits are different. They shared only 44% identity and 62% similarity (Figure 18, MultAlin sequence alignment), which gave reason to the assumption that two completely different subunits dimerize into a functional motor. Interestingly, the region of high consensus was found in the catalytic head domain (aa 1 to 365).



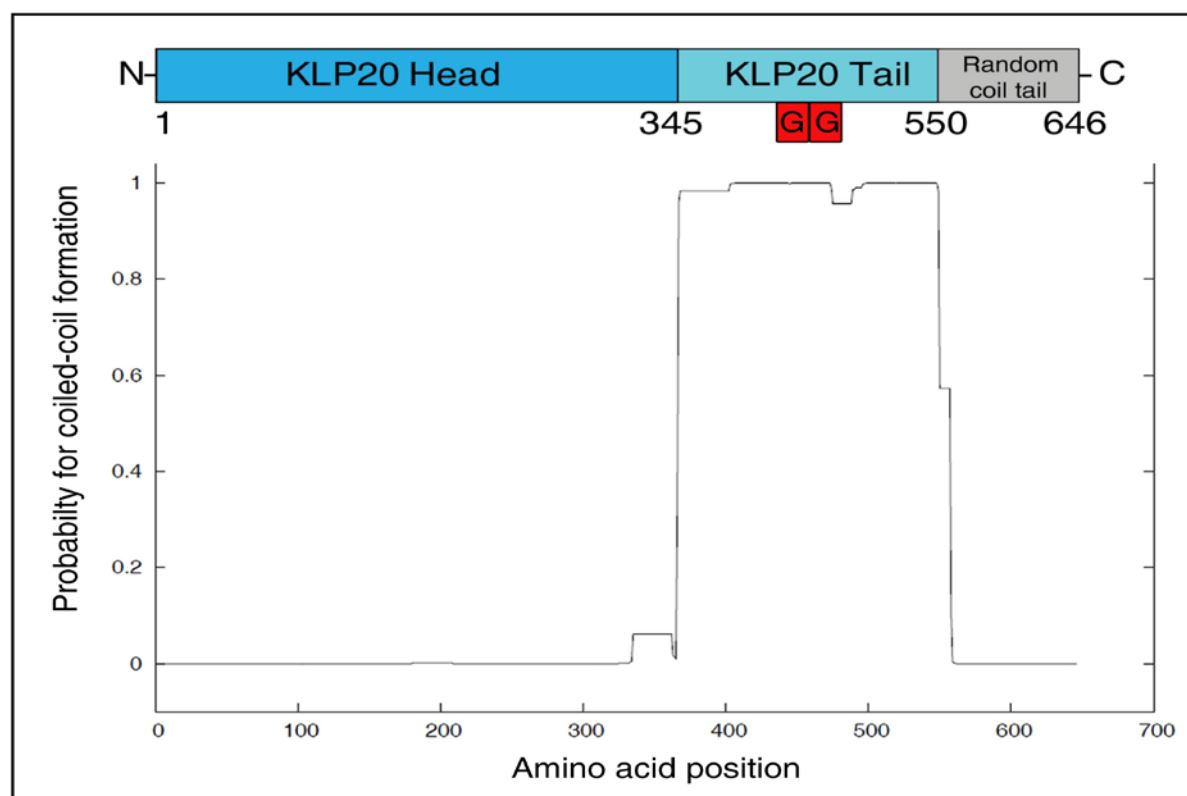
**Figure 18. Sequence alignments of full-length KLP11 and KLP20 subunits (MultAlin, [143]).** The two motor subunits shared 44% identical and 62% positive amino acids. Strikingly, the high consensus part was found in the catalytic head domain region (aa 1 to 365).

### 3. KLP11/20 exhibits a helix breaker position within its stalk region

The Wild-type KLP11 and KLP20 protein sequences were analyzed using coiled-coil prediction algorithms [144]. It should be noted, however, that these routines are limited to homodimeric coil-coil predictions. Notwithstanding, the KLP11 subunit (Figure 19) shows a kink position containing the helix-breaker residue glycine that is situated roughly in the middle of the stalk. In contrast, even though KLP20 contains two such glycines at the corresponding position (Figure 20), no disruption in the coil-coil formation is predicted. Similar to the conventional homodimeric kinesin-1, such kink positions may mediate auto-regulation in the heterodimeric kinesin-2 as well by enabling head-tail interactions [48-56, 84].



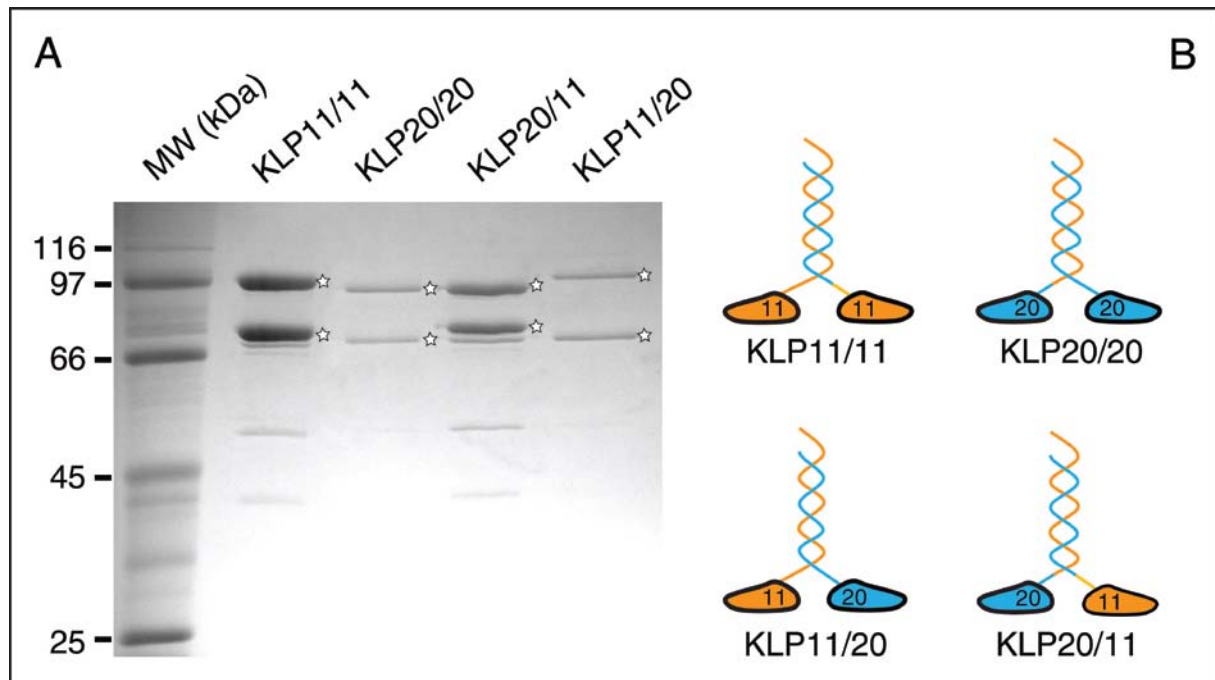
**Figure 19. Coiled-coil prediction for KLP11.** The stalk region of KLP 11 (aa 357 to aa 782) was predicted to form a coiled-coil until aa position 548, followed by a random coil until the C-terminal end of the molecule [144]. The predicted highly coiled-coil stalk region was interrupted by a helix breaker position at aa 450 (Glycine) and 451 (Serine). This position could serve as a kink allowing back-folding of the C-terminal distal tail onto the head domains for auto-regulation [84].



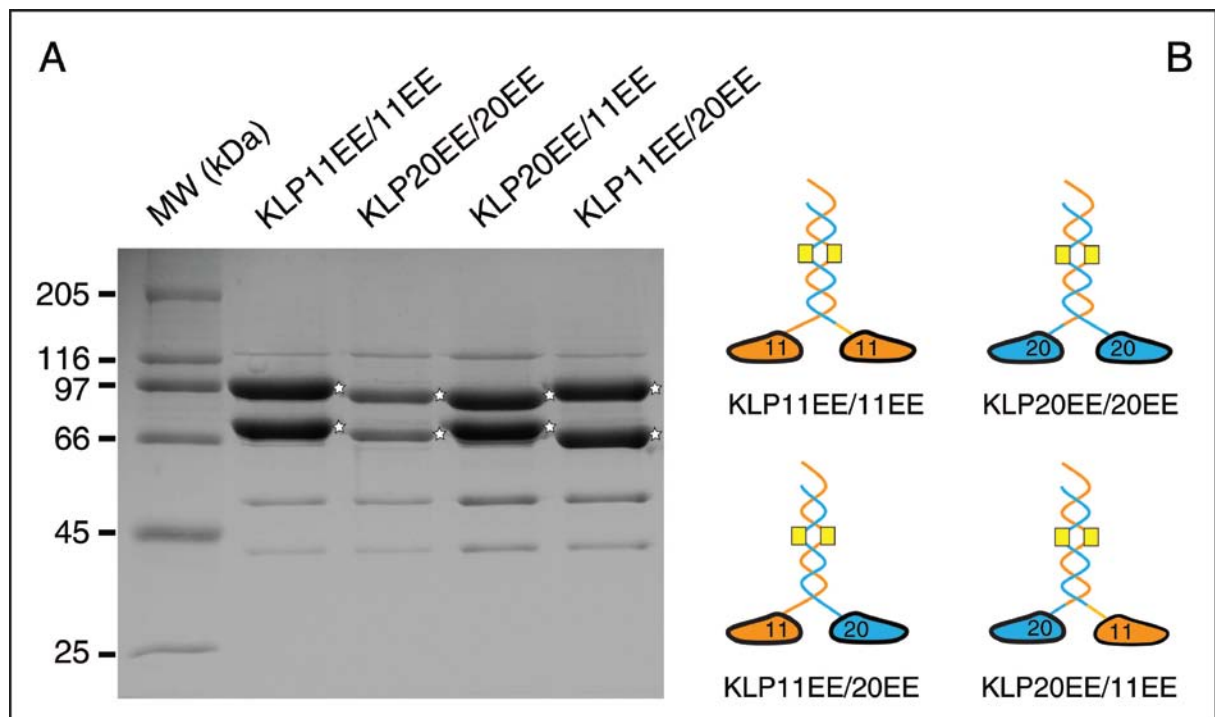
**Figure 20. Coiled-coil prediction for KLP20.** The stalk region of KLP 20 (aa 345 to aa 646) was predicted to form a coiled-coil until aa position 550, followed by a random coil until the C-terminal end of the molecule [144]. Interestingly, even though KLP20 contains two glycines (position 444 and 445) at the corresponding position where KLP11's helix breaker position is located, no disruption in the coil-coil formation of KLP20 was predicted.

## 4. Expression, purification, and quality control of the constructs

All constructs were expressed and purified using the Baculovirus Expression System (Invitrogen) in insect cells. Over-expression of the constructs in 200 to 300 ml of Sf9 cell suspensions resulted in protein concentrations typically ranging from 0.5 to 4  $\mu$ M. Affinity tag purification of the full-length motor combinations via co-immunoprecipitation (co-IP) displayed both motor subunits combined to a heterodimer in a 1:1 molar ratio, when only one of the dimerization partners contained the purification tag (Figures 21 and 22). Truncated homodimeric constructs were dimerized via the molecular zipper GCN4. Monomeric head domains were purified via FLAG-tag affinity purification (Figure 23).

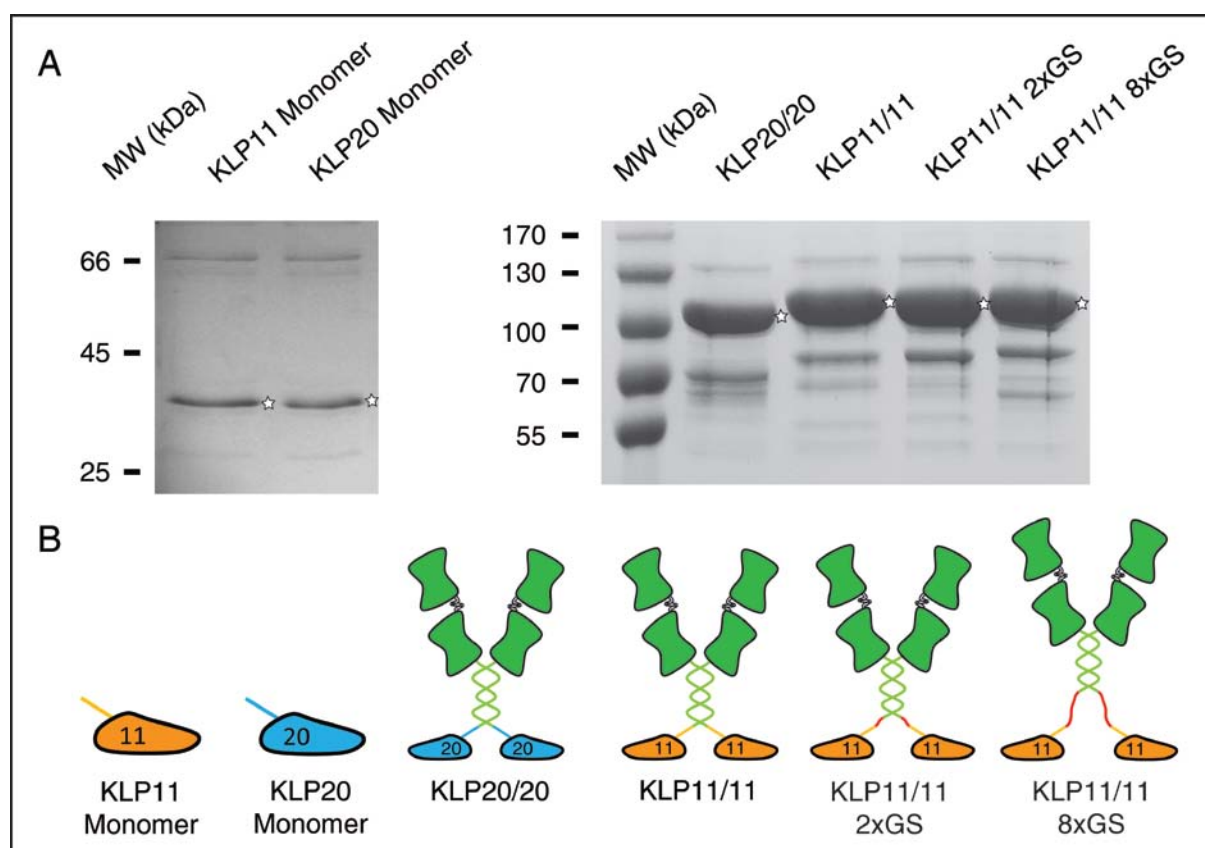


**Figure 21. Flag-affinity protein purification of kinesin-2 constructs heterodimerized via the wild type tail.** **A)** Recombinant proteins were expressed using the baculovirus expression system followed by FLAG-affinity protein purification. SDS-Page displays the purified constructs of interest marked by stars. **B)** Schematics of the purified constructs.



**Figure 22. Flag-affinity protein purification of the constructs containing the G to E and S to E mutations in the stalk domains.** **A)** Recombinant proteins were expressed using the baculovirus expression system followed by FLAG-affinity protein purification. The proteins of interest are marked with stars on SDS-Page. **B)** Schematics of the purified constructs. Mutations within the stalk domains are high-lightened by yellow boxes.



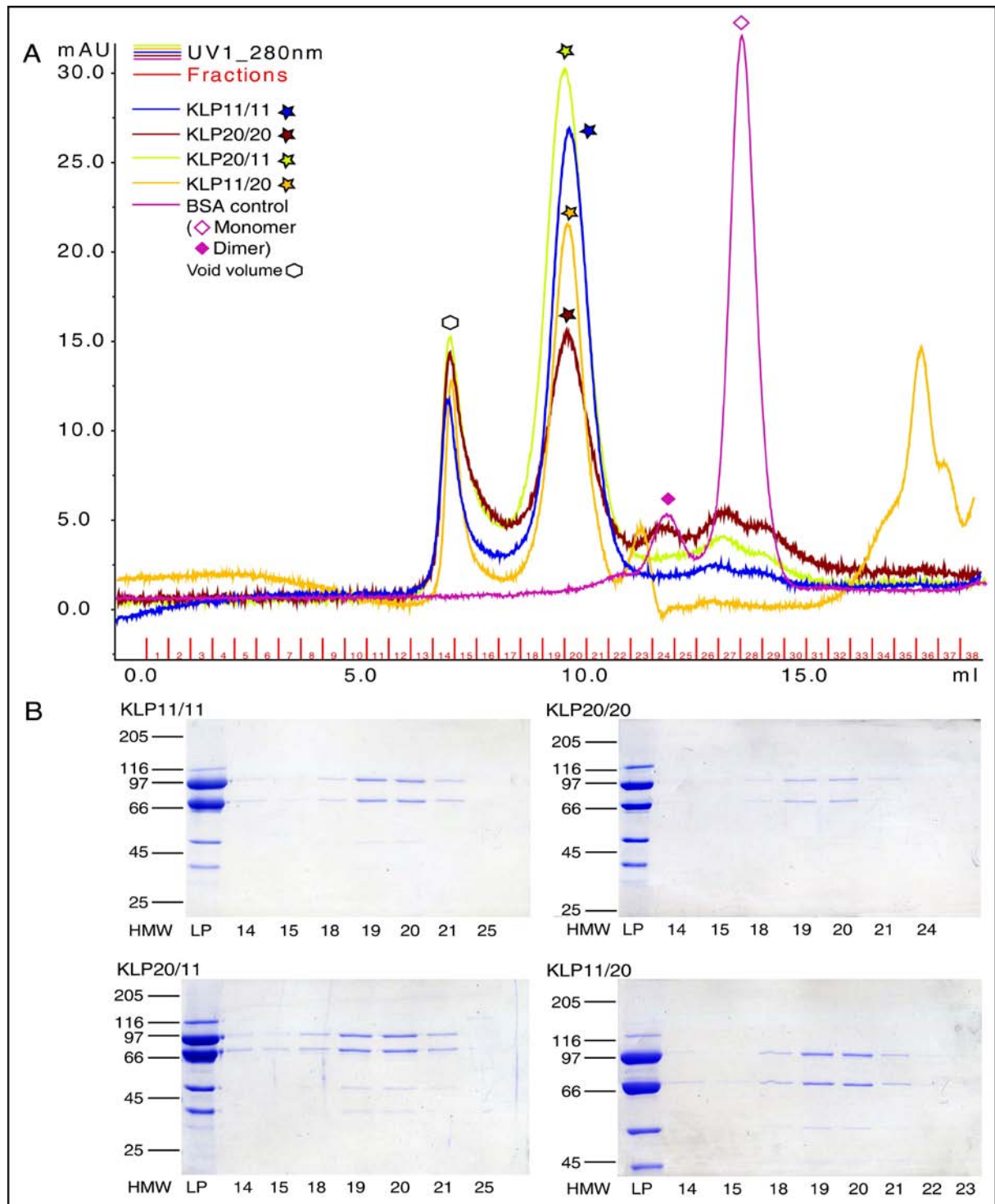


**Figure 23. Flag-affinity protein purification of the monomeric head domains and tandem SfGFP motors homodimerized via the GCN4 zipper. A)** Recombinant proteins were expressed using the baculovirus expression system followed by FLAG-affinity protein purification. Motors of interest are marked by stars on SDS-Page. **B)** Schematics of the purified constructs.

#### 4.1. Size-exclusion chromatography of the full-length constructs

Native size-exclusion chromatography coupled to multiple-angle light scattering (MALS) was carried out to characterize the molecular integrity of the purified heterodimeric constructs. BSA served as a size control for the chromatography and MALS fitting (Figure 24). The first peak in Figure 24 corresponds to the void volume of the column. The second peak contains the proteins of interest with molecular weights consistent with a dimeric state (Table IV). Eluted fractions were analyzed on SDS-PAGE and confirmed a molar ratio of 1:1 of the subunits (Figure 24, B). Monomers or aggregates were not detected.

## Results



**Figure 24. Size exclusion chromatography of the full-length constructs containing the wild type tail domains.** **A)** Aggregation or monomeric state of the generated 'WT tail' constructs was checked, and revealed a dimeric state for all constructs. KLP11/11 (blue), KLP20/20 (dark red), KLP 20/11 (green) and KLP11/20 (orange) eluted between 8.5 and 11 ml, corresponding to the second peak in the diagram. BSA as a control had a UV absorption peak at 13.6 ml (magenta). Fraction numbers and eluted volumes are depicted on the x-axis, whereas the absorption (mAu) is marked on the y-axis. **B)** Analysis of the eluted fractions on SDS-PAGE. All constructs form heterodimers with a 1:1 molar ratio. Fraction numbers of the respective elutions are given at the bottom. (LP: Loaded protein on the column)

**Table IV. Calculated and determined molecular weights of the constructs containing the wild type tail**

| Construct   | Calculated MW (kDa) | MW from MALS fit (kDa) |
|-------------|---------------------|------------------------|
| KLP11/11    | 162.2               | 143.4                  |
| KLP20/20    | 160.4               | 154.5                  |
| MC KLP20/11 | 162.3               | 178.3                  |
| WT KLP11/20 | 162.3               | 168.6                  |
| BSA control | 66.4                | 67.6                   |

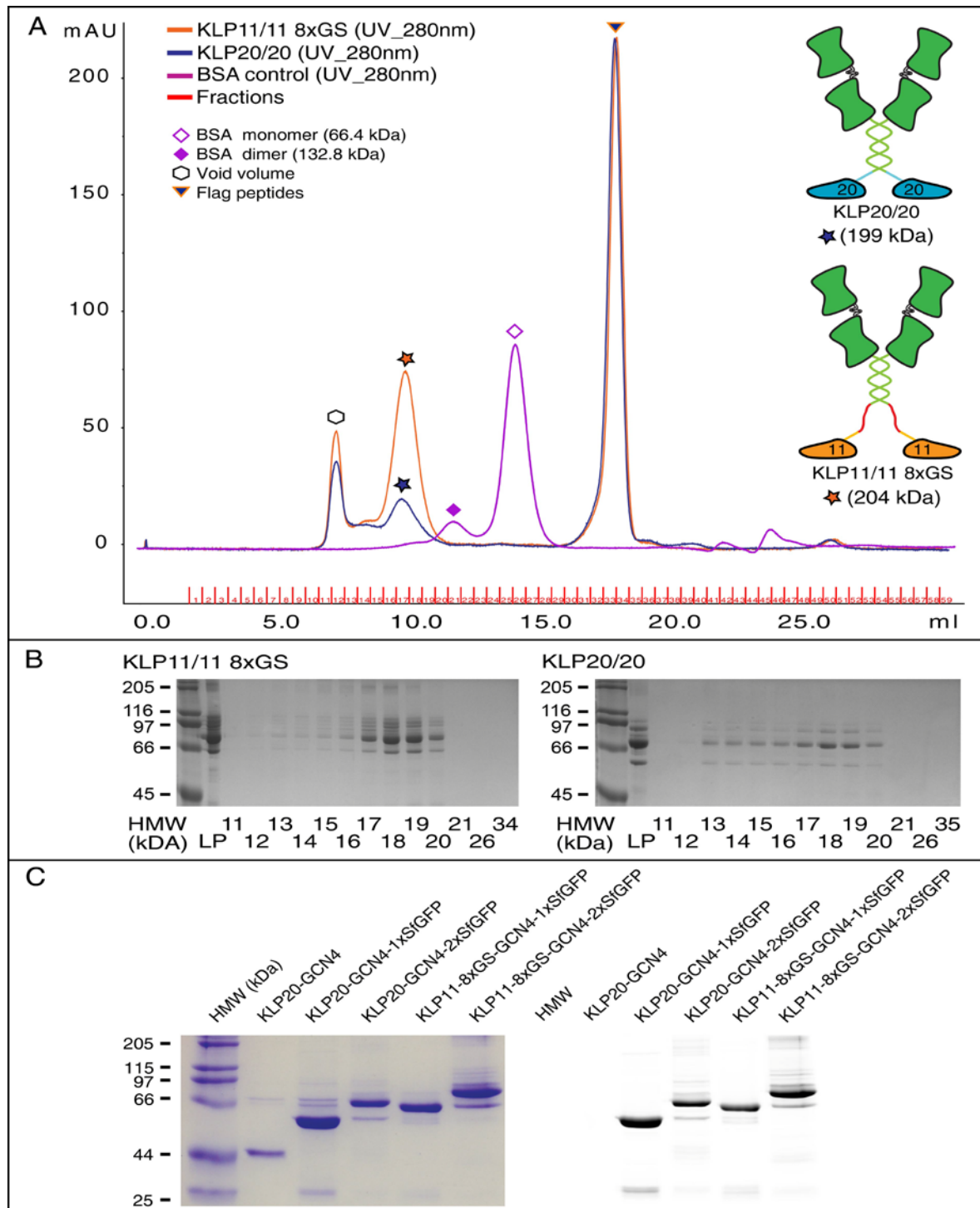
(Adapted from Brunnbauer *et al.*, 2010 [126])

## 4.2. Size exclusion chromatography of the truncated constructs

To check the molecular integrity of the truncated constructs dimerized via the molecular zipper GCN4 and conjugated to tandem Superfolder GFP (SfGFP), size-exclusion chromatography with KLP11/11 8xGS and KLP20/20 (Figure 26) was carried out. The two SfGFP molecules are separated by a 10 amino acid-long linker sequence, resulting in a dimeric motor containing four fluorophores.

The first peak (Fractions 11 and 12, blue and orange curves) in the graph corresponds to the void volume of the column, whereas the second peak (Fractions 14 to 21) contains the proteins of interest with molecular weights consistent with a dimeric state. Column resolution was checked with BSA (Figure 25, magenta). Eluted fractions were analyzed on SDS-PAGE and confirmed a non-aggregated state (Figure 25, B).

## Results



**Figure 25. Size exclusion chromatography of ‘GCN4 tail’ constructs fused to tandem Superfolder GFP (SfGFP) and confirmation via SDS-Page. A)** KLP11/11 8xGS (orange) displayed an absorption peak at 9.5 ml after injection, whereas KLP20/20 (light blue) eluted already after 9.35 ml after injection. Fraction numbers and eluted volume is depicted on the x-axis, whereas the absorption (mAu) is marked on the y-axis. Schematics of used constructs are depicted on the right. **B)** Eluted fractions (indicated at the bottom) of each run were analyzed on the SDS-PAGE and no aggregated protein fractions was observed in the void volume. High molecular weight (HMW) and fraction numbers are shown for each construct. Loaded protein on the column is marked with LP. **C)** GFP-scan of selected motors on SDS-PAGE (right) with a Typhoon Scanner (GE Healthcare) prior to coomassie stain (left) confirmed conjugation to SfGFP.

## 5. Kinetic properties of the wild type KLP11/20 and its chimeric KLP20/11

Given that wild type KLP11/20 exposed a helix breaker region in its tail domain, its ATPase activity is likely to be regulated by a mechanism similar to that of conventional kinesin-1. Conventional kinesin-1 prevents futile ATP consumption by bending of the molecule at the kink position, bringing the tail domains in close proximity of the catalytic head domains, resulting in an autoinhibition of the motor [48-56].

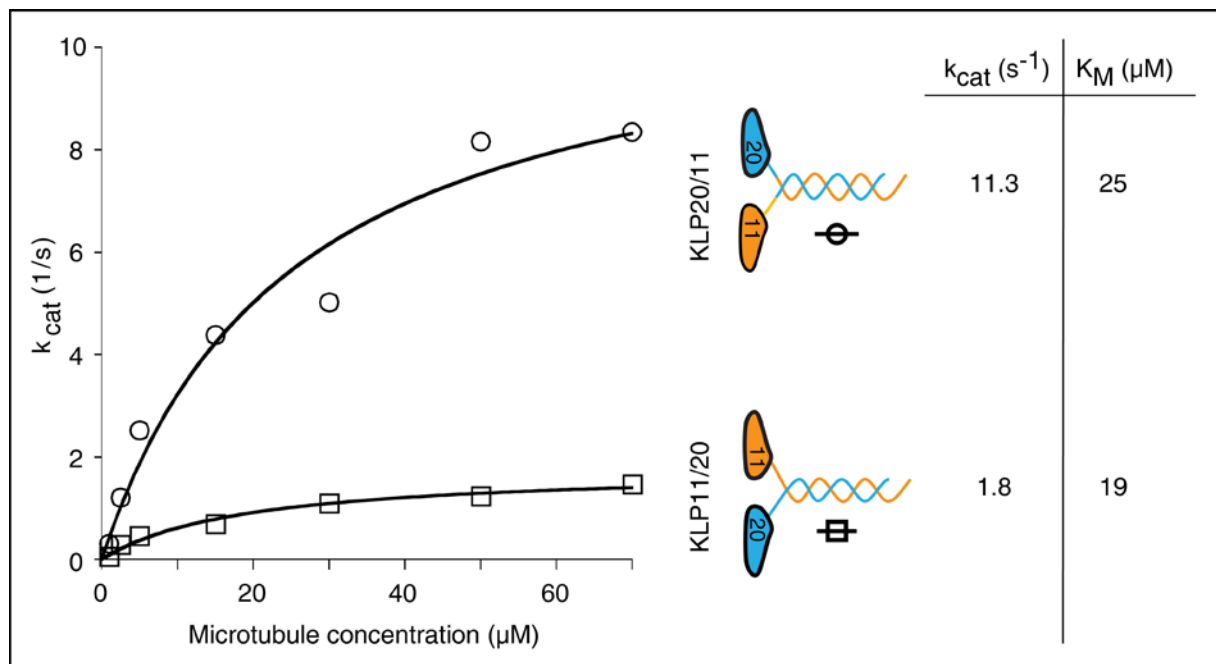
To determine the catalytic activity of the heterodimeric wild type KLP11/20, steady state ATPase and multiple motor gliding filament assays were performed. The wild type KLP11/20 construct was compared to the mixed chimera KLP20/11 with swapped head positions.

Steady-state ATPase assays at saturating ATP (3 mM) concentrations with wild type KLP11/20 and the reversed chimera KLP20/11 provided first insights into motor activity (Figure 26). While the wild type motor KLP11/20 displayed low ATPase activity ( $k_{\text{cat}} = 1.8 \text{ s}^{-1}$  (ATP turnover number),  $K_M = 19 \text{ }\mu\text{M}$ ), its corresponding chimera KLP20/11 displayed a robust ATPase activity ( $k_{\text{cat}} = 11.3 \text{ s}^{-1}$ ,  $K_M = 25 \text{ }\mu\text{M}$ ). Interestingly, the affinity of the constructs to MTs are almost in the same range, indicating, as mentioned above, that the interaction of the tail domains with the head domains in wild type KLP11/20 slows the ADP release from the catalytic head domains, leading to a reduced motor activity, while the motors affinity to microtubules is not affected [49, 51, 57-59].

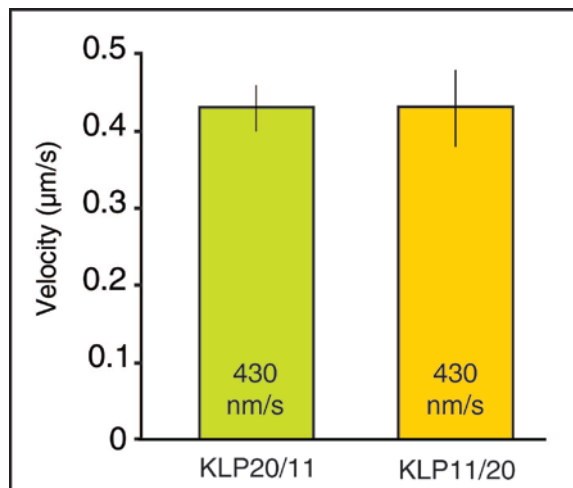
Strikingly, in contrast to the kinetic differences observed in the solution-based ATPase assays, the velocities of the KLP11/20 and the chimeric KLP20/11 were experimentally indistinguishable in multiple-motor gliding filament assays (Figure 27). This is consistent with the view of a tail-mediated inhibition of the wild type motor. In this experimental set-up (see Materials and Methods, section 2.2.7), the tail domains are attached to the glass surface, and thus disengaged from interacting with the catalytic head domains.

## Results

Taken together, these results demonstrate that WT KLP11/20 is auto-regulated in ATPase assays and that this inhibition of the catalytic heads by the tail domains is asymmetric since swapping the head domains (KLP20/11) was sufficient to circumvent the auto-regulation (Figure 26). Put differently, the positions of the head domains relative to the tail domains are crucial for an efficient inhibition of this heterodimeric motor. Consistently, disengaging the tail domains in the wild type KLP11/20 all together by binding the motor to a glass surface is equally sufficient to activate the motor's ATPase (Figure 27).



**Figure 26. Steady-state ATPase assay with wild type KLP11/20 and the chimeric KLP20/11.** The wild type motor exhibits suppressed ATPase activity and merely switching the relative positions of the head domains in the chimeric KLP20/11 is sufficient to turn on the motor's ATPase activity.

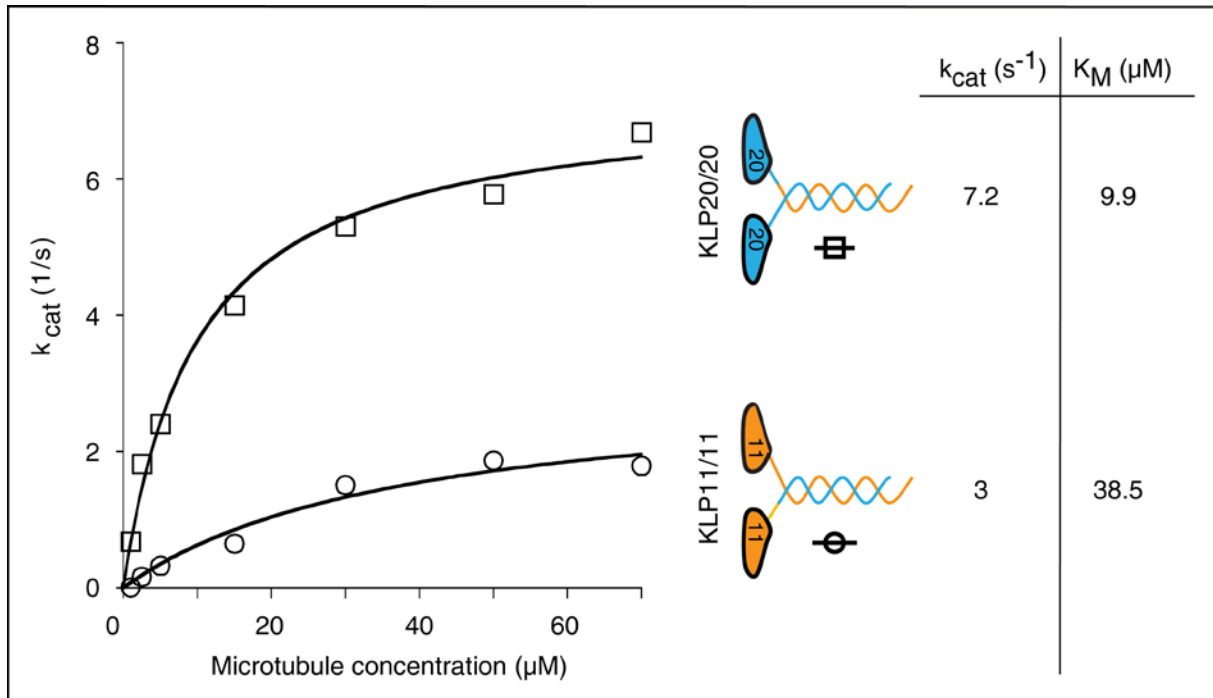


**Figure 27. Analysis of multiple motor gliding filament assays with wild type KLP11/20 and chimeric KLP20/11.** Velocities were calculated by dividing the distance a MT was displaced by multiple motors over the time. The microtubule gliding velocities of both constructs are experimentally indistinguishable (Wild type KLP11/20 ( $430 \pm 50$  nm/s (S.D.),  $n = 95$ ) and KLP20/11 ( $430 \pm 30$  nm/s (S.D.),  $n = 27$ ).

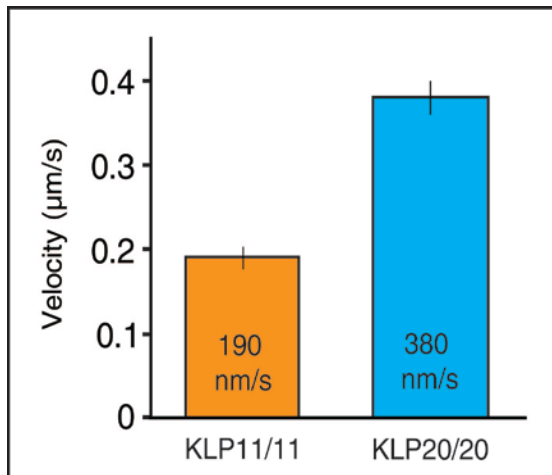
## **6. The kinetic contributions of the KLP11 and KLP20 subunits to the heterodimeric KLP11/20 motor**

To analyze the individual contributions of the two distinct catalytic subunits KLP11 and KLP20 to the overall kinetic properties of the heterodimeric KLP11/20 motor, homodimeric chimeras KLP11/11 and KLP20/20 were designed. To guarantee homodimerization of two identical head domains, the heterodimeric wild type tail domains were used as described above.

In ATPase assays, the 'homodimeric' KLP11/11 motor displayed reduced ATPase activity ( $k_{\text{cat}} = 3 \text{ s}^{-1}$ ,  $K_{\text{M}} = 38.5 \text{ }\mu\text{M}$ ) that was comparable with the wild type KLP11/20 (Figure 28 and Figure 26). In contrast, the KLP20/20 chimera ( $k_{\text{cat}} = 7.2 \text{ s}^{-1}$ ,  $K_{\text{M}} = 9.9 \text{ }\mu\text{M}$ ) was significantly more active and was rather comparable with the chimeric KLP20/11 (Figure 28 and Figure 26). To further analyze the 'homodimeric' chimeras, multiple motor gliding filament assays were performed. Consistent with result obtained from the steady-state ATPase assays (Figure 28), KLP11/11 ( $190 \pm 13 \text{ nm/s}$  (S.D.),  $n = 29$ ) displayed significantly reduced velocities when compared to KLP20/20 ( $380 \pm 20 \text{ nm/s}$  (S.D.),  $n = 30$ , Figure 29). Thus, the behavior of the KLP11/11 contrasts to that of the wild type KLP11/20 which also displayed suppressed activity in the ATPase assays (Figure 26), but showed robust gliding velocities in multiple motor gliding filament assays (Figure 27).



**Figure 28. Steady-state ATPase assay with homodimeric KLP11/11 and KLP20/20 chimeras.** The ATP turnover rates differ for the two 'homodimeric' KLP11/11 and KLP20/20. The suppressed activity of the KLP11/11 construct is reminiscent of the wild type KLP11/20 and may either represent an auto-regulated state or inherent slow kinetics of the KLP11 subunit compared to the KLP20 subunit.



**Figure 29. Multiple motor gliding filament assays with homodimeric KLP11/11 and KLP20/20 chimeras.** KLP11/11 ( $190 \pm 13$  nm/s (S.D.),  $n = 29$ ) moves the microtubule filaments at a reduced velocity ( $190 \pm 13$  nm/s (S.D.),  $n = 29$ ) when compared to KLP20/20 ( $380 \pm 20$  nm/s (S.D.),  $n = 30$ ). Thus, the differences observed in the ATPase assays between the homodimeric KLP11/11 and KLP20/20 also persist in the gliding filament assays, suggesting that the KLP11 and KLP20 subunits may indeed have distinct kinetic properties.

## 7. Relieving auto-regulation in KLP11/20 by tail mutations

The wild type KLP11/20 motor displayed a suppressed ATPase, and swapping the head positions was sufficient to activate the motor's activity (Figure 26). On the other hand, in the multiple-motor filament gliding assays where the motors were attached to the microscope slide via their tail domains (Figure 14), both constructs displayed equivalent velocities (Figure 27). This suggests that, similar to what has been



demonstrated with the kinesin-1 motor, the tail domain's capability of folding onto the head domains via the kink position may mediate the auto-regulation also in kinesin-2 [119, 120]. Coiled-coil predictions [144], indicating a helix breaker position in the tail domain of KLP11 corroborated this assumption (Figure 19). Consequently, removing the kink positions in the KLP11/20 tail domains predicts an activation of its ATPase in steady state ATPase assays.

To this end, the putative kink position situated roughly in the middle of the tail domain of the KLP11/20 motor was replaced with glutamates as described above (Material and Methods, section 2.1.11.3). Such replacement of the glycine residues with glutamates was in fact sufficient to relieve the auto-regulation in the homodimeric kinesin-2 motor from *C. elegans*, termed Osm3 [119].

### **7.1. Removing the kink in the tail domain eliminates the auto-regulation in KLP11/20**

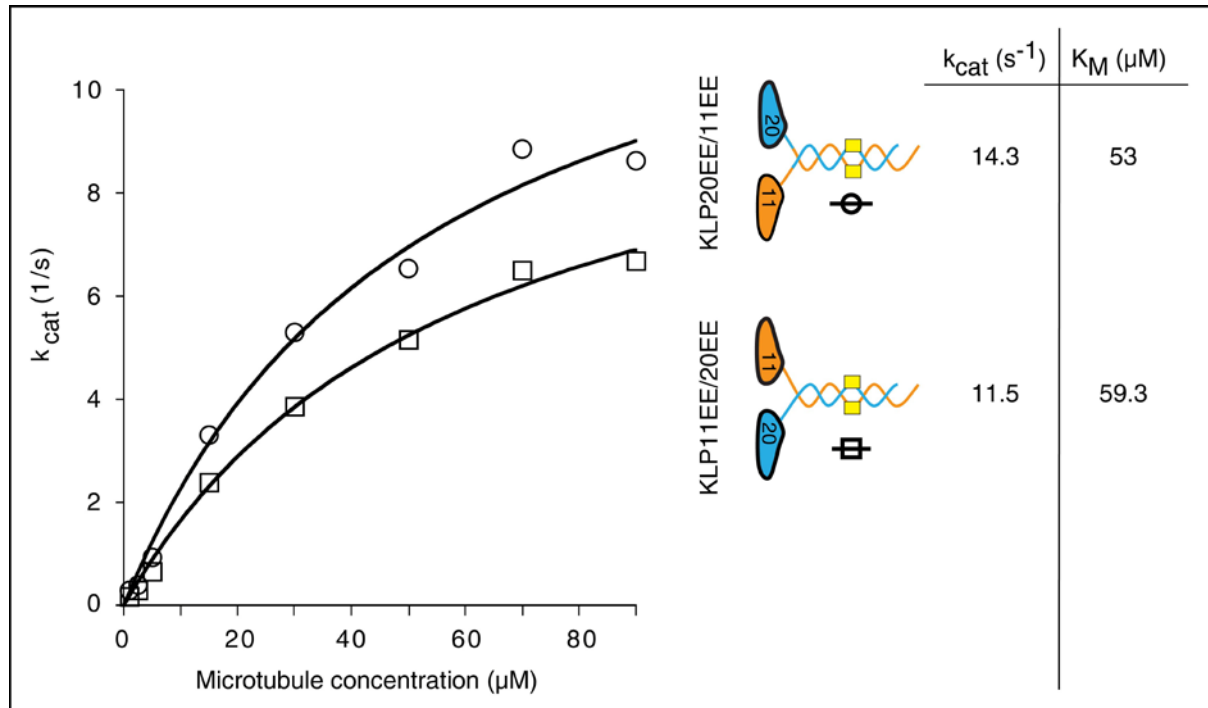
To test the catalytic activity of the KLP11/20 motor containing the glutamate residues in its tail domain (termed KLP11EE/20EE hereafter), steady-state ATPase assays and multiple motor gliding filament assays were performed. To directly compare the results obtained with the wild type tails (Figure 26), the kink in the chimeric construct with the swapped head positions KLP20/11 has also been replaced with glutamate residues, hereafter termed KLP20EE/11EE.

In microtubule-stimulated ATPase assays (Figure 30), the KLP11EE/20EE ( $k_{\text{cat}} = 11.5 \text{ s}^{-1}$ ,  $K_M = 59.3 \text{ }\mu\text{M}$ ) and KLP20EE/11EE ( $k_{\text{cat}} = 14.3 \text{ s}^{-1}$ ,  $K_M = 53 \text{ }\mu\text{M}$ ) constructs both displayed robust ATPase activities when compared to the wild type KLP11/20 (Figures 30 and 26). These results provide evidence that in addition to swapping head positions in the wild type motor, preventing the tail folding via flexible glycine residues by introduced glutamate residues also abolishes auto-regulation in the wild type KLP11/20 heterodimer.

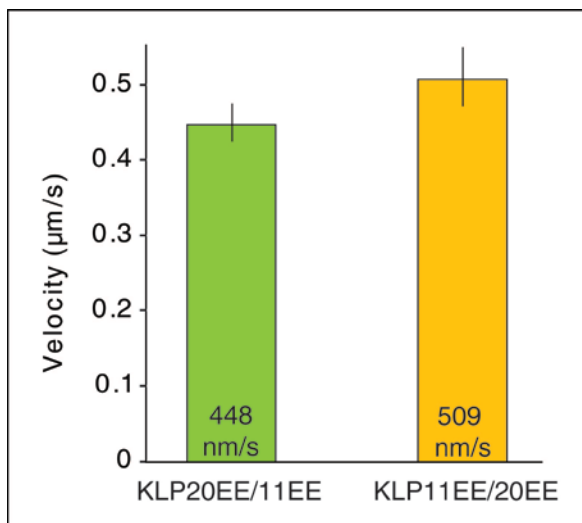
In the multiple motor gliding filament assays, the KLP11EE/20EE ( $509 \pm 39 \text{ nm/s}$ ,  $n = 30$ ) and the KLP20EE/11EE ( $448 \pm 25 \text{ nm/s}$ ,  $n = 32$ ) constructs again displayed consistent velocities (Figure 31), both among themselves and when compared to the wild type KLP11/20 and the chimeric KLP20/11 (Figure 27).

## Results

Taken together, removing the kink position in the tail domains or swapping the head positions in the wild type KLP11/20 motor is sufficient to circumvent the auto-regulation. The former is consistent with results obtained from kinesin-1 and homodimeric Osm3 kinesin-2 [52, 119] and the latter is a novel mechanism of relieving self-inhibition.



**Figure 30. Steady-state ATPase assay with KLP11EE/20EE and KLP20EE/11EE at saturating ATP concentrations (3 mM).** Both the KLP11EE/20EE and its corresponding KLP20EE/11EE chimera with swapped head positions displayed robust ATPase activity. Consistent results were obtained with 0.5mM ATP, demonstrating that the ATP concentration used in the assay was not limiting.



**Figure 31. Multiple motor gliding filament assays with KLP11EE/20EE and KLP20EE/11EE.** Upon binding of the constructs to the glass surface via their tail domains, the motors transported the fluorescently labeled microtubules at  $509 \pm 39$  nm/s (S.D.),  $n = 30$  for the KLP11EE/20EE and  $448 \pm 25$  nm/s (S.D.),  $n = 32$  for the KLP20EE/11EE.

## 7.2. Removing the kink in the homodimeric KLP11/11 does not affect the motor's activity

To rule out the possibility that the reduced ATPase activity of the homodimeric KLP11/11 motor is not due to auto-regulation mediated by the presence of the wild type tail domain containing the kink position (Figures 28 and 29), the chimeric KLP11EE/11EE construct was generated lacking such kink along with the KLP20EE/20EE construct as a control (described in Material and Methods, section 2.1.11.3).

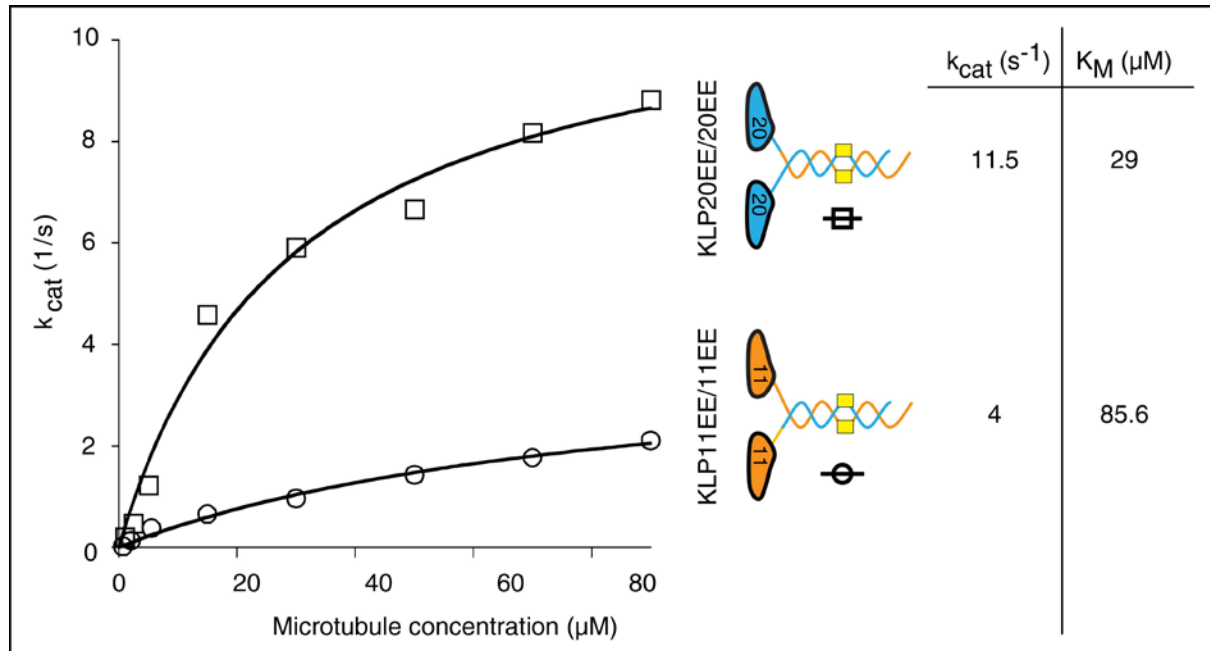
The analysis of the homodimeric KLP11EE/11EE and KLP20EE/20EE constructs using steady state ATPase (Figures 32 and 33) and multiple-motor filament gliding assays (Figure 34) again resulted in distinct kinetics as was observed with the equivalent constructs containing the wild type tails (Figures 28 and 29).

While in ATPase assays with increasing microtubule concentrations at saturating ATP concentrations (3 mM), the KLP11EE/11EE displayed a suppressed ATPase activity ( $k_{cat} = 4 \text{ s}^{-1}$ ,  $K_M = 85.6 \text{ } \mu\text{M}$ ), the KLP20EE/EE chimera showed a robust ATPase activity ( $k_{cat} = 11.5 \text{ s}^{-1}$ ,  $K_M = 29 \text{ } \mu\text{M}$ ). Consistent with this experiment, in ATPase assays with increasing ATP concentrations at low (15  $\mu\text{M}$ ) and high (30  $\mu\text{M}$ ) microtubule concentrations (Figure 33), the KLP11 subunit displayed slower activity compared to the KLP20 subunit.

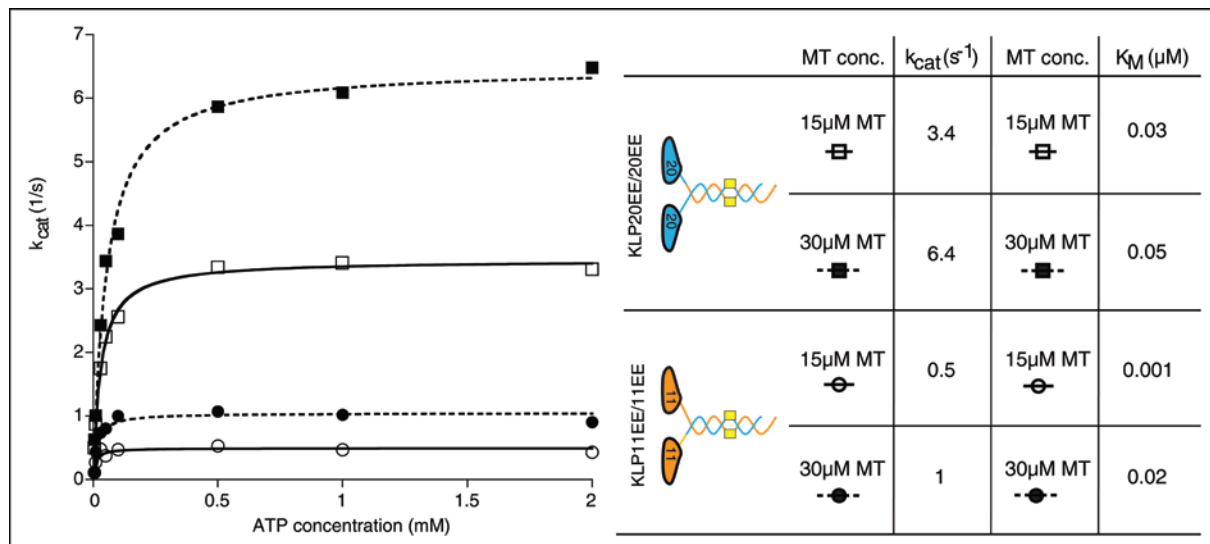
In agreement with the results obtained from the steady-state ATPase assays (Figures 32 and 33), the KLP11EE/11EE ( $232 \pm 30 \text{ nm/s}$  (S.D.),  $n = 25$ ) displayed significantly reduced velocities when compared to the KLP20EE/20EE ( $500 \pm 26 \text{ nm/s}$  (S.D.),  $n = 27$ ) in gliding filament assays (Figure 34).

Taken together, these results strengthen the view that the wild type heterodimeric KLP11/20 combines two kinetically different subunits to one double-headed motor. However, at this point a tail-mediated suppression of the ATPase of the KLP11 subunit cannot be fully ruled out as the results obtained with the KLP11EE/11EE construct addresses on the effect of the kink position. The tail domain may still impart auto-regulation onto the KLP11/11 chimera by a so far unknown mechanism.

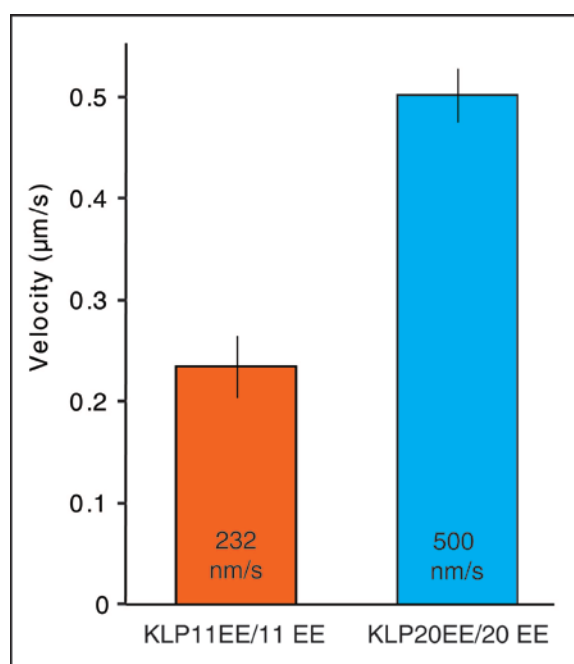
## Results



**Figure 32. Steady-state ATPase assays with KLP11EE/11EE and KLP20EE/20EE chimeras.** As observed with the equivalent constructs containing the wild type tails, the ATP turnover rates again differ for the two KLP11EE/11EE and KLP20EE/20EE chimeras in which the kink positions have been removed. The KLP11 subunit thus consistently displays a 2-3 fold slower activity compared to the KLP20 subunit.



**Figure 33. Steady-state ATPase assays with KLP11EE/11EE and KLP20EE/20EE chimeras in the presence of 15  $\mu M$  and 30  $\mu M$  microtubule.** As observed with previous ATPase experiments (Figure 32), the ATP turnover rates again differ for the two KLP11EE/11EE and KLP20EE/20EE chimeras at low and high microtubule concentrations. The KLP11 subunit consistently displays a slower activity compared to the KLP20 subunit.



**Figure 34. Multiple motor gliding filament assays with KLP11EE/11EE and KLP20EE/20EE chimera.** Consistent with the results from the ATPase assays (Figure 32 and Figure 33), the KLP11EE/11EE moves the microtubules at a reduced velocity ( $232 \pm 30$  nm/s (S.D.),  $n=25$ ) when compared to the KLP20EE/20EE ( $500 \pm 26$  nm/s (S.D.),  $n=27$ ).

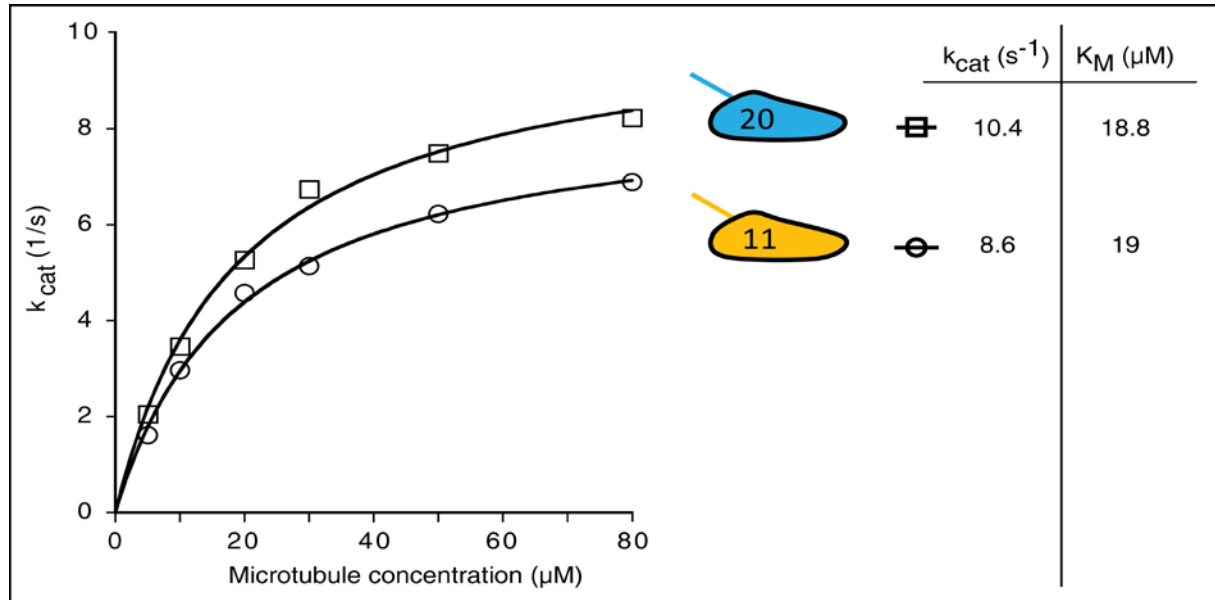
### 7.3 Monomeric KLP11 and KLP20 constructs are kinetically equivalent

The combination of two KLP11 catalytic subunits to one double-headed motor consistently displayed reduced activity compared to the combination of two KLP20 subunits (Figures 28, 32 and 33), suggesting that the wild type KLP11/20 motor may in fact employ two catalytically non-equivalent subunits.

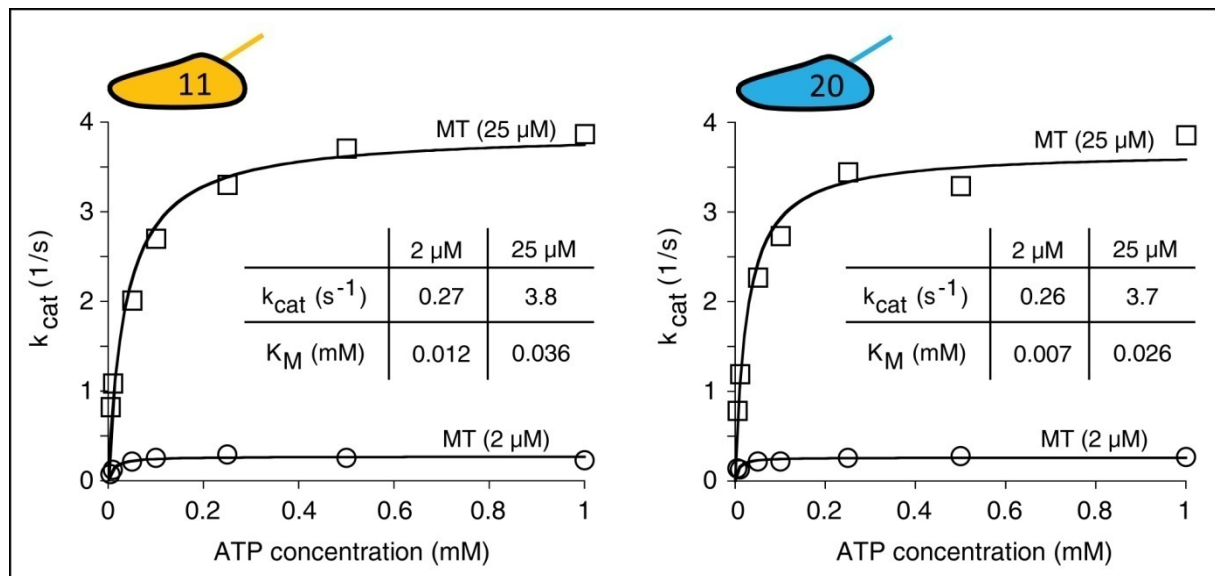
To dissect the kinetic properties of the KLP11 and KLP20 subunits without the interference of the tail region, monomeric head domains were expressed (Material and Methods, section 2.1.11.1) and probed for their activity in steady-state ATPase assays. Intriguingly, monomeric and thus unconstrained KLP11 and KLP20 head domains displayed comparable activities in the ATPase assays by microtubule titration (Figure 35, KLP11:  $k_{\text{cat}} = 8.6 \text{ s}^{-1}$ ,  $K_M = 19 \text{ } \mu\text{M}$  and KLP20:  $k_{\text{cat}} = 10.4 \text{ s}^{-1}$ ,  $K_M = 18.8 \text{ } \mu\text{M}$ ) as well as by ATP titration (Figure 36, KLP11:  $2 \text{ } \mu\text{M}$  MT:  $k_{\text{cat}} = 0.27 \text{ s}^{-1}$ ,  $K_M = 0.012 \text{ mM}$ ;  $25 \text{ } \mu\text{M}$  MT:  $k_{\text{cat}} = 3.8 \text{ s}^{-1}$ ,  $K_M = 0.036 \text{ mM}$  and KLP20:  $2 \text{ } \mu\text{M}$  MT:  $k_{\text{cat}} = 0.26 \text{ s}^{-1}$ ,  $K_M = 0.007 \text{ mM}$ ;  $25 \text{ } \mu\text{M}$  MT:  $k_{\text{cat}} = 3.7 \text{ s}^{-1}$ ,  $K_M = 0.026 \text{ mM}$ ). These results finally allow two testable conclusions: (A) the slow kinetics of the KLP11 subunit arises from the (so far unknown) interference from the tail domain or (B) the

## Results

dimerization of two KLP11 head domains into one double-headed motor is responsible for its slow kinetics.



**Figure 35. Steady-state ATPase (3 mM ATP) assays with monomeric KLP11 and KLP20 motors.** Monomeric KLP11 and KLP20 head domains display comparable activities in the absence of the tail domain, suggesting that either the tail-mediated inhibition or the dimerization into a double-headed motor may account for the differences observed with the ‘homodimeric’ KLP11/11 construct (Figures 28, 32 and 33).



**Figure 36. Steady-state ATPase assays with monomeric KLP11 and KLP20 motors in the presence of 2  $\mu M$  and 25  $\mu M$  microtubules.** Unconstrained, monomeric KLP11 and KLP20 catalytic head domains display equivalent ATP binding at saturating (25  $\mu M$ ) and sub-saturating (2  $\mu M$ ) microtubule concentrations.

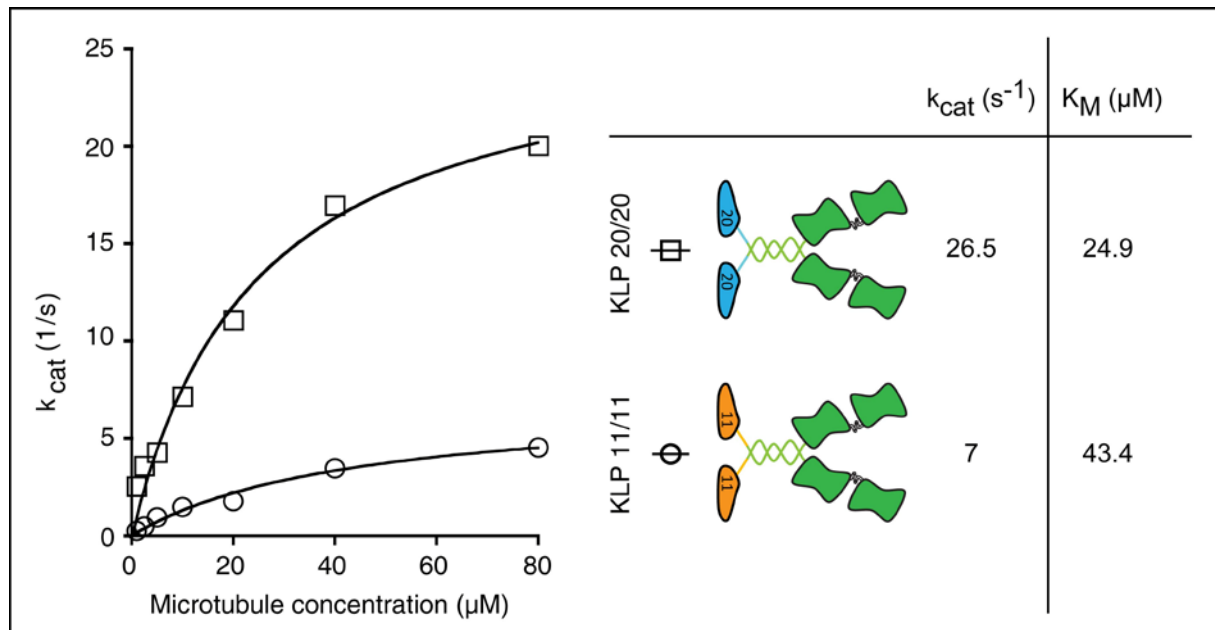
## **8. Dimerization brings about the observed kinetic distinctions in KLP11/11 and KLP20/20 chimeras**

So far, the analysis of the wild type KLP11/20 heterodimer and its corresponding KLP11/11 and KLP20/20 homodimeric chimeras revealed that (A) KLP11/20 is an auto-regulated motor, and (B) the subunits KLP11 and KLP20 may be kinetically non-equivalent. The analysis of the monomeric and therefore unconstrained KLP11 and KLP20, however, exposed that the basic catalytic subunits (devoid of the influence of the tail domain) are kinetically equivalent.

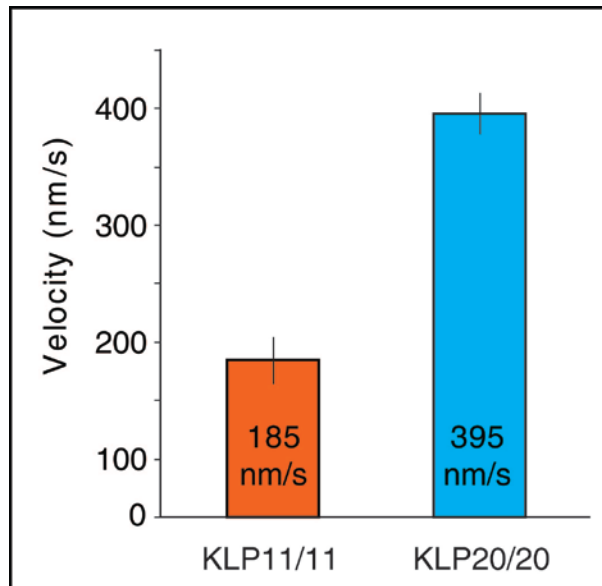
To resolve this discrepancy, KLP11 and KLP20 constructs were designed in which the tail domains have been replaced with the molecular zipper GCN4 to homodimerize the catalytic KLP11 and KLP20 head domains, respectively. In addition, flexible residues of increasing lengths have been introduced between the head domains in the KLP11/11 GCN4 to probe putative effects of dimerization on the kinetics of this homodimer. Lastly, all constructs were C-terminally tagged with tandem SfGFP to enable studies using fluorescence microscopy (Material and Methods, section 2.1.11.4).

The GCN4-mediated homodimerization of the respective KLP11 and KLP20 head domains eliminates any inhibitory effects that may arise from the presence of the tail region. If the suppressed ATPase activity of the KLP11/11 is a result of such effects, the activities of the KLP11/11 GCN4 and KLP20/20 GCN4 is expected to be similar as observed with the monomeric head domains (Figures 35 and 36). The analysis of the KLP11/11 GCN4 and KLP20/20 GCN4 homodimers in filament gliding as well as in ATPase assays revealed that the combination of two KLP11 and two KLP20 head domains in fact results in distinct kinetics (Figure 37). The suppressed ATPase activity of the KLP11 head domain is thus brought about by the homodimerization, either by its full-length stalk (Figures 28, 32 and 33) or by the molecular zipper GCN4 (Figure 37). Lastly, a tail-mediated suppression of the ATPase activity of the KLP11 can be excluded.

## Results



**Figure 37. ATPase assays with KLP11/11 and KLP20/20 constructs homodimerized via the GCN4 zipper.** As it is the case with the homodimeric KLP11/11 and KLP20/20 chimeras containing the full-length tails, the ATPase activity of the KLP11/11 head combination is suppressed when compared to the KLP20/20 head combination.



**Figure 38. Multiple motor gliding filament assays with KLP11/11 and KLP20/20 constructs homodimerized via the GCN4 zipper.** Consistent with the results from the ATPase assays (Figure 37), the KLP11/11 head combination moves the microtubules at a reduced velocity ( $185 \pm 28$  nm/s (S.D.),  $n = 38$ ) when compared to the KLP20/20 head combination ( $395 \pm 20$  nm/s (S.D.),  $n = 29$ ).

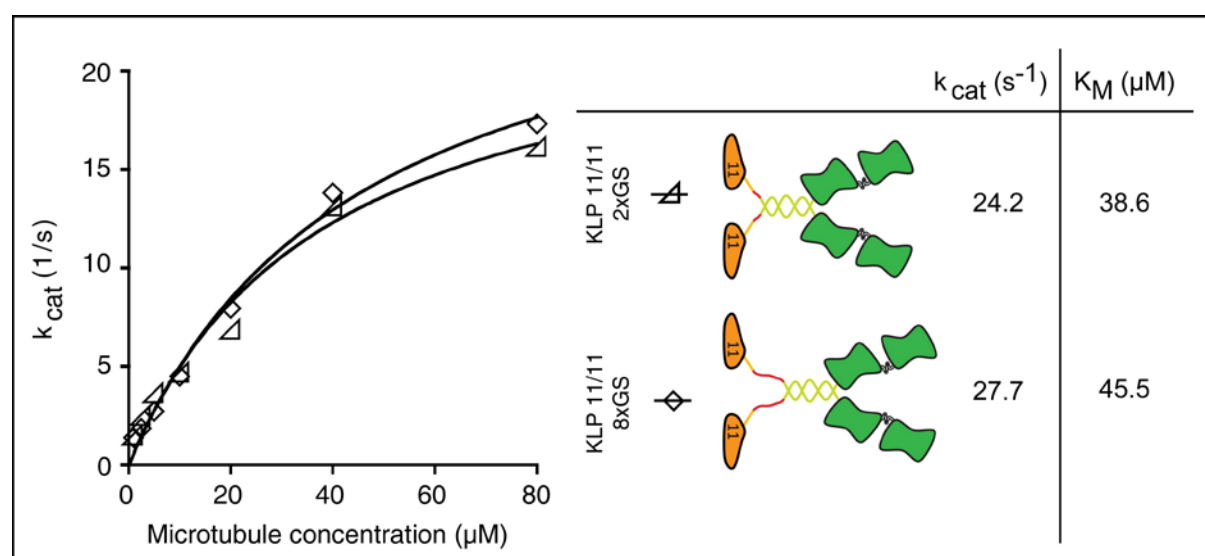


## 9. The suppression of the KLP11/11 activity is relieved by flexible residues

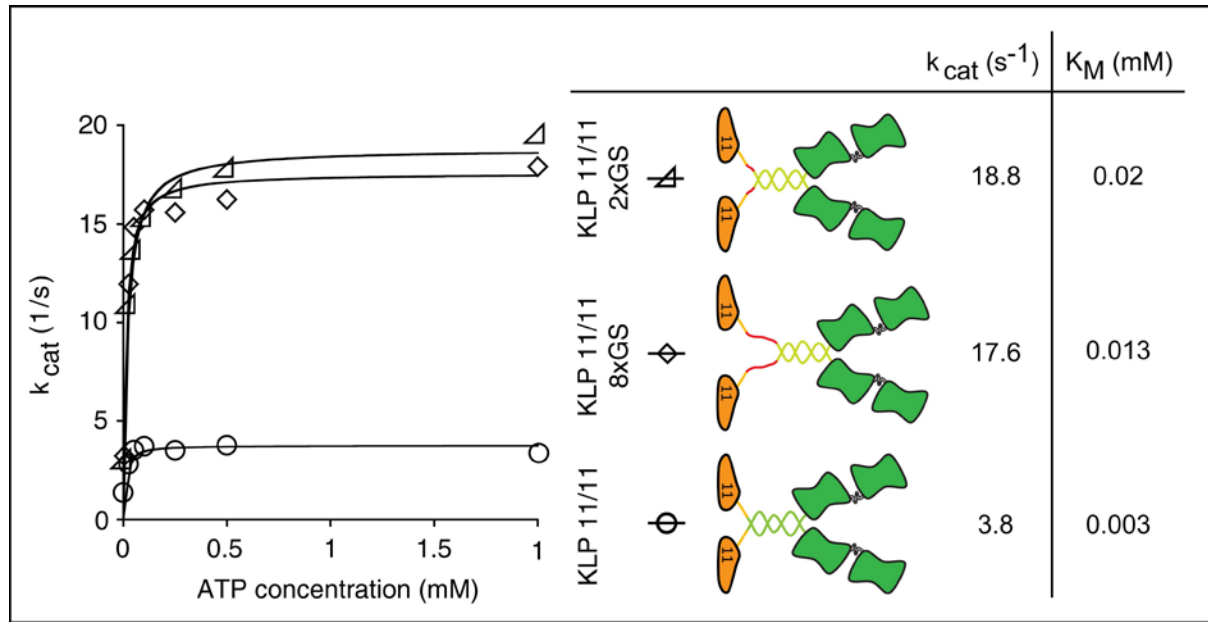
The kinetic equivalence of the monomeric KLP11 and KLP20 head domains on the one hand (Figures 35 and 36) and their non-equivalence within the dimeric context on the other hand (Figure 37) suggests that steric hindrance may account for the suppressed ATPase of the KLP11/11 constructs. To directly test this hypothesis, glycine/serine repeats of increasing lengths (2xGS and 8xGS) were introduced between the KLP11 head domains in the dimeric KLP11/11 GCN4.

Figure 39 demonstrates that the insertion of the short extension (2xGS) is already sufficient to activate the KLP11/11 GCN4 motor to levels comparable with the KLP20/20 GCN4 (Figure 37) homodimer in the microtubule-activated ATPase assay. In agreement with this experiment, complementary ATP-activated ATPase assays (Figure 40) performed at 60  $\mu\text{M}$  microtubule concentration underlined that the suppression of homodimeric KLP11/11 construct is relieved by flexible GS repeats.

To conclude, the suppressed ATPase activity of the KLP11 subunit is brought about by homodimerization that is relieved by flexible extensions situated between the KLP11 head domains. Interestingly, additional flexibility provided by 8xGS repeats does not further activate the dimeric KLP11/11 motor.



**Figure 39. Microtubule activated ATPase assays with GS extended KLP11/11 constructs in the presence of saturating ATP (3 mM).** Introducing the flexible GS extensions relieves the suppressed ATPase activity of the KLP11/11 homodimer. The ATPase rates are comparable with the values of KLP20/20 GCN4 homodimer (Figure 37).

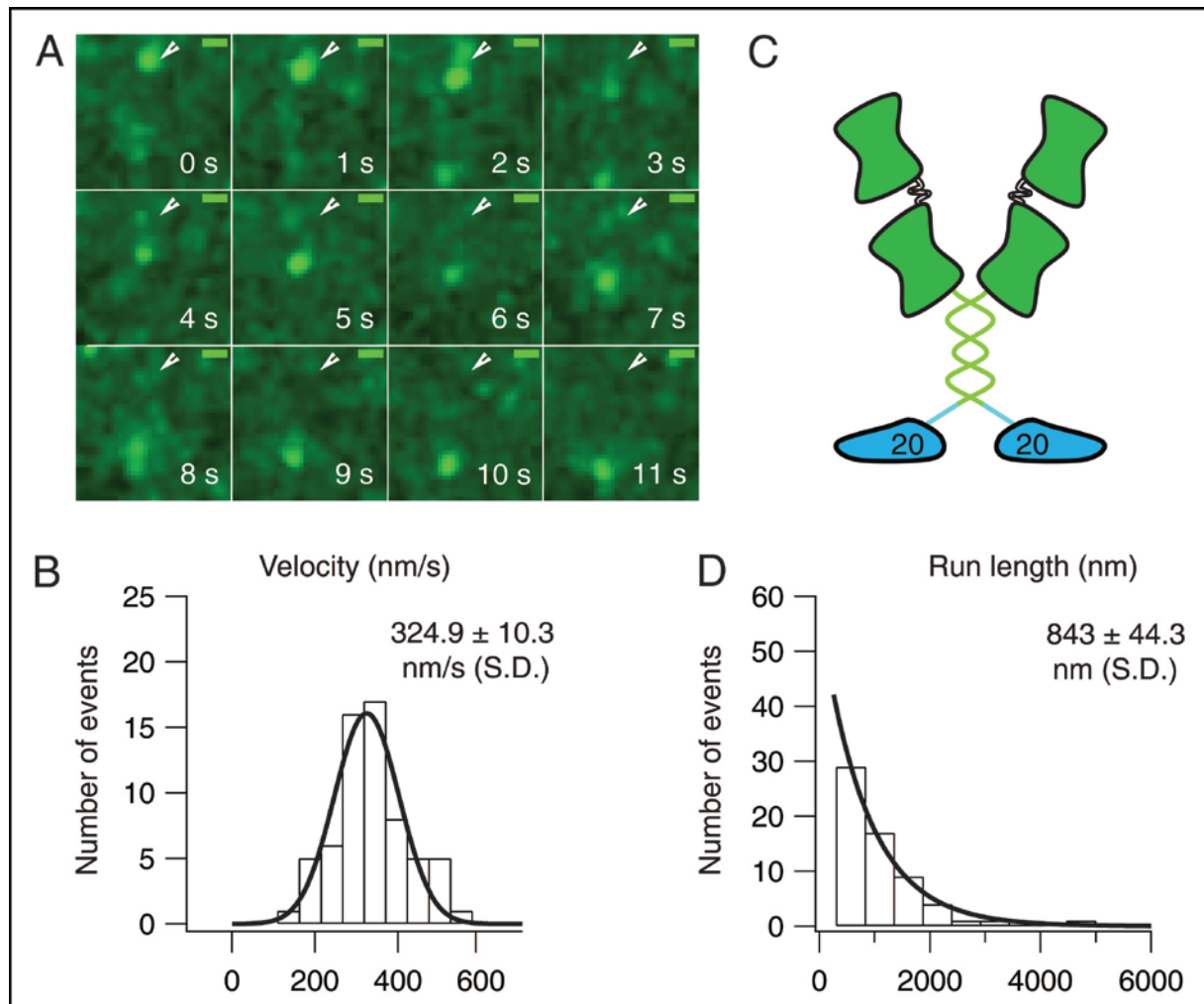


**Figure 40. ATP activated ATPase assays with GS extended KLP11/11 constructs in the presence of microtubules (60  $\mu$ M).** As observed with previous ATPase experiments (Figure 39), the GS extensions relieve the suppressed ATPase activity of the KLP11/11 homodimer.

## 10. Homodimeric KLP20/20 is processive, KLP11/11 is not

The ATPase activity of a motor, however, does not serve as an indicator of processive movement, *i.e.*, the motor's ability to take consecutive steps as a single molecule. To test whether the GCN4-mediated dimerization of the KLP11 and KLP20 head domains generates processivity, and if so, which constructs are capable of processive movement, the respective constructs were subjected to single molecule fluorescence assays. Briefly, the microtubules are attached to the surface and the movement of single, SfGFP-tagged motors is observed in the evanescent field of the TIRF microscope (Refer to section 2.2.8 in Material and Methods for experimental details).

Figure 41 shows the processive movement by the KLP20/20 motor, demonstrating that the GCN4-mediated dimerization of the KLP20 head domains is capable of generating processivity. In contrast, its corresponding KLP11/11 GCN4 motor never displayed equivalent processive movement at the single molecule level.

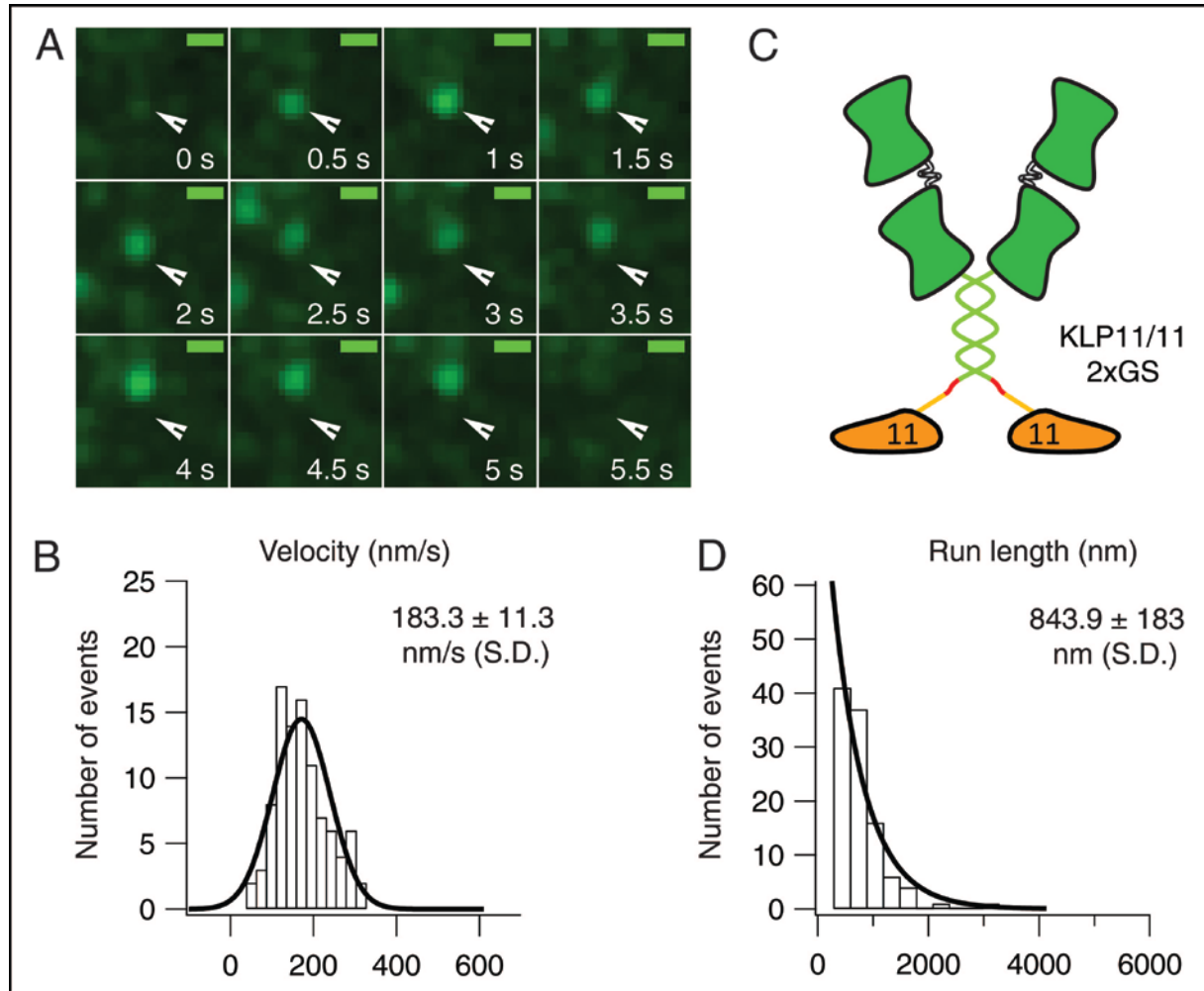


**Figure 41. Homodimeric KLP20/20 motor dimerized via GCN4 moves processively along microtubules.** **A)** TIRF microscopy image sequence showing the displacement of a single homodimeric KLP20/20 motor (indicated by white arrowheads) over time. Scale bars represent 1  $\mu\text{m}$ . **B)** Velocity histogram of the movement fitted to a Gaussian. KLP20/20 motors moved with a velocity of  $324.9 \pm 10.3$  nm/s (S.D.),  $n = 64$ . **C)** Schematics of the construct. **D)** Run length distribution plotted as histogram and fitted to a single exponential ( $n = 64$ ). KLP20/20 moved about  $843 \pm 44.3$  nm (S.D.),  $n = 64$ , along MT track.

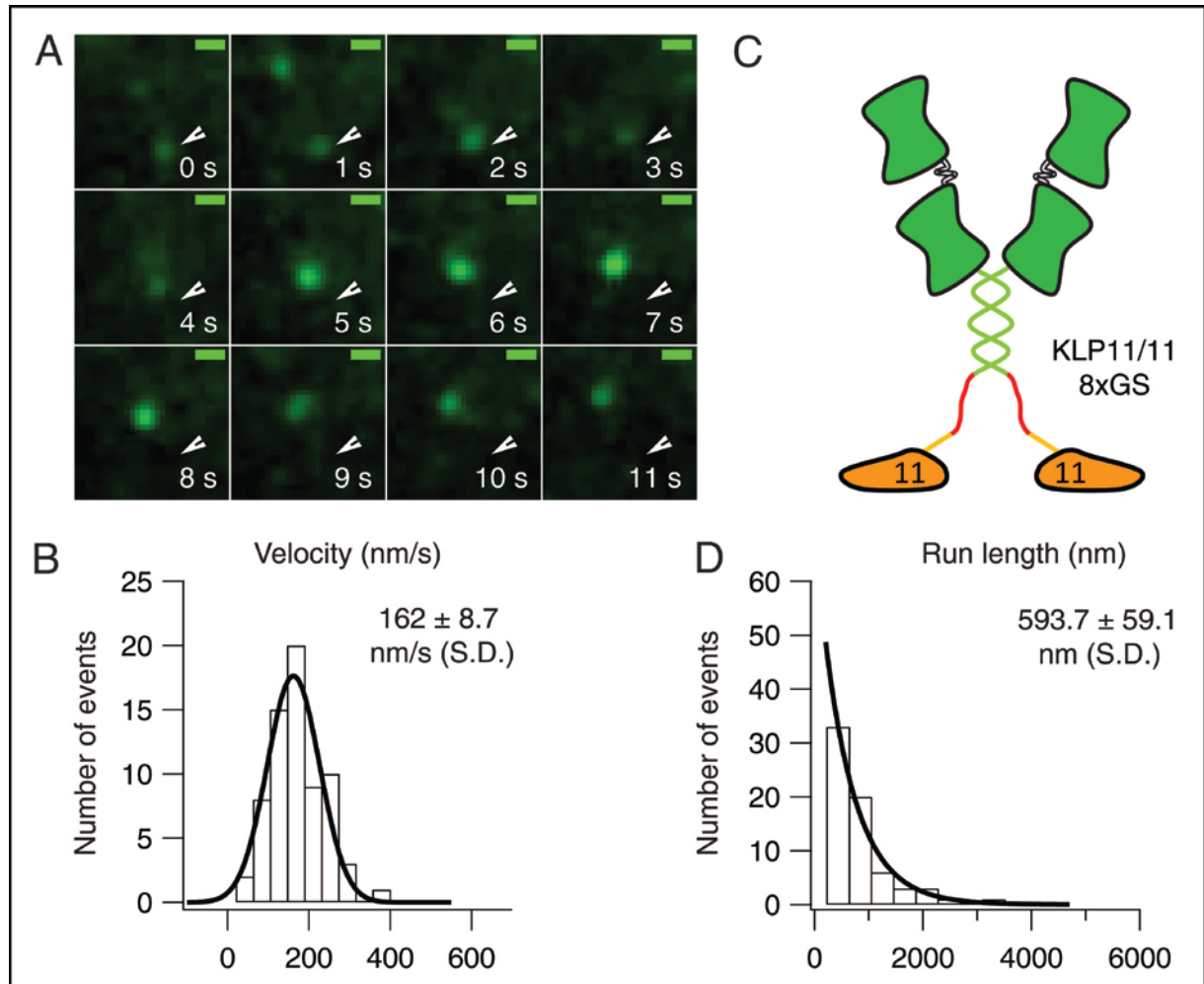
## 11. KLP11/11 GCN4 motors with flexible extensions between the head domains are processive

As described above, the GCN4-mediated dimerization of the KLP11 head domains resulted in an unprocessive motor with a suppressed ATPase activity. However, introducing flexible extensions between the head domains in the dimeric KLP11/11 motor was sufficient to activate its ATPase in microtubule-activated ATPase assays (Figures 39 and 40).

Figure 42 and Figure 43 show that circumventing the steric hindrance also results in processive movement for both KLP11/11 dimers containing the 2xGS and 8xGS repeats, respectively. Interestingly, the increasing length of the flexible extensions affects neither the velocity nor the run length of the dimeric KLP11/11 GCN4.



**Figure 42. The presence of the shortest flexible extension in the KLP11/11 GCN4 motor enables processive movement.** **A)** TIRF microscopy image sequence showing the displacement of a single homodimeric KLP11/11 GCN4 containing the 2xGS extension (indicated by white arrowheads) over time. Scale bars represent 1  $\mu\text{m}$ . **B)** Velocity histogram of the movement fitted to a Gaussian. KLP11/11 2xGS motors moved with a velocity of  $183.3 \pm 11.3$  nm/s (S.D.),  $n = 105$ , along MT track. **C)** Schematics of the construct. **D)** Run length distribution plotted as histogram and fitted to a single exponential ( $n = 105$ ). KLP11/11 2xGS moved about  $843.9 \pm 183$  nm (S.D.),  $n = 105$ , along MT track.



**Figure 43. Increasing the length of the flexible extensions does not significantly impact the kinetic parameters of the KLP11/11 GCN4.** **A)** TIRF microscopy image sequence showing the displacement of a single homodimeric KLP11/11 GCN4 motor containing 8xGS extensions between its head domains (indicated by white arrowheads) over time. Scale bars represent 1  $\mu\text{m}$  **B)** Velocity histogram of the movement fitted to a Gaussian. KLP11/11 8xGS motor moved with a velocity of  $162 \pm 8.7$  nm/s (S.D.),  $n = 68$ , along MT track. **C)** Schematics of the construct. **D)** Run length distribution plotted as histogram and fitted to a single exponential. KLP11/11 8xGS moved about  $593.7 \pm 59.1$  nm (S.D.),  $n = 68$ , along MT track.

## 12. Summary of results

Molecular engineering has enabled the dissection of the kinetic properties of the subunits KLP11 and KLP20 constituting the heterodimeric KLP11/20 motor from *C. elegans*. Four main conclusions can be drawn from these analyses:

- (A) Wild type KLP11/20 is auto-regulated and this inhibition can be relieved either by swapping the relative head positions (KLP20/11) or by replacing the flexible kink position by stiff residues (KLP11EE/20EE) or by removing the KLP11 subunit (KLP20/20).
- (B) The dimerization of two KLP11 vs. two KLP20 head domains either by the wild type tail or by the unrelated molecular zipper GCN4 results in motors with distinct kinetic properties.
- (C) The GCN4-mediated dimerization of the KLP11 subunit results in an unprocessive motor whereas the corresponding dimerization of the KLP20 subunit results in a processive motor.
- (D) Introducing flexible residues between the KLP11 head domains is sufficient to impart processivity onto the homodimeric KLP11/11 GCN4 motor.

## Results







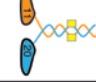
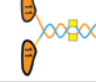
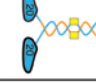



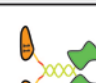

| Generated constructs                            |   | ATPase                       |                  |                               |            | Gliding filament<br>(nm/s) | Single molecule<br>(nm/s)    |
|---|---|------------------------------|------------------|-------------------------------|------------|----------------------------|------------------------------|
|   |   | $K_M$ for MT (3 mM ATP)      |                  | $K_M$ for ATP (25 $\mu$ M MT) |            |                            |                              |
|   |   | $k_{cat}$ (s <sup>-1</sup> ) | $K_M$ ( $\mu$ M) | $k_{cat}$ (s <sup>-1</sup> )  | $K_M$ (mM) |                            |                              |
| Monomeric constructs                            | 11 Monomer       | 8.6                          | 19               | 3.8                           | 0.036      |                            |                              |
|   | 20 Monomer       | 10.4                         | 18.8             | 3.7                           | 0.026      |                            |                              |
| Kinesin-2 constructs containing wild-type tails | KLP11/20         | 1.8                          | 19               |                               |            | 430 $\pm$ 50 nm/s (S.D.)   |                              |
|   | KLP11/11         | 3                            | 38.5             |                               |            | 190 $\pm$ 13 nm/s (S.D.)   |                              |
|   | KLP20/20         | 7.2                          | 9.9              |                               |            | 380 $\pm$ 20 nm/s (S.D.)   |                              |
|   | KLP20/11         | 11.3                         | 25               |                               |            | 430 $\pm$ 30 nm/s (S.D.)   |                              |
| Kinesin-2 constructs containing EE mutations    | KLP11EE/20EE    | 11.5                         | 59.3             |                               |            | 509 $\pm$ 39 nm/s (S.D.)   |                              |
|   | KLP11EE/11EE   | 4                            | 85.6             | 1                             | 0.02       | 232 $\pm$ 30 nm/s (S.D.)   |                              |
|   | KLP20EE/20EE   | 11.5                         | 29               | 6.4                           | 0.05       | 500 $\pm$ 26 nm/s (S.D.)   |                              |
|   | KLP20EE/11EE   | 14.3                         | 53               |                               |            | 448 $\pm$ 25 nm/s (S.D.)   |                              |
| Kinesin-2 constructs containing GCN4 tails      | KLP20/20       | 26.5                         | 24.9             |                               |            | 395 $\pm$ 20 nm/s (S.D.)   | 324.9 $\pm$ 10.3 nm/s (S.D.) |
|   | KLP11/11       | 7                            | 43.4             | 3.8                           | 0.003      | 185 $\pm$ 28 nm/s (S.D.)   |                              |
| Kinesin-2 constructs with flexible extensions   | KLP11/11 2xGS  | 24.2                         | 38.6             | 18.8                          | 0.02       |                            | 183.3 $\pm$ 11.3 nm/s (S.D.) |
|   | KLP11/11 8xGS  | 27.7                         | 45.5             | 17.6                          | 0.013      |                            | 162 $\pm$ 8.7 nm/s (S.D.)    |

Figure 44. Summary of generated constructs and achieved results.

## Discussion

Heteromeric kinesin-2 (KLP11/20) from *C. elegans* combines, two different motor subunits and an accessory subunit (KAP) into a heterotrimeric motor to be functional in intraflagellar transport (IFT) [115, 145]. One of the main goals of this thesis was to dissect the molecular properties of the catalytic subunits KLP11 and KLP20 kinesin-2 from *C. elegans*. It was intended to understand the benefits of a heterodimeric compared to a homodimeric motor.

### 1. Kinesin-2 (KLP11/20) from *C. elegans* is auto-regulated

It was already known, that kinesins were regulated at several levels [81], including a regulation by autoinhibition to avoid futile ATP consumption in an inactive state. In different studies, kinesin-1 [49, 51, 53-56, 58, 59] and kinesin-3 [146-148] have been shown to control motor activity by autoinhibition. Electron microscopy and FRET experiments could provide evidence that without cargo bound, conventional kinesin is in an inactive and folded conformation [56, 82]. Hereby, the flexible kink region in the middle of the stalk was crucial, allowing the folding of the tail domains onto the head domains [49, 50, 52]. By this folding, the tail domains are brought in close proximity to the catalytic head domains interacting with each other [48-56]. Folding and consequently interaction leads to slowed ADP release, whereas the ability of kinesin to bind and move along the microtubule lattice is not abolished [50]. The head-tail interaction creates a 'lock down', preventing the movement of the motor domains that is necessary to undock the neck linker and release ADP [84].

Also with homodimeric kinesin-2 from *C. elegans* (Osm-3) and mouse (Kif 17) it has been shown, that the tail domains play a major role [119, 120] in controlling motor activity. By point mutation in the predicted hinge region of Osm-3's coiled-coil stalk as well as deletion of that hinge raised the ATPase activity of the motor and additionally induced robust processive movement [119].

By analyzing the coiled-coil formation of KLP11/20 (Figures 19 and 20), we could also confirm a hinge region in the KLP11 subunit. Initial testing of the wild type KLP11/20 in ATPase assays showed a motor with low activity. Interestingly, the same motor showed gliding velocities in gliding filament assays close to values



observed from *in vivo* assays [116, 118]. This was facilitated because the stalk and tail domains of kinesin-2 interact with the glass surface in the flow chamber (Figure 14), releasing the head domains from the control of the tail domains and allowing the transport of fluorescently labeled microtubules. Interestingly, in microtubule-stimulated bulk ATPase assays, a release of the head domains in wild type KLP11/20 was prevented, providing an autoinhibited motor with very low kinetic activity. These experiments confirmed that wild type KLP11/20 is also controlled by a tail mediated autoinhibition mechanism to that of other kinesins, preventing futile ATP consumption if not activated.

Having two different KLP11 and KLP20 subunits assembling kinesin-2 provided six possible autoinhibition conformations: KLP11 tail only inhibits KLP11 head (1) or KLP20 head (2), KLP20 tail only inhibits KLP11 head (3) or KLP20 head (4), KLP11 tail inhibits KLP11 head and KLP20 tail inhibits KLP20 tail (5) or vice versa (6). Testing the 'wild type tail' chimeric constructs provided fully active KLP20/20, excluding conformations number (2) and (4), whereas the KLP11/11 combination was suppressed. Therefore, initially it was thought that only the KLP11 subunit is controlled by autoinhibition (conformations number (1) and (3)). Having an active mixed chimera KLP20/11 with swapped head positions, lead to the assumption that the regulation of the native heterodimer has to be asymmetric and depends on the correct positioning of the head domains, bringing conformations (5) and (6) in focus. Vukajlovic *et al.* (2011) [149] investigated oligomer formation in kinesin-2 from *C. elegans* and found that a C-terminal dimerization seed at the end of the stalk was necessary for heterodimerization of KLP11/20. Combining a full-length tail KLP11 with C-terminally shortened KLP20 tail and vice versa provided no heterodimerization. So, it was not possible to probe for conformations number (5) and (6) in ATPase assays. Having also active GS constructs in ATPase assays, confirming steric hindrance for KLP11/11 combinations suppression, conformations number (1) and (3) could be excluded. Taken together, with the performed experiments, pinpointing which tail inhibits which head domain was not possible.

## **2. Monomeric head domains are almost equivalent**

The chimeric constructs were generated as described by Brunnbauer *et al.* (2010) [126] in analogy to KIF3A/A and KIF3B/B chimeric constructs generated by Zhang *et al.* (2004) [150] (Figure 9) to ensure dimerization of desired motor constructs. All ATPase and gliding filament assays performed with full-length KLP11/11 combinations resulted in a suppressed motor, indicating that the KLP11/20 combines two non-equivalent subunits. So, testing for the kinetic properties of the respective minimal catalytic subunits of KLP11/20 was essential to check this hypothesis. These minimal catalytic subunits were the monomeric head domains including the neck linker region.

They were generated by cutting the head domains just after the neck linker region including an extra extension of eight amino acids of the stalk, where already the  $\alpha 7$  region started (Figure 8). Testing both monomeric head domains in ATPase assays provided two almost kinetically equivalent subunits. With these experiments, the assumption that KLP11/20 consists of two non-identical subunits whose kinetic functions differ was eliminated. Furthermore, a control of the whole motor activity by controlling only the KLP11 subunit could be excluded. The reason for suppressed activity of KLP11/11 as a full-length 'wild type tail' or 'EE tail' homodimeric construct had to be another one.

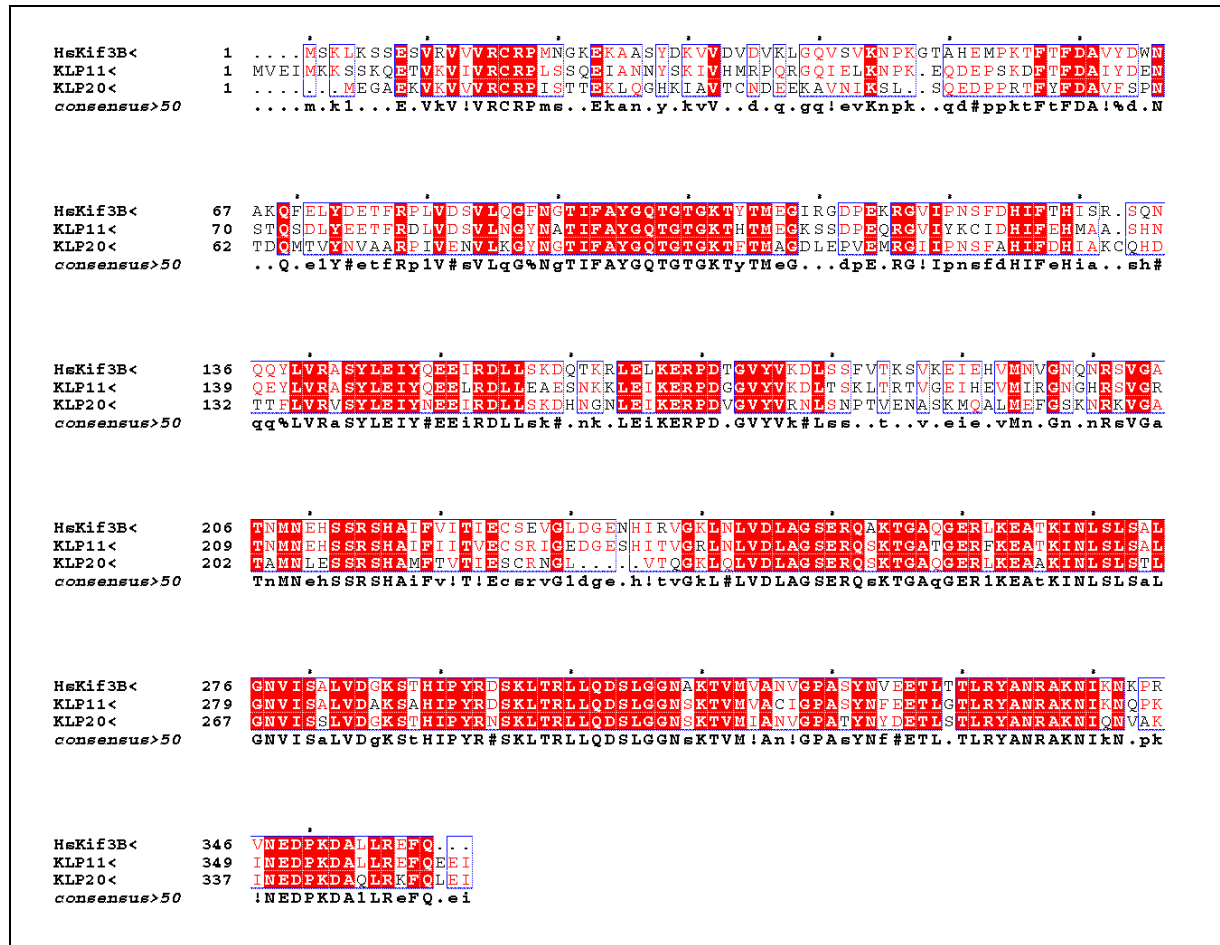
## **3. Homodimeric KLP11/11 combinations are suppressed due to steric hindrance**

Assuming that the full-length tail domains might influence motor activity by an intermolecular interaction, we generated 'GCN4 tail' constructs. A suppressed KLP11/11 GCN4 construct excluded an inhibition by the tail domains, leading to the suggestion that steric hindrance might be the reason preventing the KLP11 subunit from being as active as KLP20. 3D reconstructions based on the crystal structure of the head domain of human Kif3B as a template [151-153] showed that KLP11 was quite similar to KLP20, with slight exceptions (Figure 46, yellow circles), although they only share about 71% positive and 58% identical amino acids (Figure 45). On the other hand, KLP11 shares 81% positive and 69% identical amino acids with human Kif3B, whereas KLP20 shares 73% positive and 58% identical amino acids

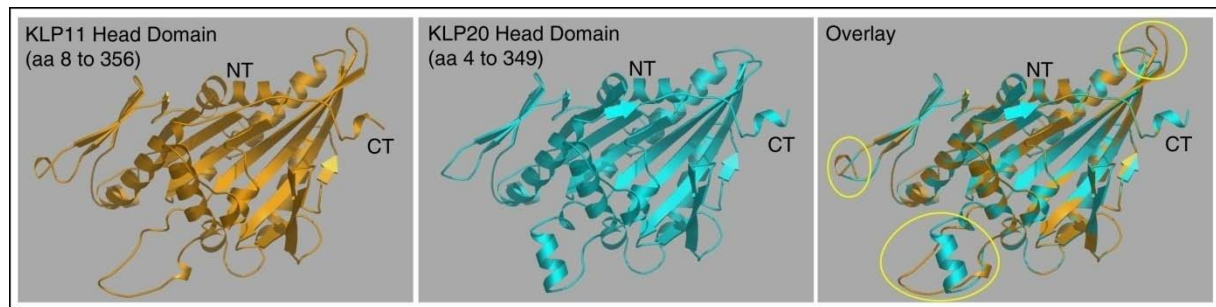
[141-143]. Measurements of the relative mean square displacement in angstrom of the KLP11 amino acid sequence versus the KLP20 amino acid sequence (Figure 47) underlined the observed difference, whereas the distance around amino acid 230 (corresponding to the 3<sup>rd</sup> peak in the graph) promised to be the crucial one. This peak in close proximity to the C-terminal region of the head domain (CT) could be of relevance in preventing the head domains to pass by each other, when combined into a homodimer, leading to steric hindrance.

By introducing additional flexible neck extensions, namely two and eight glycine and serine repeats in the neck region of the KLP11 GCN4 construct, we probed for steric hindrance. Actually, by introducing just two GS repeats in the neck linker region of KLP11 (total of 13 amino acids: four aa from GS repeats and eight aa from  $\alpha 7$ ) turned on the activity of KLP11/11 in ATPase assays (Figures 39 and 40). Interestingly, increasing the length of the flexible extensions (8xGS repeats) didn't affect the kinetic activity of KLP11/11 GCN4. With these results, evidence was provided that both subunits are kinetically similar, as already observed with monomeric head domain constructs.

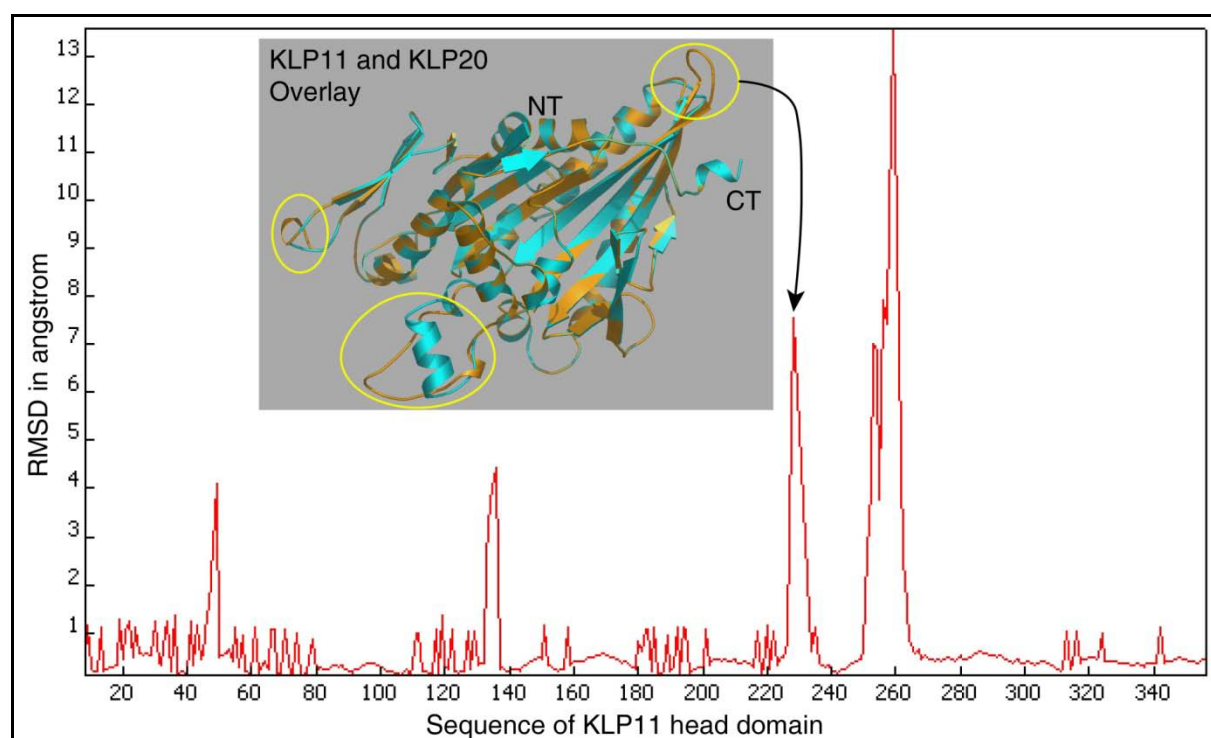
## Discussion



**Figure 45. Amino acid sequence alignment of head domains of KLP11, KLP20 and human Kif3B.** Interestingly, KLP11 and KLP20 head domains shared only 71% positive and 58% identical amino acids. On the other hand, KLP11 shared 81% positive and 69% identical amino acids to human Kif3B, whereas KLP20 shared 73% positive and 58% identical amino acids [141-143]. KLP11 head domain had more similarity to HsKif3B than to KLP20.



**Figure 46. 3D reconstruction of KLP11 and KLP20 head domains based on HsKif3B [151-153] (3b6u B subunit).** Using the HsKif3B kinesin as a template for 3D reconstructions of the catalytic head domains of KLP11 and KLP20 revealed a large structural identity for both motors although the lack of high sequence identity was given. Having only about 71% positive and 58% identical amino acids (Figure 45) gave reason to assumption that the head domains had different structures. The main differences based on the 3D reconstruction are depicted with yellow circles. The loop in close proximity to the C-terminal end of the head domain of KLP11 subunit might play a role in suppressing the head domains if KLP11 is combined to a homodimer. (CT= C-terminal, NT= N-terminal)



**Figure 47. Measurements of the relative mean square displacement in angstrom of the KLP11 amino acid sequence versus the KLP20 amino acid sequence** (NOC 3.01 software, M.E. Chen, H.X. Cang, H. Nymeyer). The calculated distance around amino acid 230 (3<sup>rd</sup> peak in the graph), corresponding to the loop of KLP11 in close proximity to the C-terminal part of the head, could play a crucial role in kinetic behavior of KLP11. This region of the head domain could be of relevance in preventing the head domains to pass by each other, leading to a steric hindrance.

#### 4. Neck linker region and kinetic activity

The neck linker was known to play a major role during the mechano-chemical cycle of kinesin molecules. On the basis of crystal structures, Hariharan and Hancock (2009) [154] defined neck linker regions for kinesin-1 as well as kinesin-2. While kinesin-1 had a neck linker region of 14 amino acids, kinesin-2's neck linker was composed of 17 amino acids. In both cases the neck linker regions were embedded between alpha helical structures, one ending the head domain ( $\alpha 6$ ) and one starting the stalk region ( $\alpha 7$ ). Muthukrishnan *et al.* (2009) [155] have investigated the processive behavior of *Drosophila* kinesin-1 and *mouse* kinesin-2 at the single molecule level and found that kinesin-2 was less processive than kinesin-1. Shastry and Hancock (2010) [156] suggested that the neck linker length determines the degree of processivity in kinesin-1 and in kinesin-2. Shortening the neck linker region of kinesin-2 enhanced its processivity [156], whereas the extension of the neck linker in kinesin-1 decreased its processivity. The same observation was made by

Muthukrishnan *et al.* (2009) [155], assuming that the mechanical tension transmitted through the neck linker domains was reduced [155]. Yildiz *et al.* (2008) [157] have intensively investigated the extension by artificial peptides of the neck linker region of kinesin-1, which led to a reduction of the intramolecular tension between the motor domains. A dramatic decrease of velocity was observed, although the processivity was not much affected. Also, strain between both motor domains was found to be responsible for reduced velocities of the constructs.

Interestingly, our GCN4 constructs included the respective neck linker region (17 aa) and an additional eight amino acids of  $\alpha$  7 (Figure 11). This 'native' elongation of the neck linker region can be assumed to reduce the tension between both head domains. In gliding filament assays and ATPase assays, a decrease in activity could not be observed for KLP20/20 GCN4 constructs containing these eight additional aa in their neck regions compared to 'wild type tail' and 'EE tail' KLP20/20 constructs lacking such an extension (Figures 28, 32 and 37). Same observations were made with KLP11/11 GCN4 constructs. Despite these eight amino acid extensions, homodimeric KLP11/11 GCN4 showed almost the same activity as the 'wild type tail' and 'EE tail' KLP11/11 constructs (Figures 28, 32 and 37). Furthermore, it lacked processive movement and displayed suppressed activity in gliding and ATPase assays (Figures 37 and 38), indicating that the additional eight aa were not sufficient to avoid a steric hindrance. Homodimeric KLP11/11 GCN4's activity in ATPase assays was turned on only by inserting additional four amino acids (2xGS construct, total of 12 aa extension) in the neck region. The 8xGS construct with its 24 aa elongation (eight aa from  $\alpha$ 7 and 16 aa as GS repeats) showed almost the same activity in ATPase assays as the 2xGS construct containing only a 12 aa extension in their neck region (Figures 39 and 40).

## 5. Neck linker region and processivity

It has been reported, that in addition to its role in force generating conformational changes, an equally important role of the neck linker is to transmit tension between the two head domains [154]. All mechanisms trying to explain processive movement of kinesin involve mechanical tension transmitted between the head domains [66,154, 158-161]. So, by inserting additional amino acids in the neck linker region of

kinesin-1, Yildiz *et al.* (2008) [157] found that the processivity of this motor was influenced. Proline extended construct's velocities decreased with the number of inserted proline residues, whereas no clear correlation between the length of the insertion and processivity could be observed. Glycine and serine extended (14 additional aa) kinesin constructs showed even lower velocities than the proline constructs, whereas the run length was not affected strikingly. Interestingly, as was observed also in our investigations with the KLP11 GCN4 GS constructs and KLP20 GCN4 constructs, the maximal microtubule-stimulated ATP turnover rates between WT kinesin-1 and the neck extended constructs were similar. This leads to the assumption that neck extended constructs were less efficient in turning ATP consumption into effective directed movement. Actually, probing for stepping behavior revealed that these constructs took highly variable as well as sideways and backward steps, leading to decreased velocities in case of neck extended kinesin-1. In agreement with this observation, Brunnbauer *et al.* (2012) [162] could provide direct evidence that kinesin's neck region determines the torque generating properties.

In our experiments, a GS extended KLP11 GCN4 construct showed an increase in the maximal microtubule-stimulated ATP turnover compared to KLP11/11 GCN4. This construct suffered steric hindrance, unable to take consecutive steps along MT tracks, resulting in an unprocessive motor. Interestingly, activated GS constructs in single molecule assays failed to reach the velocities observed with KLP20/20 GCN4, most probably for the same reason observed by Yildiz *et al.* (2009). Our neck extended GS constructs were not effective enough to turn the ATP consumption into directed movement. In contrast to the observation of Yildiz *et al.* (2009), however, our constructs showed no clear correlation between neck length and velocity as well as processivity. KLP11/11 2xGS and KLP11/11 8xGS constructs had almost same velocities in single molecule assays. These results were also in contrast to the observations made by Shastry and Hancock (2010) [156], where a clear correlation between neck shortening and processivity of kinesin-2 (Kif3A) was observed.

## Summary and Outlook

The mechanistic scrutiny of homodimeric molecular motors (e.g. kinesin-1) over the past three decades has revealed two universal kinetic signatures of such long-range transporters: (A) the ATPase activity of the motors is self-regulated via an intramolecular interaction between the catalytic heads and the distal end of the tail domains. (B) Once attached, molecular motors take multiple ATP-dependent “steps” on their respective filaments before detaching (i.e. processivity) which in turn allows the motor to efficiently transport its cargo over long distances.

This work has uncovered several kinetic properties of the heterodimeric kinesin-2 (KLP11/20) motor from *C. elegans* which agree with the concepts described above. However, the distinct identities of the motor proteins, namely KLP11 and KLP20, constituting the heterodimeric KLP11/20 allowed pinpointing the contributions of each member to the observed kinetic signatures.

The investigation of recombinantly expressed wild type and engineered constructs led to following four major conclusions: First, the wild type KLP11/20 self-inhibits its ATPase activity (auto-regulation) via its tail domains. This inhibition can be relieved either by swapping the relative head positions (KLP20/11) or by replacing the flexible kink position by stiff residues (KLP11EE/20EE) or by removing the KLP11 subunit (KLP20/20). This uncovered kinetic signature in the KLP11/20 heterodimer represents a novel concept of an asymmetric auto-regulation as merely swapping the head positions (KLP20/11) is sufficient to switch on the ATPase activity of the motor. Second, the dimerization of two KLP11 vs. two KLP20 head domains either by the wild type tail or by the unrelated molecular zipper GCN4 results in motors with distinct kinetic properties. Third, the GCN4-mediated dimerization of the KLP11 subunit results in an unprocessive motor whereas the corresponding dimerization of the KLP20 subunit results in a processive motor. Fourth, introducing flexible glycine/serine repeats between the KLP11 head domains is sufficient to turn on processivity of the homodimeric KLP11/11 GCN4 motor without affecting the motor's overall velocity.



This work provides a solid basis to further dissect the molecular interactions that allow auto-regulation in the heterodimeric KLP11/20: is the distal tail of the KLP11 or the KLP20 subunit responsible for the inhibition of the ATPase of the motor, provided the half-site inhibition model derived from the homodimeric kinesin-1 is applicable?. Or does KLP11/20 need both distal tail domains for efficient self-inhibition? Another intriguing question concerns the processivity of the dimeric KLP11 GCN4 motor containing the flexible glycine/serine extensions. In stark contrast to kinesin-1, the velocity of the KLP11-GCN4 remains constant with increasing length of the flexible elements inserted into the neck region. In kinesin-1 the stability of this neck region was shown to control the intramolecular strain which in turn is responsible for efficient stepping of the motor (i.e. one ATP hydrolysis per step). Disrupting the stability in the neck region with flexible insertions significantly decreased the velocity of the kinesin-1 motor and lead to futile ATP hydrolysis cycles that were uncoupled from mechanical stepping. Why is the combination of two KLP11 motor domains insensitive to such reduced intramolecular strain? Or in more general terms, what is the molecular basis of achieving processivity? This question is still unanswered for kinesin-1, and this work has added another flavor to the spectrum.

## Literature

1. Howard, J., *Mechanics of the motor proteins and the cytoskeleton.*, 2001, Sinauer Associates, Inc., Sunderland.
2. Schliwa, M. e., *Molecular Motors*, ed. M. Schliwa. 2003: Wiley-VCH. 604.
3. Sheetz, M.P., *Motor and cargo interactions*. Eur J Biochem, 1999. **262**(1): p. 19-25.
4. Endow, S.A., *Microtubule motors in spindle and chromosome motility*. Eur J Biochem, 1999. **262**(1): p. 12-8.
5. Goldstein, L.S. and A.V. Philp, *The road less traveled: emerging principles of kinesin motor utilization*. Annu Rev Cell Dev Biol, 1999. **15**: p. 141-83.
6. Alberts, B., *Molecular biology of the cell*, 2004, NCBI,: Bethesda, MD.
7. Vale, R., *Guidebook to Cytoskeletal and Motor Proteins*. 2001, Oxford University Press.
8. Holmes, K.C., et al., *Atomic model of the actin filament*. Nature, 1990. **347**(6288): p. 44-9.
9. Pollard, T.D. and G.G. Borisy, *Cellular motility driven by assembly and disassembly of actin filaments*. Cell, 2003. **112**(4): p. 453-65.
10. Reisler, E. and E.H. Egelman, *Actin structure and function: what we still do not understand*. J Biol Chem, 2007. **282**(50): p. 36133-7.
11. Tilney, L.G., et al., *Microtubules: evidence for 13 protofilaments*. J Cell Biol, 1973. **59**(2 Pt 1): p. 267-75.
12. Mitchison, T. and M. Kirschner, *Dynamic instability of microtubule growth*. Nature, 1984. **312**(5991): p. 237-42.
13. Howard, J. and A.A. Hyman, *Growth, fluctuation and switching at microtubule plus ends*. Nat Rev Mol Cell Biol, 2009. **10**(8): p. 569-74.
14. Wade, R.H. and A.A. Hyman, *Microtubule structure and dynamics*. Curr Opin Cell Biol, 1997. **9**(1): p. 12-7.
15. Tucker, C. and L.S. Goldstein, *Probing the kinesin-microtubule interaction*. J Biol Chem, 1997. **272**(14): p. 9481-8.
16. Schiff, P.B., J. Fant, and S.B. Horwitz, *Promotion of microtubule assembly in vitro by taxol*. Nature, 1979. **277**(5698): p. 665-7.

17. Woehlke, G. and M. Schliwa, *Walking on two heads: the many talents of kinesin*. Nat Rev Mol Cell Biol, 2000. **1**(1): p. 50-8.
18. Kull, F.J. and S.A. Endow, *Kinesin: switch I & II and the motor mechanism*. J Cell Sci, 2002. **115**(Pt 1): p. 15-23.
19. Kull, F.J., et al., *Crystal structure of the kinesin motor domain reveals a structural similarity to myosin*. Nature, 1996. **380**(6574): p. 550-5.
20. Vale, R.D., et al., *Direct observation of single kinesin molecules moving along microtubules*. Nature, 1996. **380**(6573): p. 451-3.
21. Vale, R.D., et al., *Searching for kinesin's mechanical amplifier*. Philos Trans R Soc Lond B Biol Sci, 2000. **355**(1396): p. 449-57.
22. Endow, S.A. and K.W. Waligora, *Determinants of kinesin motor polarity*. Science, 1998. **281**(5380): p. 1200-2.
23. Lawrence, C.J., et al., *Maximum likelihood methods reveal conservation of function among closely related kinesin families*. J Mol Evol, 2002. **54**(1): p. 42-53.
24. Marx, A., A. Hoenger, and E. Mandelkow, *Structures of kinesin motor proteins*. Cell Motil Cytoskeleton, 2009. **66**(11): p. 958-66.
25. Rayment, I., *Kinesin and myosin: molecular motors with similar engines*. Structure, 1996. **4**(5): p. 501-4.
26. Brady, S.T., *A novel brain ATPase with properties expected for the fast axonal transport motor*. Nature, 1985. **317**(6032): p. 73-5.
27. Vale, R.D., T.S. Reese, and M.P. Sheetz, *Identification of a novel force-generating protein, kinesin, involved in microtubule-based motility*. Cell, 1985. **42**(1): p. 39-50.
28. Lawrence, C.J., et al., *A standardized kinesin nomenclature*. J Cell Biol, 2004. **167**(1): p. 19-22.
29. Hirokawa, N. and R. Takemura, *Kinesin superfamily proteins and their various functions and dynamics*. Exp Cell Res, 2004. **301**(1): p. 50-9.
30. Wittmann, T., A. Hyman, and A. Desai, *The spindle: a dynamic assembly of microtubules and motors*. Nat Cell Biol, 2001. **3**(1): p. E28-34.
31. Lakamper, S. and E. Meyhofer, *The E-hook of tubulin interacts with kinesin's head to increase processivity and speed*. Biophys J, 2005. **89**(5): p. 3223-34.
32. Sack, S., F.J. Kull, and E. Mandelkow, *Motor proteins of the kinesin family. Structures, variations, and nucleotide binding sites*. Eur J Biochem, 1999. **262**(1): p. 1-11.

33. Ogawa, T., et al., *A common mechanism for microtubule destabilizers-M type kinesins stabilize curling of the protofilament using the class-specific neck and loops*. Cell, 2004. **116**(4): p. 591-602.
34. Hunter, A.W., et al., *The kinesin-related protein MCAK is a microtubule depolymerase that forms an ATP-hydrolyzing complex at microtubule ends*. Mol Cell, 2003. **11**(2): p. 445-57.
35. Scholey, J.M., *Kinesin-II, a membrane traffic motor in axons, axonemes, and spindles*. J Cell Biol, 1996. **133**(1): p. 1-4.
36. Hirokawa, N., Y. Noda, and Y. Okada, *Kinesin and dynein superfamily proteins in organelle transport and cell division*. Curr Opin Cell Biol, 1998. **10**(1): p. 60-73.
37. Vale, R.D. and R.J. Fletterick, *The design plan of kinesin motors*. Annu Rev Cell Dev Biol, 1997. **13**: p. 745-77.
38. Rashid, D.J., K.P. Wedaman, and J.M. Scholey, *Heterodimerization of the two motor subunits of the heterotrimeric kinesin, KRP85/95*. J Mol Biol, 1995. **252**(2): p. 157-62.
39. Yamazaki, H., et al., *KIF3A/B: a heterodimeric kinesin superfamily protein that works as a microtubule plus end-directed motor for membrane organelle transport*. J Cell Biol, 1995. **130**(6): p. 1387-99.
40. Cole, D.G., *Kinesin-II, the heteromeric kinesin*. Cell Mol Life Sci, 1999. **56**(3-4): p. 217-26.
41. Cole, D.G., et al., *Chlamydomonas kinesin-II-dependent intraflagellar transport (IFT): IFT particles contain proteins required for ciliary assembly in Caenorhabditis elegans sensory neurons*. J Cell Biol, 1998. **141**(4): p. 993-1008.
42. Miki, H., Y. Okada, and N. Hirokawa, *Analysis of the kinesin superfamily: insights into structure and function*. Trends Cell Biol, 2005. **15**(9): p. 467-76.
43. Schliwa, M., *Head and tail*. Cell, 1989. **56**(5): p. 719-20.
44. Bustamante, C., et al., *Mechanical processes in biochemistry*. Annu Rev Biochem, 2004. **73**: p. 705-48.
45. Cochran, J.C. and F.J. Kull, *A molecular motor finds its track*. Nat Struct Mol Biol, 2013. **20**(8): p. 920-1.
46. Rice, S., et al., *A structural change in the kinesin motor protein that drives motility*. Nature, 1999. **402**(6763): p. 778-84.

47. de Cuevas, M., T. Tao, and L.S. Goldstein, *Evidence that the stalk of Drosophila kinesin heavy chain is an alpha-helical coiled coil*. J Cell Biol, 1992. **116**(4): p. 957-65.
48. Hackney, D.D., J.D. Levitt, and J. Suhan, *Kinesin undergoes a 9 S to 6 S conformational transition*. J Biol Chem, 1992. **267**(12): p. 8696-701.
49. Coy, D.L., et al., *Kinesin's tail domain is an inhibitory regulator of the motor domain*. Nat Cell Biol, 1999. **1**(5): p. 288-92.
50. Friedman, D.S. and R.D. Vale, *Single-molecule analysis of kinesin motility reveals regulation by the cargo-binding tail domain*. Nat Cell Biol, 1999. **1**(5): p. 293-7.
51. Stock, M.F., et al., *Formation of the compact conformer of kinesin requires a COOH-terminal heavy chain domain and inhibits microtubule-stimulated ATPase activity*. J Biol Chem, 1999. **274**(21): p. 14617-23.
52. Seiler, S., et al., *Cargo binding and regulatory sites in the tail of fungal conventional kinesin*. Nat Cell Biol, 2000. **2**(6): p. 333-8.
53. Yonekura, H., et al., *Mechanism of tail-mediated inhibition of kinesin activities studied using synthetic peptides*. Biochem Biophys Res Commun, 2006. **343**(2): p. 420-7.
54. Cai, D., et al., *Kinesin-1 structural organization and conformational changes revealed by FRET stoichiometry in live cells*. J Cell Biol, 2007. **176**(1): p. 51-63.
55. Dietrich, K.A., et al., *The kinesin-1 motor protein is regulated by a direct interaction of its head and tail*. Proc Natl Acad Sci U S A, 2008. **105**(26): p. 8938-43.
56. Hackney, D.D., N. Baek, and A.C. Snyder, *Half-site inhibition of dimeric kinesin head domains by monomeric tail domains*. Biochemistry, 2009. **48**(15): p. 3448-56.
57. Hackney, D.D. and M.F. Stock, *Kinesin's IAK tail domain inhibits initial microtubule-stimulated ADP release*. Nat Cell Biol, 2000. **2**(5): p. 257-60.
58. Hackney, D.D. and M.F. Stock, *Kinesin tail domains and Mg<sup>2+</sup> directly inhibit release of ADP from head domains in the absence of microtubules*. Biochemistry, 2008. **47**(29): p. 7770-8.
59. Wong, Y.L., et al., *The Kinesin-1 tail conformationally restricts the nucleotide pocket*. Biophys J, 2009. **96**(7): p. 2799-807.
60. Howard, J., A.J. Hudspeth, and R.D. Vale, *Movement of microtubules by single kinesin molecules*. Nature, 1989. **342**(6246): p. 154-8.

61. Block, S.M., L.S. Goldstein, and B.J. Schnapp, *Bead movement by single kinesin molecules studied with optical tweezers*. Nature, 1990. **348**(6299): p. 348-52.
62. Svoboda, K., et al., *Direct observation of kinesin stepping by optical trapping interferometry*. Nature, 1993. **365**(6448): p. 721-7.
63. Hua, W., et al., *Coupling of kinesin steps to ATP hydrolysis*. Nature, 1997. **388**(6640): p. 390-3.
64. Schnitzer, M.J. and S.M. Block, *Kinesin hydrolyses one ATP per 8-nm step*. Nature, 1997. **388**(6640): p. 386-90.
65. Rosenfeld, S.S., et al., *Stepping and stretching. How kinesin uses internal strain to walk processively*. J Biol Chem, 2003. **278**(20): p. 18550-6.
66. Hancock, W.O. and J. Howard, *Processivity of the motor protein kinesin requires two heads*. J Cell Biol, 1998. **140**(6): p. 1395-405.
67. Cross, R.A., *On the hand-over-hand footsteps of kinesin heads*. J Muscle Res Cell Motil, 1995. **16**(2): p. 91-4.
68. Hackney, D.D., *Evidence for alternating head catalysis by kinesin during microtubule-stimulated ATP hydrolysis*. Proc Natl Acad Sci U S A, 1994. **91**(15): p. 6865-9.
69. Ma, Y.Z. and E.W. Taylor, *Interacting head mechanism of microtubule-kinesin ATPase*. J Biol Chem, 1997. **272**(2): p. 724-30.
70. Gilbert, S.P., M.L. Moyer, and K.A. Johnson, *Alternating site mechanism of the kinesin ATPase*. Biochemistry, 1998. **37**(3): p. 792-9.
71. Sablin, E.P. and R.J. Fletterick, *Nucleotide switches in molecular motors: structural analysis of kinesins and myosins*. Curr Opin Struct Biol, 2001. **11**(6): p. 716-24.
72. Endow, S.A. and D.S. Barker, *Processive and nonprocessive models of kinesin movement*. Annu Rev Physiol, 2003. **65**: p. 161-75.
73. Asbury, C.L., A.N. Fehr, and S.M. Block, *Kinesin moves by an asymmetric hand-over-hand mechanism*. Science, 2003. **302**(5653): p. 2130-4.
74. Kaseda, K., H. Higuchi, and K. Hirose, *Alternate fast and slow stepping of a heterodimeric kinesin molecule*. Nat Cell Biol, 2003. **5**(12): p. 1079-82.
75. Yildiz, A., et al., *Kinesin walks hand-over-hand*. Science, 2004. **303**(5658): p. 676-8.
76. Schief, W.R., et al., *Inhibition of kinesin motility by ADP and phosphate supports a hand-over-hand mechanism*. Proc Natl Acad Sci U S A, 2004. **101**(5): p. 1183-8.

77. McDonald, H.B., R.J. Stewart, and L.S. Goldstein, *The kinesin-like ncd protein of Drosophila is a minus end-directed microtubule motor*. Cell, 1990. **63**(6): p. 1159-65.
78. deCastro, M.J., C.H. Ho, and R.J. Stewart, *Motility of dimeric ncd on a metal-chelating surfactant: evidence that ncd is not processive*. Biochemistry, 1999. **38**(16): p. 5076-81.
79. Okada, Y. and N. Hirokawa, *A processive single-headed motor: kinesin superfamily protein KIF1A*. Science, 1999. **283**(5405): p. 1152-7.
80. Okada, Y., H. Higuchi, and N. Hirokawa, *Processivity of the single-headed kinesin KIF1A through biased binding to tubulin*. Nature, 2003. **424**(6948): p. 574-7.
81. Thaler, C.D. and L.T. Haimo, *Microtubules and microtubule motors: mechanisms of regulation*. Int Rev Cytol, 1996. **164**: p. 269-327.
82. Wedaman, K.P., et al., *Sequence and submolecular localization of the 115-kD accessory subunit of the heterotrimeric kinesin-II (KRP85/95) complex*. J Cell Biol, 1996. **132**(3): p. 371-80.
83. Coy, D.L., M. Wagenbach, and J. Howard, *Kinesin takes one 8-nm step for each ATP that it hydrolyzes*. J Biol Chem, 1999. **274**(6): p. 3667-71.
84. Kaan, H.Y., D.D. Hackney, and F. Kozielski, *The structure of the kinesin-1 motor-tail complex reveals the mechanism of autoinhibition*. Science, 2011. **333**(6044): p. 883-5.
85. Verhey, K.J. and J.W. Hammond, *Traffic control: regulation of kinesin motors*. Nat Rev Mol Cell Biol, 2009. **10**(11): p. 765-77.
86. Cole, D.G., et al., *Novel heterotrimeric kinesin-related protein purified from sea urchin eggs*. Nature, 1993. **366**(6452): p. 268-70.
87. Qiu, D., et al., *Localization and loss-of-function implicates ciliary proteins in early, cytoplasmic roles in left-right asymmetry*. Dev Dyn, 2005. **234**(1): p. 176-89.
88. Brown, J.M., et al., *Kinesin-II is preferentially targeted to assembling cilia and is required for ciliogenesis and normal cytokinesis in Tetrahymena*. Mol Biol Cell, 1999. **10**(10): p. 3081-96.
89. Signor, D., et al., *Two heteromeric kinesin complexes in chemosensory neurons and sensory cilia of Caenorhabditis elegans*. Mol Biol Cell, 1999. **10**(2): p. 345-60.
90. Scholey, J.M., *Intraflagellar transport motors in cilia: moving along the cell's antenna*. J Cell Biol, 2008. **180**(1): p. 23-9.

91. Morris, R.L. and J.M. Scholey, *Heterotrimeric kinesin-II is required for the assembly of motile 9+2 ciliary axonemes on sea urchin embryos*. J Cell Biol, 1997. **138**(5): p. 1009-22.
92. Orozco, J.T., et al., *Movement of motor and cargo along cilia*. Nature, 1999. **398**(6729): p. 674.
93. Pan, J. and W.J. Snell, *Kinesin-II is required for flagellar sensory transduction during fertilization in Chlamydomonas*. Mol Biol Cell, 2002. **13**(4): p. 1417-26.
94. Rosenbaum, J.L. and G.B. Witman, *Intraflagellar transport*. Nat Rev Mol Cell Biol, 2002. **3**(11): p. 813-25.
95. Lin, F., et al., *Kidney-specific inactivation of the KIF3A subunit of kinesin-II inhibits renal ciliogenesis and produces polycystic kidney disease*. Proc Natl Acad Sci U S A, 2003. **100**(9): p. 5286-91.
96. Scholey, J.M. and K.V. Anderson, *Intraflagellar transport and cilium-based signaling*. Cell, 2006. **125**(3): p. 439-42.
97. Kozminski, K.G., *High-resolution imaging of flagella*. Methods Cell Biol, 1995. **47**: p. 263-71.
98. Kozminski, K.G., et al., *A motility in the eukaryotic flagellum unrelated to flagellar beating*. Proc Natl Acad Sci U S A, 1993. **90**(12): p. 5519-23.
99. Pazour, G.J., et al., *The intraflagellar transport protein, IFT88, is essential for vertebrate photoreceptor assembly and maintenance*. J Cell Biol, 2002. **157**(1): p. 103-13.
100. Perkins, L.A., et al., *Mutant sensory cilia in the nematode Caenorhabditis elegans*. Dev Biol, 1986. **117**(2): p. 456-87.
101. Starich, T.A., et al., *Mutations affecting the chemosensory neurons of Caenorhabditis elegans*. Genetics, 1995. **139**(1): p. 171-88.
102. Miller, M.S., et al., *Mutant kinesin-2 motor subunits increase chromosome loss*. Mol Biol Cell, 2005. **16**(8): p. 3810-20.
103. Fan, J. and K.A. Beck, *A role for the spectrin superfamily member Syne-1 and kinesin II in cytokinesis*. J Cell Sci, 2004. **117**(Pt 4): p. 619-29.
104. Haraguchi, K., et al., *Role of the kinesin-2 family protein, KIF3, during mitosis*. J Biol Chem, 2006. **281**(7): p. 4094-9.
105. Coy, D.L. and J. Howard, *Organelle transport and sorting in axons*. Curr Opin Neurobiol, 1994. **4**(5): p. 662-7.
106. Kondo, S., et al., *KIF3A is a new microtubule-based anterograde motor in the nerve axon*. J Cell Biol, 1994. **125**(5): p. 1095-107.



107. Le Bot, N., et al., *Role of xklp3, a subunit of the Xenopus kinesin II heterotrimeric complex, in membrane transport between the endoplasmic reticulum and the Golgi apparatus*. J Cell Biol, 1998. **143**(6): p. 1559-73.
108. Tuma, M.C., et al., *Heterotrimeric kinesin II is the microtubule motor protein responsible for pigment dispersion in Xenopus melanophores*. J Cell Biol, 1998. **143**(6): p. 1547-58.
109. Kolpakova-Hart, E., et al., *Kinesin-2 controls development and patterning of the vertebrate skeleton by Hedgehog- and Gli3-dependent mechanisms*. Dev Biol, 2007. **309**(2): p. 273-84.
110. Corbit, K.C., et al., *Kif3a constrains beta-catenin-dependent Wnt signalling through dual ciliary and non-ciliary mechanisms*. Nat Cell Biol, 2008. **10**(1): p. 70-6.
111. Ocbina, P.J. and K.V. Anderson, *Intraflagellar transport, cilia, and mammalian Hedgehog signaling: analysis in mouse embryonic fibroblasts*. Dev Dyn, 2008. **237**(8): p. 2030-8.
112. Heinrich, B. and J.O. Deshler, *RNA localization to the Balbiani body in Xenopus oocytes is regulated by the energy state of the cell and is facilitated by kinesin II*. RNA, 2009. **15**(4): p. 524-36.
113. Inglis, P.N., et al., *The sensory cilia of Caenorhabditis elegans*. WormBook, 2007: p. 1-22.
114. Yamazaki, H., et al., *Cloning and characterization of KAP3: a novel kinesin superfamily-associated protein of KIF3A/3B*. Proc Natl Acad Sci U S A, 1996. **93**(16): p. 8443-8.
115. Pan, X., et al., *Mechanism of transport of IFT particles in C. elegans cilia by the concerted action of kinesin-II and OSM-3 motors*. J Cell Biol, 2006. **174**(7): p. 1035-45.
116. Snow, J.J., et al., *Two anterograde intraflagellar transport motors cooperate to build sensory cilia on C. elegans neurons*. Nat Cell Biol, 2004. **6**(11): p. 1109-13.
117. Shakir, M.A., et al., *C. elegans osm-3 gene mediating osmotic avoidance behaviour encodes a kinesin-like protein*. Neuroreport, 1993. **4**(7): p. 891-4.
118. Ou, G., et al., *Functional coordination of intraflagellar transport motors*. Nature, 2005. **436**(7050): p. 583-7.
119. Imanishi, M., et al., *Autoinhibition regulates the motility of the C. elegans intraflagellar transport motor OSM-3*. J Cell Biol, 2006. **174**(7): p. 931-7.
120. Hammond, J.W., et al., *Autoinhibition of the kinesin-2 motor KIF17 via dual intramolecular mechanisms*. J Cell Biol, 2010. **189**(6): p. 1013-25.

121. Guydosh, N.R. and S.M. Block, *Backsteps induced by nucleotide analogs suggest the front head of kinesin is gated by strain*. Proc Natl Acad Sci U S A, 2006. **103**(21): p. 8054-9.
122. Rosenfeld, S.S., et al., *Measuring kinesin's first step*. J Biol Chem, 2002. **277**(39): p. 36731-9.
123. Uemura, S. and S. Ishiwata, *Loading direction regulates the affinity of ADP for kinesin*. Nat Struct Biol, 2003. **10**(4): p. 308-11.
124. Sambrook J, F.E.M.T., *"Molecular cloning: a laboratory manual."*. 1989: Cold Spring Harbor Laboratory Press.
125. Mullis, K., et al., *Specific enzymatic amplification of DNA in vitro: the polymerase chain reaction*. Cold Spring Harb Symp Quant Biol, 1986. **51 Pt 1**: p. 263-73.
126. Brunnbauer, M., et al., *Regulation of a heterodimeric kinesin-2 through an unprocessive motor domain that is turned processive by its partner*. Proc Natl Acad Sci U S A, 2010. **107**(23): p. 10460-5.
127. Cai, D., K.J. Verhey, and E. Meyhofer, *Tracking single Kinesin molecules in the cytoplasm of mammalian cells*. Biophys J, 2007. **92**(12): p. 4137-44.
128. Miller, L.K., *Baculoviruses as gene expression vectors*. Annu Rev Microbiol, 1988. **42**: p. 177-99.
129. Carbonell, L.F., M.J. Klowden, and L.K. Miller, *Baculovirus-mediated expression of bacterial genes in dipteran and mammalian cells*. J Virol, 1985. **56**(1): p. 153-60.
130. Luckow, V.A., et al., *Efficient generation of infectious recombinant baculoviruses by site-specific transposon-mediated insertion of foreign genes into a baculovirus genome propagated in Escherichia coli*. J Virol, 1993. **67**(8): p. 4566-79.
131. Laemmli, U.K., *Cleavage of structural proteins during the assembly of the head of bacteriophage T4*. Nature, 1970. **227**(5259): p. 680-5.
132. Bradford, M.M., *A rapid and sensitive method for the quantitation of microgram quantities of protein utilizing the principle of protein-dye binding*. Anal Biochem, 1976. **72**: p. 248-54.
133. Huang, T.G. and D.D. Hackney, *Drosophila kinesin minimal motor domain expressed in Escherichia coli. Purification and kinetic characterization*. J Biol Chem, 1994. **269**(23): p. 16493-501.
134. Lange, G., et al., *Tubulin oligomers and microtubule oscillations. Antagonistic role of microtubule stabilizers and destabilizers*. Eur J Biochem, 1988. **178**(1): p. 61-9.

135. Haid, E., P. Lehmann, and J. Ziegenhorn, *Molar absorptivities of beta-NADH and beta-NAD at 260 nm*. Clin Chem, 1975. **21**(7): p. 884-7.
136. Peloquin, J., Y. Komarova, and G. Borisy, *Conjugation of fluorophores to tubulin*. Nat Methods, 2005. **2**(4): p. 299-303.
137. Axelrod, D., *Total internal reflection fluorescence microscopy*. Methods Cell Biol, 1989. **30**: p. 245-70.
138. Schneckenburger, H., *Total internal reflection fluorescence microscopy: technical innovations and novel applications*. Curr Opin Biotechnol, 2005. **16**(1): p. 13-8.
139. Sako, Y. and T. Uyemura, *Total internal reflection fluorescence microscopy for single-molecule imaging in living cells*. Cell Struct Funct, 2002. **27**(5): p. 357-65.
140. Downard, K.M.F.W.A., *The man Behind the Mass Spectrograph*. European Journal of Mass Spectrometry 2007(13): p. 177-190.
141. Altschul, S.F., et al., *Gapped BLAST and PSI-BLAST: a new generation of protein database search programs*. Nucleic Acids Res, 1997. **25**(17): p. 3389-402.
142. Altschul, S.F., et al., *Protein database searches using compositionally adjusted substitution matrices*. FEBS J, 2005. **272**(20): p. 5101-9.
143. Corpet, F., *Multiple sequence alignment with hierarchical clustering*. Nucleic Acids Res, 1988. **16**(22): p. 10881-90.
144. Lupas, A., M. Van Dyke, and J. Stock, *Predicting coiled coils from protein sequences*. Science, 1991. **252**(5009): p. 1162-4.
145. Scholey, J.M., *Kinesin-2 motors transport IFT-particles, dyneins and tubulin subunits to the tips of Caenorhabditis elegans sensory cilia: relevance to vision research?* Vision Res, 2012. **75**: p. 44-52.
146. Lee, J.R., et al., *An intramolecular interaction between the FHA domain and a coiled coil negatively regulates the kinesin motor KIF1A*. EMBO J, 2004. **23**(7): p. 1506-15.
147. Yamada, K.H., T. Hanada, and A.H. Chishti, *The effector domain of human Dlg tumor suppressor acts as a switch that relieves autoinhibition of kinesin-3 motor GAKIN/KIF13B*. Biochemistry, 2007. **46**(35): p. 10039-45.
148. Hammond, J.W., et al., *Mammalian Kinesin-3 motors are dimeric in vivo and move by processive motility upon release of autoinhibition*. PLoS Biol, 2009. **7**(3): p. e72.

149. Vukajlovic, M., et al., *How kinesin-2 forms a stalk*. Mol Biol Cell, 2011. **22**(22): p. 4279-87.
150. Zhang, Y. and W.O. Hancock, *The two motor domains of KIF3A/B coordinate for processive motility and move at different speeds*. Biophys J, 2004. **87**(3): p. 1795-804.
151. Arnold, K., et al., *The SWISS-MODEL workspace: a web-based environment for protein structure homology modelling*. Bioinformatics, 2006. **22**(2): p. 195-201.
152. Kiefer, F., et al., *The SWISS-MODEL Repository and associated resources*. Nucleic Acids Res, 2009. **37**(Database issue): p. D387-92.
153. Peitsch, M., *Protein modeling by Email*. Bio/Technology, 1995. **13**: p. 658-660.
154. Hariharan, V. and W.O. Hancock, *Insights into the Mechanical Properties of the Kinesin Neck Linker Domain from Sequence Analysis and Molecular Dynamics Simulations*. Cell Mol Bioeng, 2009. **2**(2): p. 177-189.
155. Muthukrishnan, G., et al., *The processivity of kinesin-2 motors suggests diminished front-head gating*. Curr Biol, 2009. **19**(5): p. 442-7.
156. Shastry, S. and W.O. Hancock, *Neck linker length determines the degree of processivity in kinesin-1 and kinesin-2 motors*. Curr Biol, 2010. **20**(10): p. 939-43.
157. Yildiz, A., et al., *Intramolecular strain coordinates kinesin stepping behavior along microtubules*. Cell, 2008. **134**(6): p. 1030-41.
158. Endow, S.A., *Determinants of molecular motor directionality*. Nat Cell Biol, 1999. **1**(6): p. E163-7.
159. Hancock, W.O. and J. Howard, *Kinesin's processivity results from mechanical and chemical coordination between the ATP hydrolysis cycles of the two motor domains*. Proc Natl Acad Sci U S A, 1999. **96**(23): p. 13147-52.
160. Hirose, K., et al., *Three-dimensional cryoelectron microscopy of dimeric kinesin and ncd motor domains on microtubules*. Proc Natl Acad Sci U S A, 1996. **93**(18): p. 9539-44.
161. Hoeng, J.C., et al., *High-resolution crystal structure and in vivo function of a kinesin-2 homologue in Giardia intestinalis*. Mol Biol Cell, 2008. **19**(7): p. 3124-37.
162. Brunnbauer, M., et al., *Torque generation of kinesin motors is governed by the stability of the neck domain*. Mol Cell, 2012. **46**(2): p. 147-58.

